INDUCTION GENERAL, INC. • PITTSBURGH, PA
ANALYSIS • DESIGN • DEVELOPMENT • PROTOTYPES
ELECTRIC POWER EQUIPMENT AND SYSTEMS

NASA CR - 175071

(NASA-CR-175071) HIGH FREQUENCY POWER DISTRIBUTION SYSTEM Final Report (Induction General, Inc.) 159 p LIMIT DOMESTIC X86-10292
Unclas
G4/33 16078

CONTRACT NO. NAS3 - 23894

HIGH FREQUENCY POWER DISTRIBUTION SYSTEM

FINAL REPORT

by

Induction General, Inc.
GM Industrial Court
3253 Old Frankstown Road
Pittsburgh, PA 15239

Mikund R. Patel
Project Engineer

Prepared for

NASA Lewis Research Center
Space Station Systems Section
Cleveland, OH 44135

David D. Renz
NASA Project Manager

April, 1986

(NASA-CR-175071) HIGH FREQUENCY POWER DISTRIBUTION SYSTEM Final Report (Induction General) 159 p CSCL 09C
N88-23939
Unclas
G3/33 0146364

or in part.
Review for general release April 88

APR 1986
RECEIVED
NASA STI FACILITY
ACCESS DEPT.

NASA CR - 175071

CONTRACT NO. NAS3 - 23894

HIGH FREQUENCY POWER DISTRIBUTION SYSTEM

FINAL REPORT

by

Induction General, Inc.
GM Industrial Court
3253 Old Frankstown Road
Pittsburgh, PA 15239

Prepared for

NASA Lewis Research Center
Space Station Systems Section
Cleveland, OH 44135

Mikund R. Patel

Approved
Mikund R. Patel, President

April 1986

ACKNOWLEDGMENT

Induction General, Inc. gratefully acknowledges contributions from several sources towards the timely and successful completion of the work documented in this report: Messrs. D. D. Renz and I. G. Hansen of NASA Lewis Research Center, who provided continuous guidance throughout the project; Ms. Sarla Patel, who significantly contributed in the early configuration analysis; Messrs. R. F. Meserve and A. R. Copp of New England Electric Wire, who contributed in sharing their valuable manufacturing experience during the design stage and also in manufacturing the cable; and Ms. Rosalie T. Grenelle, who diligently prepared the manuscript.

NASA CR - 175071

HIGH FREQUENCY POWER DISTRIBUTION SYSTEM

ABSTRACT

The objective of this project was to provide the technology of high frequency, high power transmission lines to the 100 kW power range at 20 kHz frequency. In addition to the necessary design studies, a 150 m long, 600 V, 60 A transmission line was built, tested and delivered to NASA LeRC for full vacuum tests.

The configuration analysis on five alternative configurations resulted in the final selection of the three parallel Litz straps configuration, which gave a virtually concentric design in the electromagnetic sense. Low inductance, low EMI and flexibility in handling are the key features of this configuration. The final design was made after a parametric study to minimize the losses, weight and inductance. The construction of the cable was completed with no major difficulties. The R,L,C parameters measured on the cable agreed well with the calculated values. The corona tests on insulation samples showed a safety factor of 3. The EMI test results exceeded the MIL-STD-462 RE01 limit due to small non-concentricity introduced by the manufacturing variations. Certain manufacturing improvements are recommended to reduce EMI.

The project was funded by NASA Lewis Research Center under Contract No. NAS3-23894, and was monitored by Mr. D. D. Renz.

KEY WORDS: Electrical power, Transmission lines, Distribution, Space station, High voltage, High frequency, Resistance, Inductance, Capacitance, Analysis, Prototype, Corona, EMI.

TABLE OF CONTENTS

		PAGE
	EXECUTIVE SUMMARY	v
1.0	INTRODUCTION TO PROJECT OBJECTIVE	1.01
2.0	CONFIGURATION ANALYSIS	2.01
2.1	Initial Alternative Configurations	2.01
2.2	Parameters of Hollow Configurations	2.05
2.3	Parameters of Two Parallel Litz Straps	2.05
2.3.1	Factors Influencing 2-Strap Line Parameters	2.05
2.3.2	Effect of Stranding and Spiraling	2.05
2.3.3	Skin Effect	2.06
2.3.4	Proximity Effect	2.07
2.3.5	Resistance Calculation	2.11
2.3.6	Inductance Calculation	2.12
2.3.7	Capacitance Calculation	2.12
2.3.8	Mechanical Force Calculation	2.15
2.3.9	Mass Calculation	2.17
3.0	PARAMETRIC STUDY ON INITIAL CONFIGURATIONS	3.01
3.1	Hollow Configurations	3.01
3.2	Two Parallel Litz Straps	3.01
3.3	Parameter Optimization in 2-Strap Cable	3.04
3.4	Discussion on Initial Configuration Designs	3.04
4.0	THREE PARALLEL LITZ STRAPS CONFIGURATION	4.01
4.1	3-Strap Configuration Analysis	4.01
4.2	Shielding and End Insulation Considerations	4.03
4.3	Comparison Between 2-Strap and 3-Strap Configurations	4.05
4.4	Design Optimization in 3-Strap Configuration	4.07

TABLE OF CONTENTS

		PAGE
4.5	Cable Ratings Revised	4.07
4.6	Line Parameters of the Selected 3-Strap Design	4.09
5.0	MATERIAL SELECTION	5.01
5.1	Conductor Materials	5.01
5.2	Inherent Material Limitations on Loss x Mass Product	5.04
5.3	Dielectric Materials	5.05
5.3.1	Strand Insulation	5.05
5.3.2	Major Insulation	5.05
5.4	Low Loss Insulating Material	5.06
5.5	Dielectric Loss Calculation	5.13
6.0	CORONA CONSIDERATIONS	6.01
6.1	Corona Inception Voltage Vs. Maximum Permissible Void Size	6.01
6.2	Dielectric Stress Concentration in End-Insulation	6.05
6.3	Corona Resistance	6.07
7.0	OTHER CONSIDERATIONS	7.01
7.1	Environmental Considerations	7.01
7.2	Manufacturing and Flexibility Considerations	7.01
7.3	Joints and Termination Consideration	7.02
8.0	ALL THE ALTERNATIVES COMPARED FOR FINAL SELECTION	8.01
9.0	THERMAL DESIGN CALCULATIONS	9.01
9.1	Radiation Cooling Alone	9.01
9.2	Conduction Cooling to Continuous Base Plate	9.03
9.3	Conduction Cooling by Intermittent Mounting Supports	9.05
9.4	Summary of Thermal Design Calculations	9.09
10.0	MECHANICAL FORCE CALCULATIONS	10.01

TABLE OF CONTENTS

		PAGE
11.0	ELECTROMAGNETIC INTERFERENCE	11.01
11.1	EMI Flux Density Estimate	11.01
11.2	EMI Shielding	11.03
12.0	FINAL DESIGN SUMMARIZED	12.01
12.1	Discussion on the Final Design	12.01
12.2	Summary of Basic Formulas for 3-Strap Design	12.04
13.0	FAILURE MODES AND EFFECTS ANALYSIS	13.01
13.1	Exposure to Free Space Temperature	13.01
13.2	Exposure to Ultraviolet Radiation	13.01
13.3	Voids in Insulation	13.02
14.0	SAMPLE CONSTRUCTION AND TESTS	14.01
14.1	One Meter Long Sample	14.01
14.2	3.7 Meter Long Sample	14.01
14.3	Five Meter Long Sample	14.05
15.0	CONSTRUCTION OF FULL CABLE	15.01
16.0	TESTS ON FULL CABLE	16.01
16.1	AC Corona Tests	16.01
16.2	R,L,C Tests	16.04
16.3	EMI Tests with Cable Terminals Inside the Chamber	16.13
16.4	EMI Tests with Cable Terminals Outside the Chamber	16.14
APPENDIX A:	EDDY LOSSES IN LITZ STRAP LINES DUE TO TRANSVERSE FLUX	A.01
APPENDIX B:	PARAMETRIC STUDY ON 2-STRAP CABLE CONFIGURATION	B.01
LIST OF FIGURES		L.01
LIST OF TABLES		L.05
LIST OF REFERENCES		L.07
DISTRIBUTION LIST		L.09

EXECUTIVE SUMMARY

The objective of this project was to provide the technology of high voltage, high power transmission lines to deliver power at 1000 Vrms and 100 Arms levels, operating at 20 kHz in vacuum. In addition to the necessary design studies, a 150-meter long, 600 V, 60 A transmission line was built, tested and delivered to NASA Lewis Research Center for vacuum testing. The analysis, design, manufacturing and test results obtained during the course of the project are documented in this report.

In the initial part of the report, four alternative configurations have been analyzed, namely, the hollow coaxial, hollow stranded coaxial, hollow parallel and two parallel Litz straps. A parametric study and the design optimizations on these configurations, along with the manufacturing considerations, led us to recommend the two parallel Litz straps cable configuration. Three attractive features of this configuration are low inductance, good manufacturability and flexibility in handling. Further improvements were achieved by splitting one of the two straps in two parts and locating the split halves on two sides of the full strap. As shown in the report, the resulting three-strap configuration is a virtually concentric cable in an electromagnetic sense. For a given cable width, it reduces the inductance to less than one-half. Furthermore, since the magnetic flux is now internally contained (see sketch below), it offers lower EMI. At the same time, it maintains

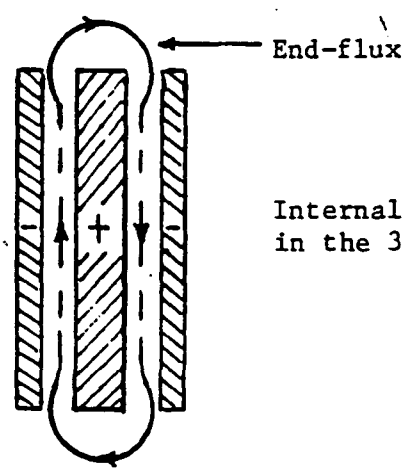

Internal flux containment in the 3-strap configuration

other attractive features of the 2-strap configuration, including the flexibility in manufacturing and handling. The 3-strap configuration, therefore, was adopted for the final design.

Alternative conductor materials were evaluated. It is shown that for a given conductor material, the loss x mass product of the cable is invariant. Copper meets the set goal on loss x Mass product at the anticipated operating temperature. Aluminum would exceed the goal but would pose severe limitations on manufacturing, joints and terminations. Copper was chosen as the conductor material for its solderability. Alternative insulating materials were also investigated. Polypropylene was selected as the major insulating material for low dielectric loss.

From corona considerations, the maximum permissible void size in the insulation has been established. This has a bearing on selecting the manufacturing process and operating practice for the cable. For example, the failure mode and effect analysis on the cable showed a possibility of creating a delamination void between the middle and the outer straps that may exceed the permissible void size of 5 mils. Bleeding nitrogen along the length of the cable may be necessary to avoid corona under such delamination. Embrittlement and cracking of the insulation at low temperatures is another possible source of voids in the insulation.

Two inch wide cable was initially selected as an optimum design for the originally specified 1000 V, 100 A cable. However, the manufacturing investigations during the final design phase revealed that the existing cable extrusion process would allow only 1.5 inch wide cable. The decreased cable width required increased cable thickness, resulting in the aspect ratio of 3.2 versus at least 5 desired for a good flexibility in handling. Upon reviewing this constraint and the near term power requirement, the cable rating was revised to 600 V, 60 A. The 1.5 inch wide extrusion die limitation, however, is not of a

fundamental nature. Wider extrusion dies and tools can be developed for higher cable ratings when required. Such cost, however, was considered unnecessary at this time.

For the 600 V, 60 A cable with 3-strap configuration, the copper conductor and polypropylene insulation were selected in the final design. The cable dimensions, design parameters and design formulas are summarized in Section 12.0. The losses in the final design are 3.755 watts/m, inductive voltage drop 0.203 v/m, capacitive charging current 0.227 A/m and the mass 1.102 kg/m. If one side of the cable is radiating to free space at 80°K (liquid nitrogen temperature), the operating cable temperature is expected to be tens of degrees below 0°C. If the cable is mounted continuously on a 60°C base plate, the operating temperature of the cable would be 61°C. The low temperature rises are due to low losses and large surface area available for cooling. The mechanical and electrical stresses in the insulation are adequately low.

Pre-production cable samples were constructed and tested for R,L,C parameters. The measurements on these samples checked well with their calculated values. The test results, therefore, indicated the validity of the design formulas developed for the cable. The design was then formally reviewed and released for the construction.

There were several problems encountered during the manufacture of the cable. First of all, maintaining accurate dimensions of Litz straps during and after the manufacturing processes was difficult. Generally, the strap thicknesses came out 15 to 20% oversize. In the second manufacturing step, applying a 25 to 30 mil polypropylene jacket (major insulation) over the middle strap with no tearing or pinholes was a smooth process and was completed with no difficulties. In the last step, applying the outer PVC jacket over the 3-strap assembly, however, proved difficult because of the fluid pressure which built up at the corners of the rectangular extrusion die. Because of this, the

outer straps became narrower than the middle strap and the PVC penetrated excessively inbetween the middle and outer straps. To eliminate this problem, one-mil teflon tape was half-lapped around the 3-strap assembly before extruding the outer PVC jacket. This considerably improved the cable construction.

A detailed Test Plan for testing the cable was prepared for R,L,C,corona and EMI tests. Several flat samples of polypropylene were tested for AC corona under ASTM standard brass electrodes. Twenty mils thick samples gave 1550 Vrms corona inception voltage and 1400 Vrms corona extinction voltage. For a 440 V operating voltage, this gives a safety factor of 3 for the solid insulation. The previously mentioned delamination voids may cause corona under vacuum at a lower voltage.

From a theoretical consideration, the 3-strap cable configuration was expected to give negligible EMI. However, due to manufacturing variations, the inductances of the two individual outer straps with respect to the middle strap were unequal. This caused unequal currents in the outer straps. The resulting solenoidal flux radiating from the cable was sufficient to exceed the MIL-STD-462, Section RE01 limit of 27 db over one picotesla at 20 kHz. Further manufacturing improvements and/or shielding will be necessary in the future to meet the EMI requirement.

The R,L,C tests were made on full length cable under 20 kHz excitation at full current and full voltage. The resistance agreed well, while the inductance was slightly higher and the capacitance slightly lower than the calculated values. The deviations in the L and C are attributed to the oversized dimensions that resulted in the final manufacture. Accounting for the oversize, the R,L,C test results clearly proved the validity of the virtually concentric 3-strap cable concept and also verified the formulas developed for calculating the circuit parameters.

1.0 INTRODUCTION TO PROJECT OBJECTIVE

NASA studies have projected the power requirements of large spacecrafts, power platforms and space stations in the megawatt level by the year 2000. Analysis on near term power needs has identified a variety of missions and space station configurations requiring significant increase in electrical power up to the hundred kilowatt level. As the need for space power grows larger, so do the requirements for the power distribution system grow in size, sophistication, and complexity. Studies by NASA have shown that significant advantages in weight, cost, efficiency, and design flexibility can be achieved if power transmission and distribution could be accomplished at high voltage and high frequency.

A critical element in high voltage, high power distribution system is a high frequency, high power transmission line which has low loss, low weight and low reactive voltage drop. This project is to provide this technology for high frequency, high power transmission lines to the 100 kW power range at 20 kHz, 1000 V and 100 A in a vacuum.

The original specifications and goals for a prototype of such a line are summarized in Table 1.1. During the course of the project, the ratings of the first prototype line were changed to 600 V, 60 A capacity. In addition to the necessary design studies to meet the set specifications, the goals included a 150 meter long transmission line to be built, tested and delivered to NASA Lewis Research Center for vacuum testing.

TABLE 1.1: SPECIFICATIONS AND GOALS AS SET BY NASA

INITIAL GOALS

A. RATINGS

Voltage - 1000 volts (rms)
Current - 100 amps (rms)
Frequency - 20 kHz

B. DESIGN GOALS

I^2R Loss - .01% per meter (measured at full load current)
Weight - .01 kg per kW per meter
Reactive drop - 1 volt per meter

C. TEMPERATURE

The system shall be designed to reject its heat to a grounded 60°C base plate or mounting points as required.

D. DESIGN LIFE

The design life shall be ten (10) years of continuous operation in a vacuum at rated conditions.

E. EMI

The system shall be designed to meet MIL-STD-462 sections

1) RE01 - 30 Hz to 30 kHz
2) RE02 - 14 kHz to 12.4 GHz
3) RE04 - 20 Hz to 50 kHz

F. LENGTH

System shall be 50 meters in length.

REVISED RATINGS

The ratings of the first prototype were later revised to 600 V, 60 A, with proportionate changes in the loss, weight and inductance. At the same time, the length was changed to 150 meters.

2.0 CONFIGURATION ANALYSIS

Five alternative configurations were investigated in two phases. The initial phase consisted of four different configurations, including two parallel Litz straps. A thorough parametric study was conducted on this group for minimizing the loss, weight and inductance of the cable. At this stage, a new three parallel straps configuration was conceived and was analyzed in the second phase.

2.1 INITIAL ALTERNATIVE CONFIGURATIONS

As for the alternative configurations of the targeted transmission line, the following four options were initially studied:

1) Hollow coaxial cable (with solid sheet conductor)
2) Hollow stranded coaxial cable
3) Hollow round parallel lines
4) Two parallel Litz straps

The first three configurations have been thoroughly investigated by Jefferies and Renz in a NASA study [1], and are depicted in Figure 2.1. These configurations with central part filled with conductor (instead of hollow) offer other three options, which are theoretically included in the above study with the inner radius equal to zero. To avoid duplication, the NASA study is not reproduced here. The interested reader must read Reference 1 as a complement to this report. However, the results of that study have been used in the present investigations.

Coaxial cable with hollow center conductor was the configuration selected in Reference 1 for high frequency distribution of space power. Nearly equal radii of the inner and outer conductor minimized inductance. To provide cable flexibility, stranded rather than solid conductors were considered. A 5 mm inside radius stranded coax cable with 0.5 mm conductor thickness was cited as an example to transmit 100 kW at a voltage of 1000 V AC for a distance of 50 m. This cable would have

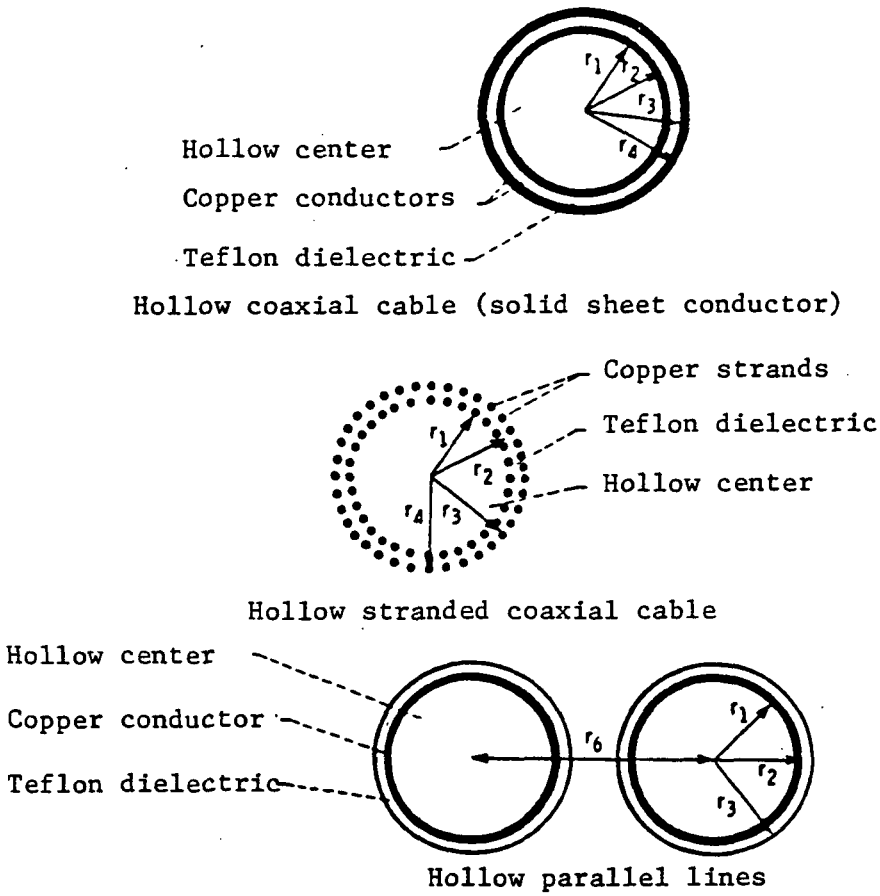

(a) Configurations investigated.

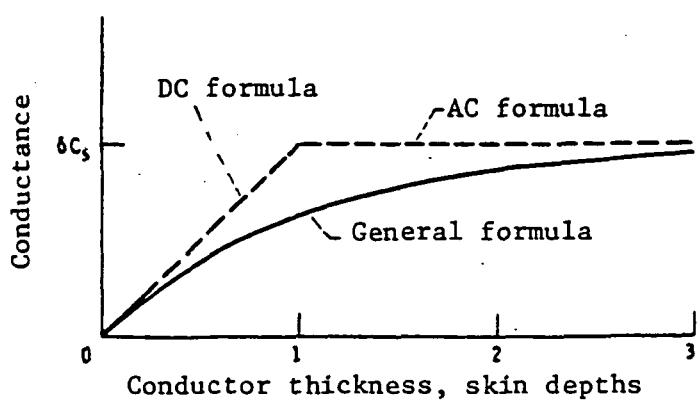

(b) Conductance versus conductor thickness.

FIGURE 2.1: Hollow Configurations Investigated by Previous Workers (Reference 1).

a power loss of 1900 W, an inductance of 1.45 μH and a capacitance of 0.07 μF. Reference 1 could be used to determine characteristics of other cable sizes.

There are some disadvantages attached with the hollow coaxial configurations:

(a) With solid conductor, the cable is rigid and extremely difficult to handle in practical applications.

(b) With stranded conductor, the inner conductor may buckle under inward radial electromagnetic force . A support structure in the center can prevent such collapse, but would add weight.

(c) The central hollow space adds unnecessary volume.

The third configuration, the hollow round parallel lines, have all the above disadvantages, plus two more. It has much higher reactance and occupies almost double the volume compared to the coaxial configurations.

The fourth configuration, namely the two parallel Litz straps (Figure 2.2) appears to be a more attractive configuration, and has been thoroughly investigated in this section. This configuration, having longer leakage flux path, produces less magnetic flux per ampere, and hence offers a lower reactance design compared to round parallel lines. The strap configuration has two parameters, a and d, which can be conveniently changed to meet the specified reactance. This configuration also appears to be easy to manufacture and install on site.

From thermal viewpoint, the flat straps provide more heat dissipation area. Dielectrically, by rounding the strip edges, we can achieve more or less a uniform field pattern between the two straps. Thus, from all major design considerations, flat strap configuration appears to be more favorable for meeting the objectives of the project. It is therefore evaluated as a serious condidate to compete with the first three options.

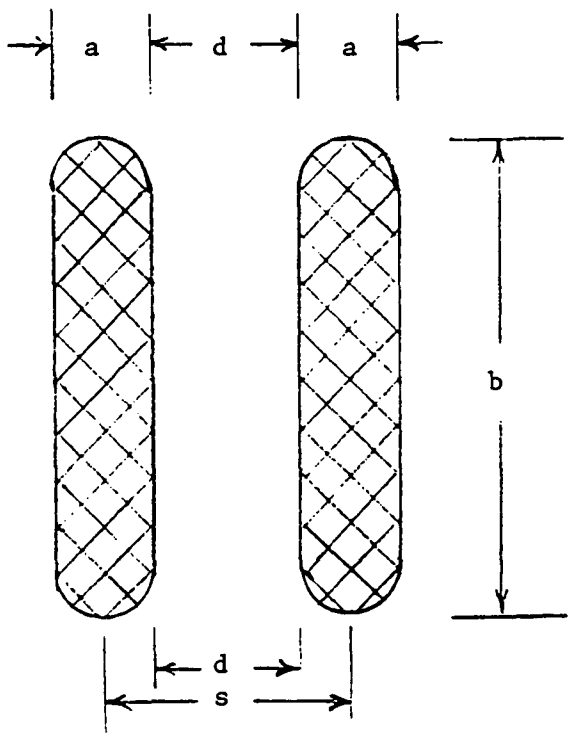

FIGURE 2.2: Two Parallel Litz Strap Lines.
It offers longer flux-leakage path and hence
lower inductance.

2.2 PARAMETERS OF HOLLOW CONFIGURATIONS

The design parameters of the first three alternative configurations (referred to as hollow lines from now on in this report) are fully documented in Reference 1, which we will refer to for further details.

2.3 PARAMETERS OF TWO PARALLEL LITZ STRAPS

Three basic circuit parameters required for the proposed design are series resistance R to calculate the I^2R losses, series inductance L to calculate the reactive voltage drop and line-to-line capacitance C to calculate the charging current. Other constants, such as capacitance and conductance to ground may also be required for detailed calculations, but are not considered in the present study.

2.3.1 FACTORS INFLUENCING 2-STRAP LINE PARAMETERS

The major influence factor on the line parameters is, of course, the geometrical spacings, which will be considered in detail in latter sections. Before that, the effects of the following factors are considered below:

a. Effect of stranding and spiraling
b. Skin effect
c. Proximity effect

2.3.2 EFFECT OF STRANDING AND SPIRALING

Because numerous thin and completely transposed strands are to be used in the proposed line, the current can be assumed to be uniformly distributed for inductance and resistance calculations, except for small eddy loss corrections as discussed in the next section. The capacitance of a stranded line is very nearly equal to that of a solid conductor having the same periphery, and needs no correction.

As for the effect of spiraling, the resistance would be higher due to longer strand length required to cover the given line length. This depends on the transposition pitch and is taken into account in calculating the resistance. On the

other hand, inductance depends only on the geometrical arrangement of the conductors. Since the current, on average, is parallel to the axis of the line, the line length, and not the strand length, is used in the inductance calculation. The same argument applies for the capacitance calculations.

The increase in length and hence resistance due to cabling (stranding and spiraling) is difficult to calculate from an analytical expression, as it depends on many manufacturing process variables. The easiest way of calculating this resistance increment factor K_c due to cabling is:

$$K_c = \frac{\text{Manufacturers catalog weight for given cable length}}{\text{Theoretically calculated weight based on straight length}}$$

2.3.3 SKIN EFFECT

Alternating currents at high frequencies concentrate near the outer surface (skin) of the conductor. The skin depth δ is given by

$$\delta = \sqrt{\frac{\rho}{\pi \mu f}} \tag{2.1}$$

where ρ = resistivity of the conductive material, Ωm
μ = permeability of the material, H/m
f = frequency, Hz

For copper, δ is 9 mm at 60 Hz and 0.5 mm at 20 kHz. In order to keep the eddy losses low, it is necessary to keep the wire diameter smaller than the skin thickness. Experience in high frequency design indicates that copper wires for 20 kHz application should be smaller than 0.5 mm (20 mils) in diameter. Clearly, the high current carrying capacity will require numerous strands of fine wires in parallel. To keep the eddy losses low in such bundles of wires, individual strands must be insulated and continuously transposed to occupy all the possible locations in the bundle along the full length of the transmission line. Cables of round shapes, such as Litz cables used in radio frequency transmission lines, can be

used. Alternatively, flat braided straps can also be used, as proposed for the present lines. Calculating the high frequency AC resistance is complex and involves ber and bei functions. Practical curves to find the ratio of effective AC resistance R to DC resistance R_o have been derived by Grover [3] and published by the U.S. Bureau of Standards for values of mr up to 100, where r = wire radius and m = $\sqrt{2}/\delta$. As seen in Figure 2.3, the R/R_o ratio becomes excessive beyond mr value of 2. This indicates that the strand's r/δ ratio should be smaller than $\sqrt{2}$ at a given frequency to keep the skin effect ratio $K_s = R/R_o$ less than 1.08.

The skin effect decreases the internal inductance of the conductor. However, in the stranded flat strap configuration, this decrease is negligible.

2.3.4 PROXIMITY EFFECT

Consider the case of two parallel cylindrical conductors in close proximity as shown in Figure 2.4. Here, the current density varies both radially and azimuthally. We may say that the current strive to occupy the two facing zones of the two conductors due to the proximity of each other.

The effect is still more striking in two parallel tubular conductors. If the tube wall is small, there is no noticeable radial variation in the current density, and there is, thus, no simple skin effect. The proximity effect, however, introduces an asymmetry in the peripheral distribution large enough to make R and L appreciably different from those calculated by assuming axisymmetrically uniform current distribution. It appears that this effect is ignored in calculating R and L of the hollow round parallel lines in Reference 1. If so, the actual R and L will be considerably higher than those calculated in that study. For the stranded flat strap configuration, because the strand size would be much smaller than the skin depth, the proximity effect on the line parameters will be small, as discussed below.

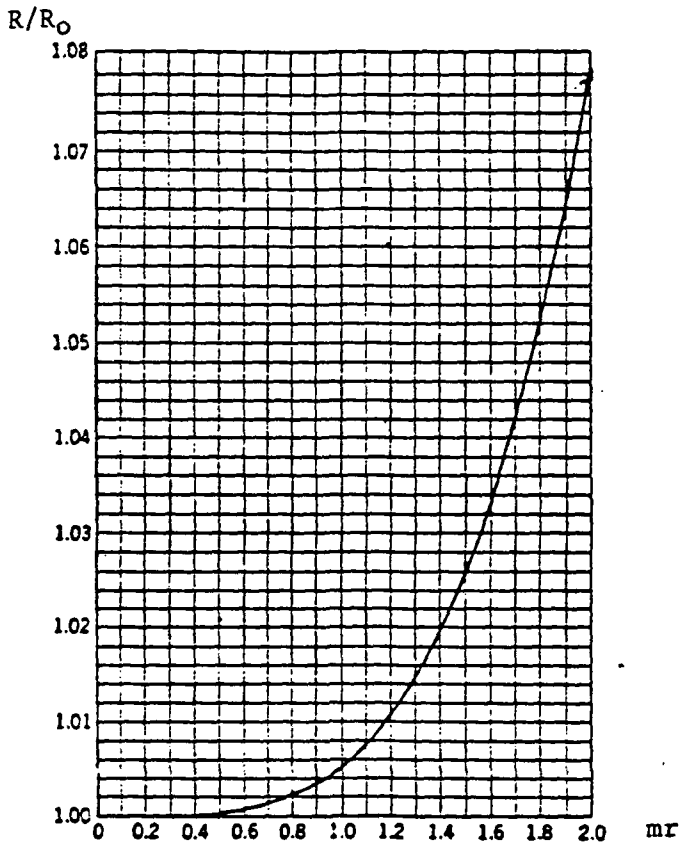

FIGURE 2.3: Ratio of AC to DC Resistance for a Round Wire in self magnetic field, where r is the wire radius and $m = \sqrt{2}/\delta$

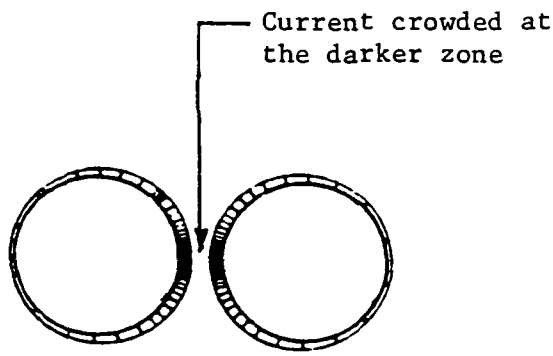

FIGURE 2.4: Characteristic of Proximity Effect on the peripheral distribution of current density. Notice that the current is crowded at the facing zones of the two conductors.

The equivalent of the above proximity effect in stranded cables is the eddy losses due to transverse flux perpendicular to the strand axis. If a single strand of diameter d_o is placed in transverse flux density B, the resulting eddy loss, as derived in Appendix A, is:

$$P_{et} = \frac{f^2 B^2 d_o^4}{\rho} \quad \text{watts/meter} \qquad (2.2)$$

The leakage (transverse) flux density in the flat strap configuration varies linearly from maximum at the inner faces to zero at the outer faces. The maximum flux density B_o is then:

$$B_o = \mu_o H_o = \mu_o \frac{I}{b} \quad \text{in SI units}$$

If there are N total number of strands, integrating individual strand losses and converting them into the ratio of AC to DC resistance, we obtained the following transverse eddy loss factor in Appendix A:

$$K_t = 1 + \frac{0.8\ f^2 N^2 d_o^6}{\rho^2 b^2 El2} \quad \text{in SI units} \qquad (2.3)$$

The conclusion of this subsection is that the basic R, L and C parameters of the stranded flat strap configuration can be calculated assuming uniform current distribution without significant loss of accuracy, except for a small skin effect and transverse flux eddy loss corrections in R. Accordingly, the R, L and C calculations of the stranded flat strap configuration follows.

2.3.5 RESISTANCE CALCULATION

If K_f = overall fill factor of conductor

$$= \frac{\text{conductor cross section}}{\text{total cross section}}$$

a,b,d = geometrical dimensions (Figure 2.2)

ρ = resistivity of the conductor

Subscript 1 refers to the parameter per meter of the lines.

Then, the DC resistance per meter loop of the cable (i.e. one meter lead and one meter return) is given by:

$$R_{dc1} = \frac{2\rho L}{A} = \frac{2\rho}{K_f ab} \quad \text{ohms/m loop} \qquad (2.4)$$

For copper at 20°C, ρ = 1.77 E-8 ohm m. At higher temperature T°C, it can be calculated by the following IEEE standard formula:

$$\frac{\rho_T}{\rho_{20}} = \frac{234.5 + T}{234.5 + 20} \qquad (2.5)$$

Now, recalling that K_c = cabling (stranding and spiraling) factor

K_s = skin effect eddy loss factor

K_t = proximity-effect (transverse flux) eddy loss factor

With all these factors multiplied, the total resistance of a cable is:

$$R_{ac1} = K_s K_t K_c R_{dc1} \quad \text{ohms/m loop} \qquad (2.6)$$

DC resistance increases with temperature, while K_s and K_t decreases with increasing temperature. For this reason,

it would be inaccurate to correct R_{ac} according to Equation (2.5). For large temperature deviations, R_{dc}, K_s and K_t should be separately corrected.

2.3.6 INDUCTANCE CALCULATION

The exact inductance calculation of this configuration is mathematically involved. The exact formula has been derived in the Bureau of Standards Bulletin, Vol. 3, No. 1, Pg. 6, as reproduced in graphical form in Figure 2.5. These curves are plotted at 60 Hz reactance per foot length one-way. However, since they neglect skin effect and assume uniform current distribution, reactance of high frequency stranded cables can be taken in the proportion of the frequencies as long as the current distribution is uniform, as in the present case. If the conductors were solid bus bars, instead of finely stranded straps, these curves would be invalid at higher frequencies.

Since width b of the straps is likely to be much larger than the strap thickness a and the insulation thickness d, the inductance of this configuration can be simply calculated by thick infinitely long solenoid (or transformer) type formula without significant loss of accuracy. Neglecting the fringing flux at the ends and the magnetomotive force consumed in the external return flux path, the inductance per meter length can be shown to be:

$$L_1 = \frac{\mu o}{b} \left(d + \frac{2a}{3}\right) \quad \text{H/m loop} \qquad (2.7)$$

This formula agrees well with Figure 2.5 at the lower end.

2.3.7 CAPACITANCE CALCULATIONS

Ignoring the fringing of the electrostatic field (Figure 2.6), the capacitance per meter loop of the line is given by the following approximate but simple flat electrodes formula:

ORIGINAL PAGE IS
OF POOR QUALITY

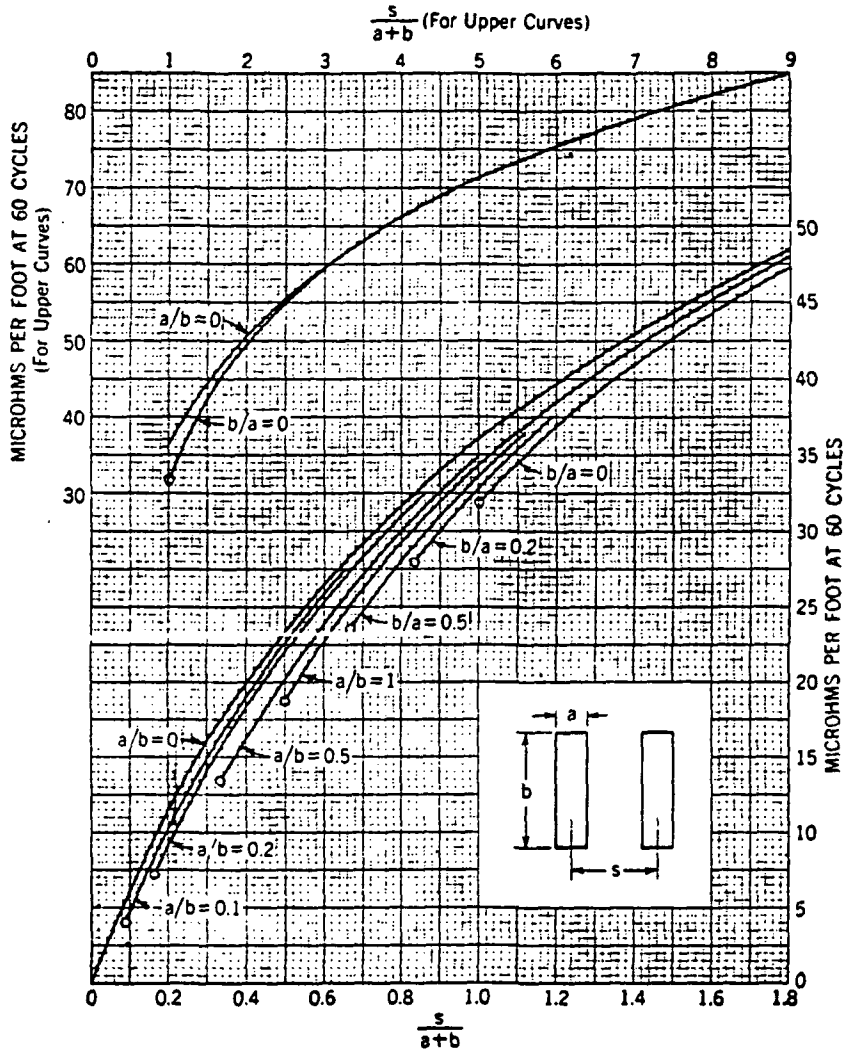

FIGURE 2.5: Reactance of Rectangular Flat Conductors at 60 Hz ($\mu\Omega$ per foot one-way). Source: Bureau of Standards.

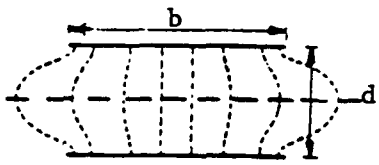

FIGURE 2.6: The Strap Lines as a Capacitor

$$C_1 = \frac{\varepsilon A}{d} = \frac{\varepsilon b}{d} \quad \text{F/meter loop} \tag{2.8}$$

where A = electrode area = b per meter length

ε = permittivity of dielectric between electrodes

d = separation between electrodes

The fringing (stray) field introduces significant complexity in the capacitance calculations. Maxwell took this into account by using the method of conformal transformation and derived the following accurate formula [4]:

$$C_1 = \varepsilon \left[\!\!\left[\frac{b}{d} + \frac{1}{\pi} \left[1 + \text{Ln} \left\{ \frac{\pi b}{d} + 1 + \text{Ln} \left(\frac{\pi b}{d} + 1 \right) \right\} \right] \right]\!\!\right] \tag{2.9}$$

The first term is the familiar expression for the ideal line without fringing, while the second term gives the edge correction. The formula is accurate within 0.3% for b=d and much better for larger b. It can, therefore, be considered exact for the present application.

The total capacitance for the 50-meter long line is $C = 50\ C_1$ and the total charging current at the receiving end at voltage V is:

$$I_c = VC\omega \text{ amps} \tag{2.10}$$

2.3.8 MECHANICAL FORCE CALCULATION

The force on two round thin parallel straight wires carrying currents I_1 and I_2, Ø degrees out of phase, distance s meters apart has been shown to be:

$$F' = \frac{2I_1 I_2 \cos Ø}{s} \quad \text{N/meter loop} \tag{2.11}$$

The force between two straps, each of cross section a x b, placed opposite each other at distance s, is given by:

$$F_1 = KF' \tag{2.12}$$

where K is the correction factor as plotted in Figure 2.7[5].

ORIGINAL PAGE IS
OF POOR QUALITY

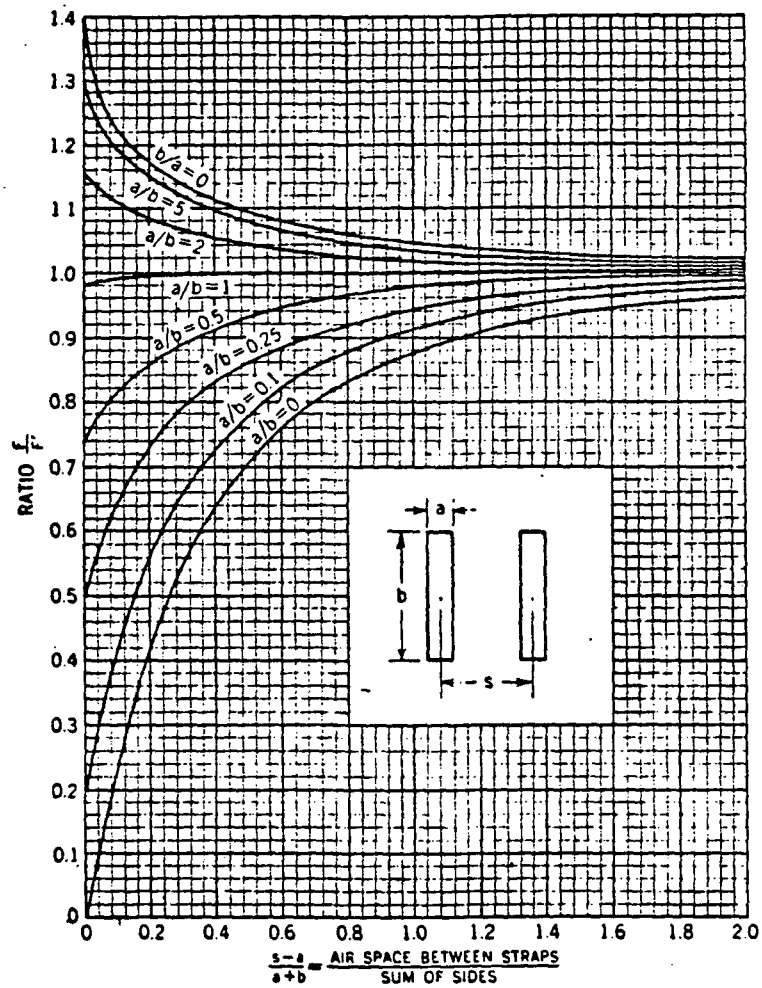

Repulsion between strap conductors.
F = repulsion between two equal long parallel straps.
F' = repulsion between two long parallel straight wires.

$$= 5.40 \frac{I_1 I_2 \cos\theta}{s} 10^{-7} \text{ pounds per foot of circuit,}$$

where θ is the phase angle between I_1 and I_2 which are in amperes, and where s is the axial spacing in inches. F and F' are average forces.

FIGURE 2.7: Force between Rectangular Flat Conductors for different geometrical spacings

The above force, in steady state conditions, will have twice the basic frequency, i.e., 40 kHz. This, over a ten year period, will amount to 12.6×10^{12} cycles of tensile stresses. The conventional fatigue studies are done over a few million cycles. Since the present requirement is much beyond this conventional range, the tensile stresses in the major insulation have to be kept exceptionally low. Thermal aging adds into the complexity in evaluating the electrical degradation of the insulation. McNutt and Patel [6] have studied the combined effects of mechanical stresses and thermal degradation on one class of insulating materials. Such considerations, based on experience and judgement, can be applied for designing the system to endure the mechanical fatigue over the functional life of about ten years at 20 kHz.

2.3.9 MASS CALCULATION

If γ is the conductor mass density, K_c and K_f are the cabling and fill factor, and a x b are the cross sectional dimensions, the mass per meter loop of the line is simply given by:

$$M_l = 2K_cK_fab\gamma \quad \text{kg/m loop} \tag{2.13}$$

3.0 PARAMETRIC STUDY ON INITIAL CONFIGURATIONS

The effects of various design parameters on the initial four configurations of the transmission lines are discussed in this section in order to establish their trade-off values.

3.1 HOLLOW CONFIGURATIONS

The parametric studies on these configurations have been extensively made by Jefferies, Renz and others [1,2]. To avoid duplication, this NASA study is not reproduced here. However, its results are used to derive the optimum designs for each of the three hollow configurations depicted in Figure 2.1. These designs are summarized in rows 3 to 7 of Table 3.1.

3.2 TWO PARALLEL LITZ STRAPS

The equations developed in Section 2.3 are simple enough for a hand calculator. However, for performing numerous calculations for a parametric study, a computer program was prepared. The details of this program are given in Appendix B. The AC resistance, inductance, capacitance and weight of the lines with two parallel Litz straps were calculated for both copper and aluminum conductors. The insulation mass density of 1340 kg/m^3 (that of PVC) has been assumed in the weight calculations. Computations were made for major insulation thickness d ranging from 1 to 3 mm, strap thickness a from 1 to 4 mm, and strap width b from 50 to 100 mm. The results are summarized in Figures B.1 to B.5 of Appendix B. From these curves, three alternative designs with copper are given in rows 8 to 10 of Table 3.1. Similar designs with aluminum conductor are given in rows 11 to 13.

TABLE 3.1: COMPARISON OF VARIOUS CONFIGURATIONS FOR
100 kW, 1000 V, 100 A, 20 kHz, 50 m LONG TRANSMISSION LINE

Sr.	No.	CONFIGURATION	RmΩ	L μH	C μF	MASS kg	LOSS w	IX v	VOLUME m^3	DIELECTRIC STRESS E V/mm	DIELECTRIC STRESS E V/mil	TEMP RISE °C
*1	1	Goals per meter	1mΩ	.08μH	-	.01 kg/kW	.01%/m	1 v/m	-	-	-	-
	2	Goals for 50 m cable	50mΩ	4μH	-	50 kg	500 w	50 v	-	-	-	-
*2 Cu	3	Hollow copper coaxial with Ri = 32 mm	50	0.2	0.41	60	500	2.5	.171	2000	50	23 *6
	4	Hollow stranded coaxial with Ri = 41 mm	50	0.2	0.52	71	500	2.5	.277	2000	50	20 *6
	5	Hollow parallels with Ri = 33 mm	50	5.5 *7	.006	61	500	68.8	.363	1000	25	10 *6
*3 Cu	6	Hollow copper coaxial with Ri = 36 mm	50	0.15	-	84	500	1.88	.215	2000	50	-
	7	Hollow copper coaxial with Ri = 30 mm. From Table I of Ref. 2 *8	51.4	0.217	.376	-	514	2.71	.151	-	-	-
*4 Cu	8	2 Litz copper straps a=2,b=65,d=1 mm *9	50	2.2	.078	67	500	27.5	.023	1000	25	-
	9	2 Litz copper straps a=2,b=50,d=1 mm	66	2.9	.06	51	660	36.3	.018	1000	25	-
	10	2 Litz copper straps a=3,b=50,d=1 mm	47	3.7	.06	71	470	46.3	.023	1000	25	-
*5 Al	11	2 Litz Al. straps a=3,b=72,d=1 mm	50	2.6	.087	43	430	32.5	.032	1000	25	-
	12	2 Litz Al. straps a=3,b=83,d=1 mm	43	2.3	.100	50	500	28.8	.037	1000	25	-
	13	2 Litz Al. straps *10 a=4,b=60,d=1 mm	46	3.75	.072	45	450	46.9	.033	1000	25	-

*See next page for notes and stars and Figures 2.1 and 2.2 for dimensions.

NOTES & STARS FOR TABLE 3.1

NOTES:

- o Losses taken as the most severe constraint. That is, most designs start with meeting the losses.
- o All hollow designs are with 0.2 mm (8 mil) copper conductor and 0.5 mm (20 mil) teflon dielectric.
- o Center support mass not included in the hollow designs.
- o Two parallel Litz straps designs include insulation mass and use conductor fill factor of 0.4.
- o Hollow designs used ρ = 1.77E-8 and parallel Litz strap designs used ρ = 2.2E-8 as the copper resistivity. The former is at 40°C temperature and the latter is at 100°C.

STARS:

- * 1 Goals set by NASA for the present contract work.
- * 2 Designs from Ref. 1 (shield not included).
- * 3 Design from Ref. 2 (shield included).
- * 4 Design from Figure B.1 of this report.
- * 5 Design from Figure B.2 of this report.
- * 6 Rise across one dielectric layer due to radiation.
- * 7 Conductors 1 mm apart.
- * 8 After correcting an apparent misprint in Ref. 2.
- * 9 See Figures 2.1 and 2.2 for dimensions.
- *10 From design considerations alone, this is the best of all configurations considered in this table, meeting all the goals with 10% extra margin. Further improvements with 3-strap configuration are discussed in Section 4.0.

3.3 PARAMETER OPTIMIZATION IN 2-STRAP CABLE

As will be discussed in Section 5.2, there is no theoretical scope for optimizing the conductor Loss x Mass product, which remains constant for a given material. If both loss and mass are evaluated with equal importance by NASA, one can factor the two in any combination. If one is more important than the other, than the important attribute can be favorably factored in the final design.

However, an optimization opportunity exists in the insulation weight. For minimum cable weight, the insulation should be as thin as possible while keeping the cable corona-free. There is, however, another limitation in making the insulation thin. The extrusion process of applying the insulation on the straps requires certain minimum thickness to avoid tearing of the insulation during the manufacturing process. Experience indicates that a minimum of 25 to 30 mils insulation thickness is required for a tear-free extrusion.

Once the insulation thickness is fixed, the total conductor and insulation mass can be minimized by selecting the minimum strap width b while choosing the strap thickness a to meet the losses and the reactance. Since the loss depends on the product a x b, for a fixed loss, i.e. for a fixed a x b, the reactance increases with increasing a and decreasing b, while the mass of insulation of given thickness decreases with increasing a, as there is now less insulation thickness in proportion to the strap thickness. For a given loss and insulation thickness, the cable weight can, therefore, be minimized by decreasing b and increasing a until the reactance increases to its permissible limit. This is done in row 13 of Table 3.1 for aluminum straps, leaving about 6 to 10% margin in all the parameters, i.e. loss, mass and the reactance. The same optimization logic also applies for copper straps.

3.4 DISCUSSION ON INITIAL CONFIGURATION DESIGNS

Table 3.1 indicates that in the first group of four alternative configurations, the hollow copper coaxial lines

meet the goals on losses and reactance, but not the mass, and occupy large volume. The hollow parallel line meets only the loss goal, but misses both the reactance and the mass goals, and occupies much larger volume.

Two parallel Litz straps with copper conductor can meet the reactance goal and either loss or mass goal, but not both exactly. This is also true for the hollow coaxial configurations with copper conductor. The aluminum straps, on the other hand, meet all the goals comfortably, leaving 6 to 10% margin for final design adjustments. The parallel straps occupy the least volume.

Thus, among the four configurations evaluated in this phase, the parallel Litz straps appear to be the best, the hollow coaxials rank next best and the hollow parallel ranks the last.

From only the design point of view, the parallel straps configuration with aluminum strands is the most optimum configuration. However, as discussed in Section 7.0, aluminum poses difficulties in manufacturing and joining. The flat straps with copper strands offer an optimum configuration from both the design and manufacturing considerations.

4.0 THREE PARALLEL LITZ STRAP CONFIGURATION

4.1 3-STRAP CONFIGURATION ANALYSIS

The design and manufacturing considerations studied so far led us to recommend the two parallel Litz straps configuration. The subsequent study showed that the three parallel straps configuration results in even better design, in which the middle strap carries full rated current at the rated voltage, and each of the grounded outer straps carry one-half of the return current. Such a birfurcated design makes the cable virtually concentric in the electromagnetic sense, as evolutionary shown in Figure 4.1. The advantages of the three-strap over the two-strap design are as follows:

1) The magnetic flux density B in the major insulation region is now one-half. The reactance is a measure of the magnetic energy $B^2/2\mu_0$ stored in the configuration space. Since there are now two major insulation gaps, the net effect is to reduce the cable reactance to less than

$$2 \times (B/2)^2/B^2 = 1/2.$$

2) The magnetic flux in the two major insulation regions is now in a push-pull mode, thus containing the flux within the cable volume itself. This significantly reduces the EMI shield requirement. The main flux in the two-strap design, on the other hand, returns external to the cable (like an air-cored solenoid).

3) Due to one-half B, the eddy losses by the transverse flux reduces to one-quarter. This is only a minor gain, as the eddy losses are already kept small by using thin strands. However, this may allow thicker strands if desired for other reasons.

4) The repulsive force between the central strap and the outer straps carrying half the current now reduces to one-fourth. Again, this gain is not much useful, as the forces are already low.

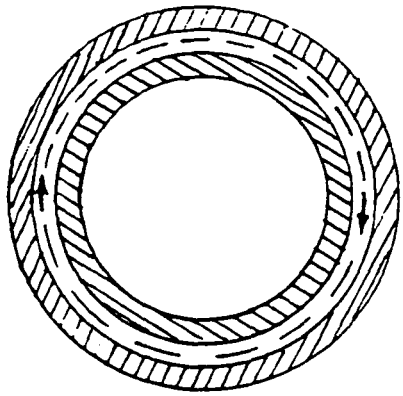

(a) Take a Hollow
Coaxial Cable

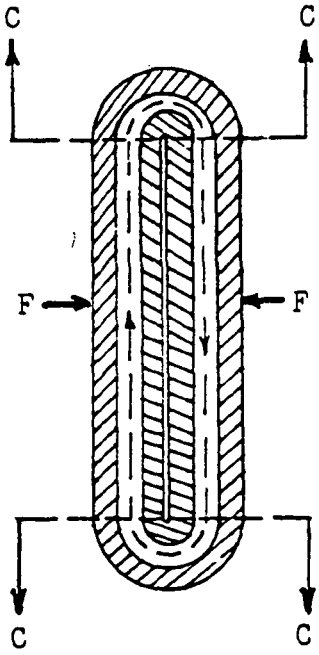

(b) Squash it and cut
top and bottom ends

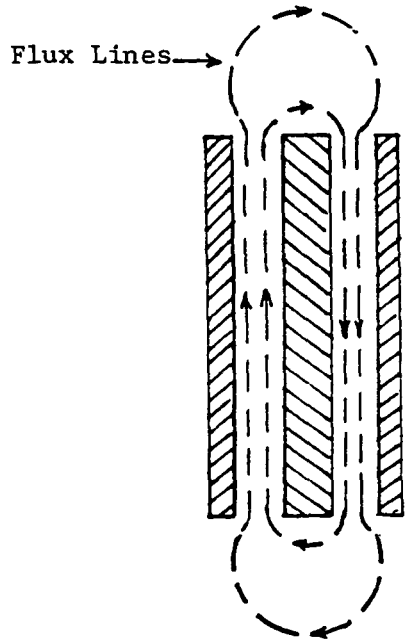

(c) Remainder, which can be
made with 3 parallel straps

FIGURE 4.1: Three Parallel Straps Configuration.
See how it evolves to be virtually concentric, while
keeping the flexibility in manufacturing and handling.

5) The flexibility in manufacturing, handling, splicing and terminating are still maintained.

6) Thermally, the three-strap configuration is not much different than the two-strap configuration. Due to large flat surfaces available for cooling, the operating temperatures are anticipated to be much below the material limits.

Among the above gains, the substantial reduction in the reactance is viewed most favorably for the overall power system management in large space stations.

4.2 SHIELDING AND END-INSULATION CONSIDERATIONS

Since the main magnetic flux in this configuration is internally contained, the EMI at some distance away from the cable would be negligible. However, there exists some fringing flux at the ends, as shown in Figure 4.1(C). The extent of this flux is difficult to calculate by hand. To obtain a quantitative picture of this fringe region, the in-house literature was searched. A set of three-phase bus bars at the instant when the middle bus carries 1.0 per unit and the outer buses -0.5 per unit currents closely resembled the virtually concentric configuration under present study. A finite-element magnetostatic flux plot of the three-phase buses is depicted in Figure 4.2. Notice the internal containment of the main flux. Also notice that most of the fringing flux at the ends returns within about one-half the distance between the outer buses.

Since the EMI shield has to now contain only the fringing flux, as compared to the main flux in the two-strap configuration, the shield requirement in the three-strap design is significantly lower.

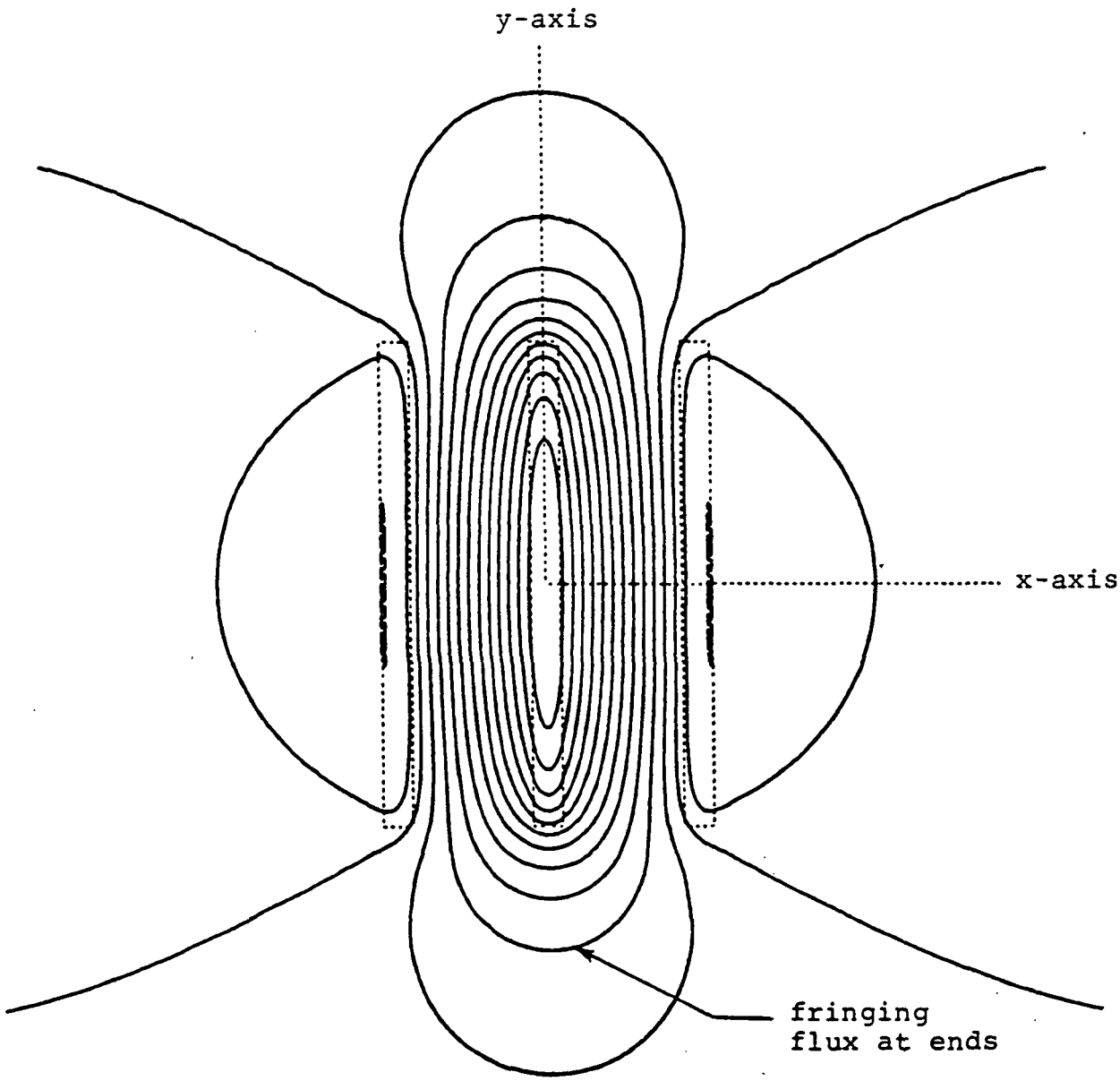

FIGURE 4.2: Finite-element flux plot of 3-phase bus bars with central bus carrying peak current. Notice the internal containment of the main flux and that most of the fringing flux at ends returns within about one-half the distance between the outer buses. The dotted lines are the bus bars.

The three-strap design can be further improved by indenting the middle strap (i.e. stepping it down) with respect to the outer straps as shown in Figure 4.3. This has two advantages:

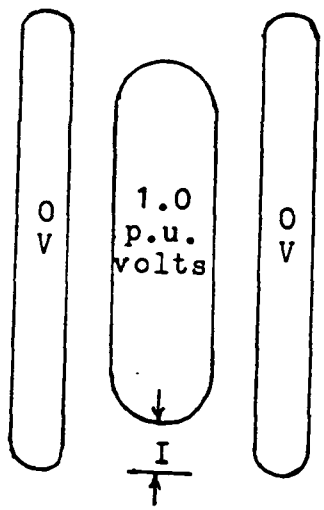

Figure 4.3: Indentation of the middle strap improves EMI and end-insulation design.

- The end flux is pulled inward, thus further reducing the shield requirement.
- The additional end-insulation for the middle strap operating at full line voltage would be adequate to withstand nonuniform dielectric stress even without an electrostatic shield over the cable.

4.3 COMPARISON BETWEEN 2-STRAP AND 3-STRAP CONFIGURATIONS

Table 4.1 compares a 50 mm (2 inch) wide 2-strap and 3-strap designs for 1000 V, 100 A ratings. Clearly, the three-strap configuration is superior with respect to the inductance, tensile stress and EMI shield requirement points of view,

TABLE 4.1

Comparison between 2-strap and 3-strap 1000 V, 100 A cable designs. The latter has less than one-half the inductance, double the capacitance and the same resistance, mass and volume.

Configuration	R mΩ	L μH	C μF	Mass kg	Volume m^3	Volts/mil	Tensile Stress Relative	Shield Requirement
Goals for 50 m cable	50	4	--	50	--	--	--	--
Two Litz Straps with a=3, b=50, d=1 mm	47	3.7	.06	71	.023	25	100	Yes
Virtually concentric Three straps Indented a=1.5,3.0,1.5 b=50, d=1 mm	47	1.5	.12	71	.023	25	25	Much reduced

while comparable with the two-strap design in all other major considerations. The 3-strap configuration is, therefore, selected as the final configuration.

4.4 DESIGN OPTIMIZATION IN 3-STRAP CONFIGURATION

Once the 3-strap configuration had been selected as the most optimum configuration, the design calculations were made for optimizing the line resistance, inductance and mass of the 3-strap design. The general optimization guidelines discussed in Section 3.3 for the 2-strap configuration also apply for the 3-strap configuration. That is, for a given cross-section of the straps (i.e. for a given resistance) and a given insulation thickness:

- Wider straps result in lower inductance and higher capacitance.
- Narrower straps result in higher inductance and lower insulation mass.
- The loss x mass product of the conductor remains constant irrespective of the strap width.

Within these guidelines and the 2-strap parametric calculations reported earlier, an optimum design for the initially specified 1000 V, 100 A line is depicted in Figure 4.4. Notice that the aspect ratio of this cable is 2/0.39 = 5.1. For adequate flexibility in handling such a cable, the aspect ratio of at least 5 is considered desirable.

4.5 CABLE RATINGS REVISED

The process which is most likely to be used for manufacturing the line is the extrusion process, in which the conductor passes through a reservoir of insulating material under heat and pressure. The insulating material melts and gets deposited on the conductor continuously. This process requires an extrusion die which is the heart of the process.

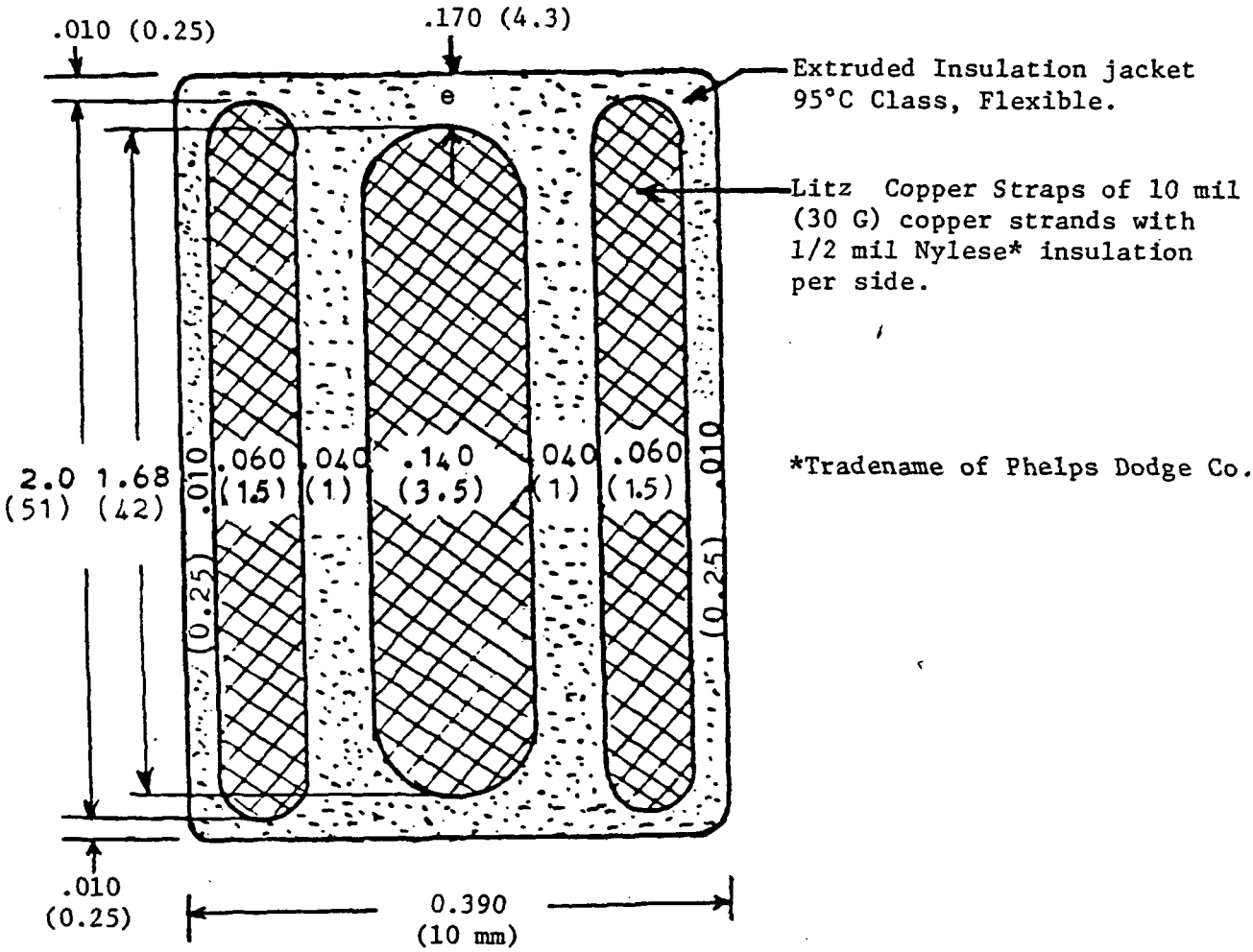

FIGURE 4.4: Three-Strap 2.0 inch wide design for 1000 V, 100 A cable, with aspect ratio of 5.1. All dimensions in inches (mm in the brackets)

Two leading cable manufacturers, New England Electric Wire and Cable Company, Lisbon, NH, and Brand Rex Industrial Cable Corporation, Willimantic, CT, showed interest in manufacturing such cable. However, they are presently limited in the extrusion width of 1.5 inches. A wider die has to be specially made and the wider extrusion process has to be tried out before making the cable. To avoid the excessive cost of special tooling for the first prototype, the 1000 V, 100 A cable was redesigned for 1.5 inch width. The aspect ratio of this design came to 3.2, which is much less than the desired value of at least 5. After reviewing the available funds, the aspect ratio constraints and the near term power requirement, the cable ratings were revised to 600 Vrms and 60 Arms. With 0.85 power factor load, this cable would deliver about 30 kW power.

The cable was redesigned for the new rating, as shown in Figure 4.5. Notice the aspect ratio of 38/7.1 = 5.4 which is mid-way between the desired range of 5 to 6.

It should be pointed out that the extrusion die width limitation is not of a fundamental nature. Wider dies are within the state of the extrusion art. They can be made and used when needed. Furthermore, the cable configuration and the design method are scalable to higher ratings with no technical barriers. Hence, the selected cable configuration has no fundamental design or manufacturing barriers for scaling to higher ratings.

4.6 LINE PARAMETERS OF THE SELECTED 3-STRAP DESIGN

The final design, as it was released for manufacture, is shown in Figure 4.5 with 20 mil major insulation. However, as mentioned in Section 15.0, it was necessary to increase the major insulation jacket thickness to 30 mils to avoid tearing in the insulation during extrusion. This increases the inductance by 19% (not 50%, as the copper-build

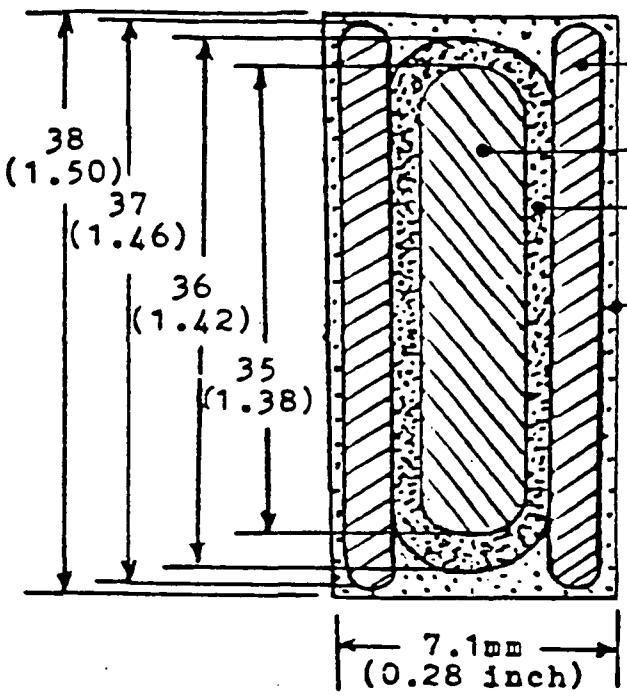

Outer straps 1.3 mm (.050 inch) thick
37 mm (1.46 inch) wide

Middle strap 3.0 mm (.120 inch) thick
35 mm (1.38 inch) wide

Middle insulation jacket, Polypropylene
0.5 mm (.020 inch) thick

Outer insulation jacket, PVC
0.25 mm (.020 inch) thick

No. of strands in the middle strap=1056 approximately (copper)

No. of strands in each outer strap=480 approximately (copper)

Strand Insulation: Solderable

Flexible (Aspect Ratio 5.4)

CALCULATED LINE PARAMETERS

Parameter	Unit	with major insulation 20 mils	30 mils
Resistance (100°C)	mΩ/m	1.043	1.043
Inductance	μH/m	.027	.032
Capacitance	μF/m	.003	.002
Mass	kg/m	1.102	1.103
Losses	Watts/m	3.755	3.755
IX drop	Volt/m	.203	.241
Charging current	Amp/m	.227	.151
Dielectric stresses	Volts/mil	30	20

FIGURE 4.5: Three-straps 1.5 inch wide design for 20 kHz, 600 V, 60 A cable. Aspect ratio 5.4.

Prepared By: Mikund R. Patel

ID No. MRP - 850731

Approved By: Mikund R. Patel

Date: July 31, 1985 Rev. 2

contributes more in the inductance than the major insulation gap). The table in Figure 4.5 summarizes the line parameters of the selected design with both 20 mil and 30 mil insulation, everything else being the same.

5.0 MATERIAL SELECTION

5.1 CONDUCTOR MATERIALS

Conductor materials that may be used are listed in Table 5.1. For a conceptual optimization, consider the following:

$$\text{Loss} = I^2R = I^2\rho L/A$$

and

$$\text{Mass} = \gamma AL$$

where I = Line current

L, A = length and cross sectional area of the line

ρ, γ = resistivity and mass density of the conductor material

$$\therefore \quad \text{Loss} \times \text{Mass} = \rho\gamma I^2L^2 \qquad (5.1)$$

Taking the product L x M (Loss x Mass) as an indicative figure of demerit, it can be minimized for given I and L by minimizing the product $\rho \times \gamma$. Table 5.1 shows that the optimum materials in this respect are sodium and lithium. These materials, however, are difficult to fabricate and require special storage. The next optimum material is aluminum, which is widely used as an electrical conductor. However, it is difficult to join. Moreover, its low ductility makes it difficult to draw in fine strands. The next optimum common conductor is copper. Copper is much heavier than aluminum but is much easier to join and draw in fine strands. Thus, from these considerations, aluminum and copper emerge as the potential candidates for the proposed lines. Aluminum offers low weight, while copper offers better joints. Both aluminum and copper have been considered in the parametric study in Section 3.0. Their electrical and mechanical properties are given in Table 5.2.

TABLE 5.1: ALTERNATIVE CONDUCTOR MATERIALS

Material	Resistivity, Micro Ohm-cm (20°C)	Density g/cm^3 (20°C)	Resistivity x Density (20°C)
Aluminum	2.828	2.7	7.64
Beryllium	5.9	1.82	10.73
Copper (annealed)	1.724	8.89	15.32
Lithium	8.55	0.54	4.62
Magnesium	4.6	1.74	8.00
Silver	1.629	10.5	17.10
Sodium	4.3	0.97	4.17

TABLE 5.2

ELECTRICAL AND MECHANICAL PROPERTIES
OF COMMON CONDUCTORS

Material	Density kg/m^3	Resistivity $\mu\Omega m$ (at 100°C)	Thermal Conductivity w/(m°C)	Young's Modulus psi	Tensile Strength psi
Copper	8640	.022	387	15×10^6	30,000
Aluminum	2700	.0364	219	10×10^6	10,000

5.2 INHERENT MATERIAL LIMITATIONS ON LOSS X MASS PRODUCT

Ignoring the insulation weight for the time being, we now derive the inherent material limitations on the Loss x Mass product with copper and aluminum as the conducting materials. Using Equations (2.2), (2.4) and (2.5), the L X M product of 50-meter long line carrying 100 A current is:

$$LxM = 50\ I^2R_{acl}x50\ M_l = 50^2x100^2xK_sK_tK_c\ \frac{2\rho}{K_fab}\ x2K_cK_fab\gamma$$

$$= 100\ E6xK_sK_tK_c{}^2\rho\gamma \quad \text{watts.kg} \qquad (5.2)$$

Notice that this product is doubly sensitive to the cabling factor K_c as compared to the skin effect factor K_s and the transverse flux eddy loss factor K_t. Manufacturers' catalogs indicate that K_c for the present line would be about 1.15 and the calculations indicate K_s and K_t near unity. At 100°C, $\rho\gamma$ is 190 E-6 for copper and 98 E-6 for aluminum. Substituting these values in Equation (5.2), we get:

L x M = 25,128 watts.kg for copper, and
L x M = 12,961 watts.kg for aluminum.

These are the minimum theoretical L x M product values that can be achieved with these materials at 100°C, regardless of the configuration chosen.

The L x M product goal set for the 100 A line is 500 x 50 = 25,000 watts.kg, which is about the inherent material limitation of copper. Since the above values do not include the insulation weight, we can therefore say that the bare copper conductor's L x M product just nearly meets the goal. The mass of the most optimum design with any configuration with copper conductor will therefore exceed by the mass of the insulation and the shield.

On the other hand, the limiting L x M product for aluminum is 12,961, which is much below the goal of 25,000. Aluminum can, therefore, exceed the goal.

5.3 DIELECTRIC MATERIALS

Two kinds of insulating materials will be required, the major insulation to the ground and the minor inter-strand insulation.

5.3.1 STRAND INSULATION

A variety of film insulations on magnet wires is available in the market to meet different ANSI and military temperature requiements. For example, polyimide film is good for continuous service temperature of 220°C. However, one disadvantage of this wire lies in stripping the strands for joints at termination. This can be overcome by the use of Nylese (registered tradename of Phelps Dodge Copper Products Corporation) strand insulation which permits solder pot tinning when done with care. There are other types of solderable insulation available. Of these, Nylese has the highest temperature rating of 130°C. Such an insulation has been used by Hensen [7], along with degassed Urethane polymer potting, in manufacturing a 2.3 kW, 20 kHz power transformer for space applications.

5.3.2 MAJOR INSULATION

The major insulation between the straps should be as thin as possible for compact and light weight design and for low inductance. On the other hand, thin insulation raises the operating electrical stresses and the associated corona activity. Corona considerations are further discussed in Section 6.0.

Low dielectric loss factor is an important material property any major insulation in high frequency application must possess. The next section discusses some of the candidate materials for the major insulation in the cable under design.

5.4 LOW LOSS INSULATING MATERIAL

Polyvinyl Chloride (PVC) was initially proposed as the major insulating material due to its good extrudibility. With 0.01 loss factor, the dielectric loss calculated from Equation 5.1 in Section 5.5 was 175 watts in PVC in the 100 kW cable design, where the conductor losses were 470 watts. This dielectric loss being not acceptable, a new search for a low-loss insulating material was made. Table 5.3 contains the material properties, and Table 5.4 summarizes manufacturing aspects of the candidate materials. From these tables, it is seen that Teflon exhibits the least dielectric loss factor. However, it cannot be extruded over wide straps with the presently available manufacturing processes. The PVC and Silicone rubber exhibit high losses. This leaves two suitable candidates for the present application, namely, the Polypropylene and Polyethylene. At room temperature and 1 kHz, the latter has lower loss. However, the stability of this loss at the operating temperature and frequency is yet another factor which must be considered in the final design. The frequency dependence of the loss in Figure 5.1 shows that both the polyethylene and polypropylene are fairly stable between 1 kHz and 1 MHz frequencies. However, the temperature dependence of the loss in Figure 5.2 indicates that polypropylene is much stable with respect to temperature changes than polyethylene. From these points of view, polypropylene has been chosen for the major insulation over the middle strap.

For each class of polymer, there are usually hundreds of different grades available from different commercial suppliers, each exhibiting some differences in critical material properties. For this reason, a specific grade of polypropylene which meets the desired low loss requirement over the operating temperature and frequency range was searched from different manufacturers of primary cable insulation. The grade which was initially identified to meet the requirement

TABLE 5.3: PROPERTIES OF MAJOR ELECTRICAL INSULATING MATERIALS

PHYSICAL PROPERTIES	Plasticized Polyvinyl Choride	Poly-ethylene	Polypro-pylene	Polytetra-fluoroethy-lene (Teflon)	Silicone Rubber
Specific gravity	1.35	0.93	0.90	2.15	1.90
Tensile strength (psi)	1000-3000	1900-2600	3300	2500	4200
Elongation (%)	200-400	200	300	200-300	--
Abrasion resistance	Good	Good	--	Good	Poor
Cont. operating temp. °C	95°C	80°C	120°C	260°C	200°C
Melting temperature °C	200°C	120°C	200°C	330°C	>375°C
Flexibility at -180°C	Cracks	Cracks	Cracks	Good	Cracks
Flamability (in/min)	self-extinguishing	1	1	Nonflamable	10-80
Dielectric strength (v/mil) (short time)	1000	500	600	500	400
Dielectric constant	2.7	2.3	2.25	2.2	4.2
Dielectric loss factor at 1 kHz, 20°C	.004	.0002[1]	.0005[1] to	.00005[1]	.004
at 1 kHz, 100°C	--	--	.0018	--	--
at 20 kHz, 20°C	--	--	.0003	.00003[3]	--
at 20 kHz, 100°C	.010*	--	.0003[2]	.00003[3]	.010*

*Estimated

1. Machine Design, April 1985 issue (Ref. 9)
2. Mfrs. catalog of Hercules, Inc. (Table 5.5)
3. Electrical Insulation, Bradwell, IEE (Ref. 10)

TABLE 5.4: CANDIDATE INSULATING MATERIALS COMPARED FROM MANUFACTURING VIEWPOINTS

MANUFACTURING CONSIDERATIONS	Plasticized Polyvinyl Choride	Polyethylene	Polypro-pylene	Teflon	Silicone Rubber
Compatibility with strand insulation during extrusion process	Excellent	Good	Good	Will damage strand insulation	Will damage strand insulation
Extrudability	Excellent	Good	Good	Equipment not available for straps	Thick wall jacket difficult to cure
Dielectric losses	High	Low to Medium	Low	Lowest	High
Flexibility	Good	Good	Excellent	Excellent	Good

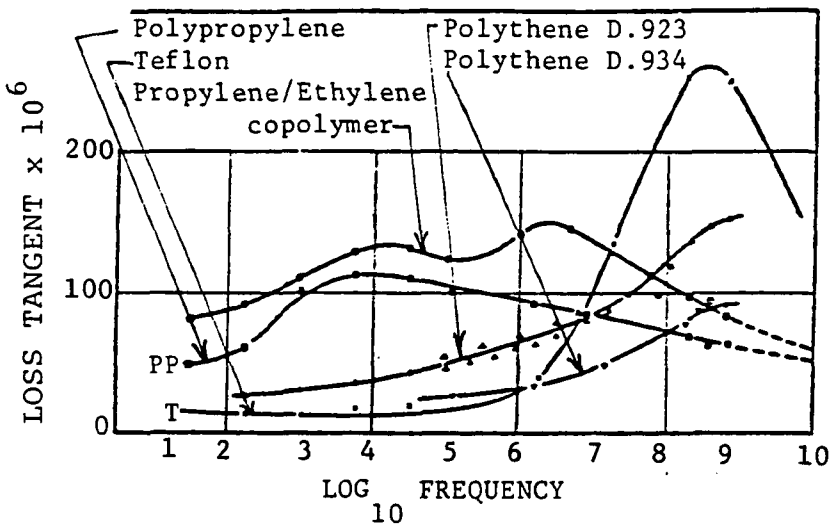

FIGURE 5.1: Dielectric Loss Tangent Vs. Frequency at room temperature for some low-loss insulating materials (Ref. 10). Polypropylene losses are fairly stable between 1 kHz and 1 MHz.

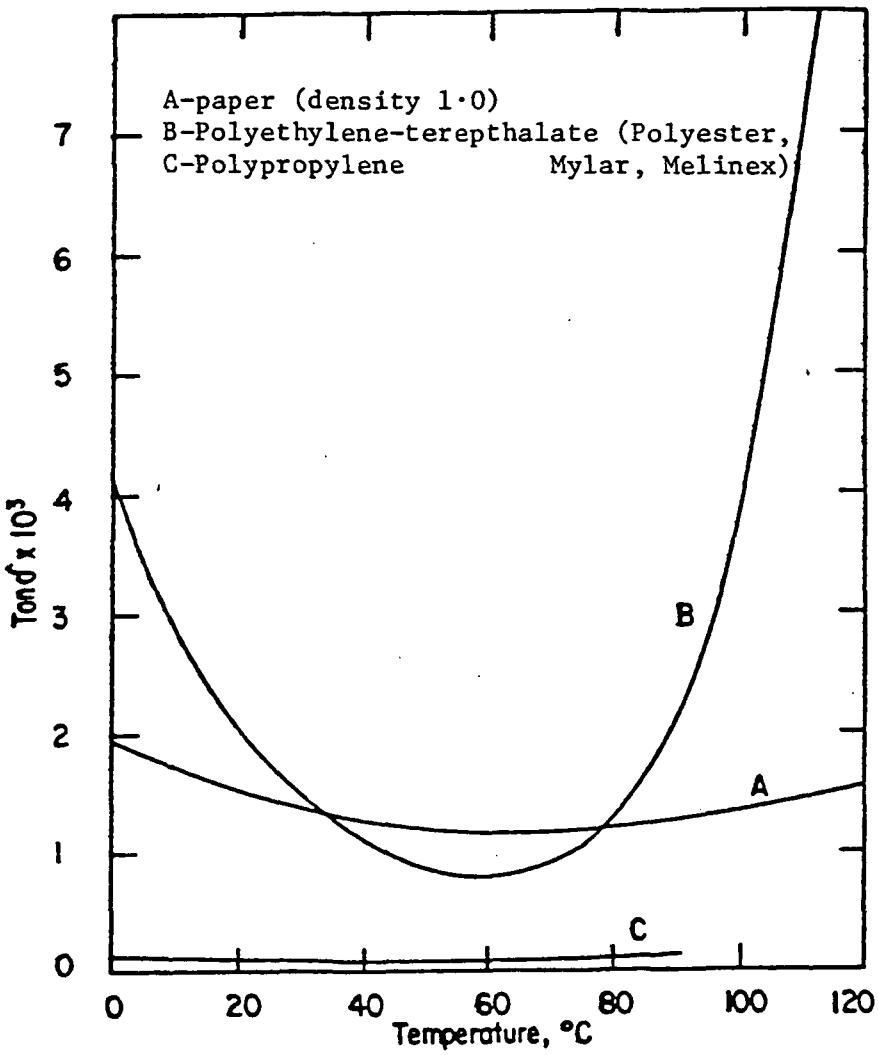

FIGURE 5.2: Dielectric Loss Tangent Vs. Temperature for some insulating materials (Ref. 10). Polypropylene losses are low and fairly stable between 0 and 90°C.

was Pro-Fax SE-023 of Hercules, Inc., Willmington, DE. This grade, however, was later found to be replaced with an improved version of SE-191. The manufacturer's catalog sheet on this insulation is depicted in Table 5.5. Compared to PVC, this material has three advantages:

- Low dielectric loss (the primary reason for choosing this as the major insulation).
- It has lower dielectric constant, 2.25 versus 2.7 for PVC. This results in lower dielectric stresses in voids in series with the solid insulation, thus raising the corona inception voltage of the cable.
- It has lower mass density, 0.904, versus 1.34 g/cm^3, thus resulting in lower insulation mass.

A disadvantage of Pro-Fax polypropylene is its lower short time dielectric puncture strength, 600 v/mil versus 1000 v/mil for PVC. However, this is of no real concern, since the operating dielectric stress in the major insulation is only 600 v/20 mils = 30 v/mil. The more likely insulation failure mode in the cable is due to corona degradation, as analyzed in detail in Section 6.0.

Since the outer jacket contributes heavily to the area-moment of inertia in flexural stiffness of the cable, a flexible material is desired for the outer jacket to keep the cable stiffness low. Polyvinyl chloride can be made more flexible than polypropylene by adding required plasticizer in it. For this reason, the PVC has been selected for the outer jacket. The outer jacket sees no dielectric stress, hence no losses, as the outer straps would be grounded in the normal operation.

TABLE 5.5

PROPERTIES OF THE SELECTED MAJOR INSULATING MATERIAL, PRO-FAX SE-191 PROPYLENE COPOLYMER OF HERCULES, INC.

Propylene Copolymer for Wire and Cable Primary Insulation

CHARACTER

Pro-fax SE-191 is an electrical-grade, high-impact-resistant propylene copolymer designed for maximum toughness at low temperatures, with minimum sacrifice in tensile strength, heat resistance, hardness, and processibility. It is especially suited for use in filled telephone cable because its unique stabilizer system resists extraction by petroleum-jelly-based filling compounds.

TYPICAL PROPERTIES

PROPERTY	TYPICAL PRO-FAX SE-191	TEST METHOD
Melt flow (condition L)	2.0	D 1238L 1_2 at 230°C
Density at 23°C, g/cm^3	0.900	D 792
Tensile strength at yield, psi (MPa) (0.075-in. specimen—D 1708)	3,350 (23.1)	D 638 2 in./min
Tensile elongation at break, % (0.075-in. specimen—D 1708)	300	D 638 2 in./min
Brittleness temperature, °C	−15	D 746
Environmental stress-crack resistance, hrs	>500 No failures	REA PE-210
Thermal stress-crack resistance, 100°C, hrs	>500 No failures	REA PE-210
Cu/Al dish stability, % change	<100	REA PE-210
Dielectric constant, 1 KHz 1 MHz	2.25 2.25	D 1531
Dissipation factor, 1 KHz 1 MHz	0.0003 0.0003	D 1531
DC resistivity, volume, ohm-cm	>1.0 × 10^{15}	D 257

5.5 DIELECTRIC LOSS CALCULATION

All insulating materials, when subjected to alternating dielectric stresses, produce internal heat at a rate

$$P_i = 2\pi f \varepsilon_0 \varepsilon_\ell E^2 \text{ watts/m}^3 \quad \text{or} \quad 2\pi f C_1 \tan\delta V^2 \text{ watts/m length} \qquad (5.1)$$

where E = dielectric stress Vrms/m; ε_0 = permittivity of free space; ε_ℓ and $\tan\delta$ = loss factor and loss tangent of the insulating material; f = frequency, Hz; V = rated rms voltage and C_1 = capacitance per meter length.

For the cable design of Figure 4.5, the dielectric stress in the major insulation is 600/.0005 = 1.2E6 v/m. For the chosen grade of polypropylene for this insulation, the loss factor ε_ℓ at 20 kHz and 100°C is 0.0003. The dielectric loss per cubic meter is then:

$$P_i = 2\pi \times 20{,}000 \times 8.85\text{E-}12 \times .0003 \times (1.2\text{E}6)^2$$
$$= 480 \text{ watts/m}^3.$$

The major insulation volume is

$$2 \times .0005 \times .036 = 36\text{E-}6 \text{ m}^3\text{/meter length of cable.}$$

$$\therefore \text{ Dielectric loss} = 480 \times 36\text{E-}6 = 0.017 \text{ w/m loop.}$$

For 50-meter long cable, this loss would be .017 x 50 = 0.85 watt, which is now negligible.

6.0 CORONA CONSIDERATIONS

6.1 CORONA INCEPTION VOLTAGE VS. MAXIMUM PERMISSIBLE VOID SIZE

A critical quantity needed for evaluating an insulation subject to corona is E_i, which is the partial discharge inception voltage stress. This can be obtained directly by a partial discharge inception measurement, from extrapolation of the volt-breakdown time curve, and from careful analysis of the voltage stress at a conductor edge or in a void if the necessary geometric parameters are known. The dielectric stress is εE in laminar voids and $3\varepsilon E/(1+2\varepsilon)$ for spherical voids, where the total void thickness is much smaller than the insulation thickness and E is the stress in solid insulation. Partial discharges occur in a void when the product of the pressure in the gas and the void thickness (electrode separation) exceeds the breakdown voltage according to the characteristic Paschen curve shown in Figure 6.1 [11]. It shows that the electrical strength of a gas decreases with pressure up to a certain value of pressure, below which the strength again rises as the pressure drops towards vacuum.

Since the laminar voids produce more stress concentration than the spherical voids, the former is assumed in the following analysis. If a laminar void of size d_o is developed between the middle and an outer strap due to any reason, the breakdown voltage across such a void will depend on the gas pressure in the void. Since this pressure may vary over a wide range in and around the spacecraft at different times of the journey, we shall use the minimum Paschen breakdown voltage in the calculations, which is about 297 V peak or 210 Vrms between copper electrodes.

There are now two dielectrics in series, a gap of laminar thickness d_o and the solid insulation of thickness d. If the dielectric stresses are E_o and E in the gap and the solid, respectively, the voltage across the copper straps would be $V = E_o d_o + Ed$. With the relative dielectric constant

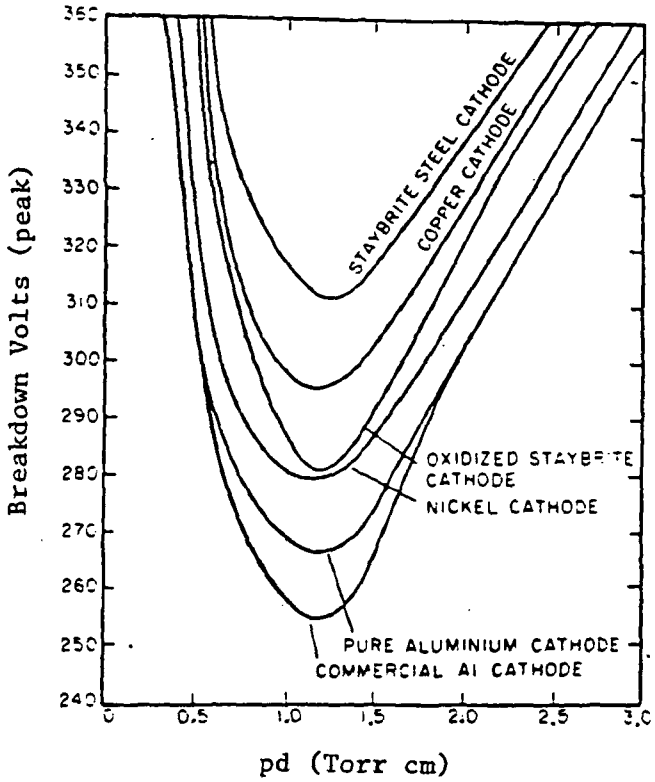

FIGURE 6.1: Paschen Curve, Electrical Breakdown Voltage versus pd for air (Reference 10).

of 2.25, the polypropylene insulation would take 1/2.25 times the gap stress, i.e. $E = E_o/2.25$. With d = 20 mils as an example, the above voltage then becomes

$$V = E_o d_o + \frac{E_o}{2.25} \times 20 = E_o d_o + 8.89 E_o = E_o d_o \left(1 + \frac{8.89}{d_o}\right)$$

where d_o is in mils. The product $E_o d_o$ is the voltage across gap, which has the minimum Paschen value of 210 Vrms. The corona would start at this voltage across the gap. The corona inception voltage of the cable is then

$$V_i = 210 \left(1 + \frac{8.89}{d_o}\right) \tag{6.1}$$

Equation (6.1) is plotted in Figure 6.2, which shows that it takes about 5 mils delamination gap for corona to start at 600 volts rms. This condition would not normally lead to an immediate failure, but eventually would under gradual corona degradation. Should the gap completely fail, the dielectric stress in the solid insulation would be 600/20 = 30 v/mil, which is two orders of magnitude lower than the solid insulation's short time breakdown strength.

As seen in Figure 6.2, the corona inception voltage decreases with increasing gap size and asymptotically approaches the minimum Paschen value of 210 Vrms. This is because the Paschen minimum is a constant value, although occurring at different pressures for different gap sizes. As the gap increases, the corona inception voltage across the gap remains constant at 210 V, while the voltage contribution of the decreasing dielectric stress in the solid insulation decreases.

It should be emphasized that the above corona inception voltage calculations are based on the worst possible combination of the gap pressure and the gap size (i.e. the minimum Paschen value). It is likely that there is always some pressure in the void due to continuous outgassing of the insulation.

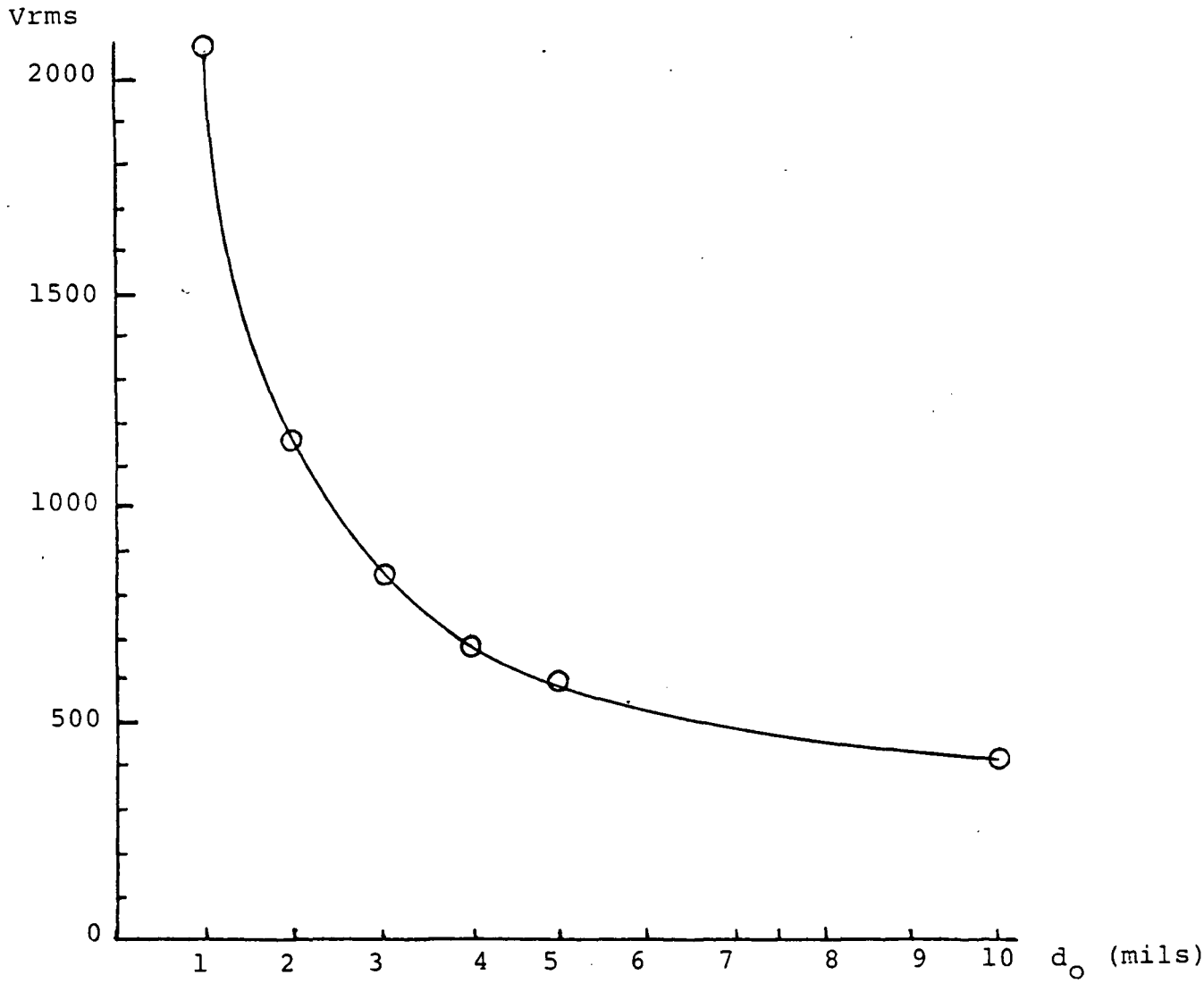

FIGURE 6.2: Corona Inception Voltage Vs. Laminar Void of size d_o
With increasing void size, the voltage asymptotically decreases to the Paschen minimum, which remains constant. With large voids, the solid insulation contributes less.

The location of the gap along the cable length also matters. If the gap develops at mid-length of the cable, outgassing may take a long time due to high gas-flow resistance offered by a long narrow duct.

For increased reliability, it may be desirable to bleed some gas (such as nitrogen) along the length of the cable insulation. This would assure the desired gas pressure to maintain the required dielectric strength of the cable. Another alternative is to use a suitable adhesive at the interface of the solid insulation and the conductor straps to avoid possible delamination. However, the conductor strands would now have strong bonds with the insulation, and may break while splicing. For easy preparation and high reliability of joints and terminations, it is desirable to have the insulation jackets peelable as in the present design. Furthermore, the planned manufacturing process requires anti-stick insulation for easy and smooth extrusion. Adding an adhesive at the conductor-insulation interface may require special process development before it can be tried on the present cable. Another reason for having anti-stick peelable insulation is the cable flexibility. The inter-woven strands in the straps bonded with the insulation jacket at the interface would significantly increase the rigidity of the cable. Based on the above considerations, we proceeded with the peelable insulation for the first prototype cable.

6.2 DIELECTRIC STRESS CONCENTRATION IN END INSULATION

In the hollow coaxial configurations, the dielectric stress between the conductors is nearly uniform, and so is in the parallel strap configuration. However, the stress at the ends of the parallel straps is not uniform. With respect to the grounded external shield, the rounded edge of the conductor makes a cylinder-to-plane configuration in which the dielectric stress gets concentrated near the conductor edge. If the

conductor radius is r and end distance e, as shown in the following figure, then the maximum dielectric stress, from the published literature [11], is very nearly

$$E_{max} = \frac{V}{e}\left(1 + 0.25\,\frac{e}{r}\right) \qquad (6.2)$$

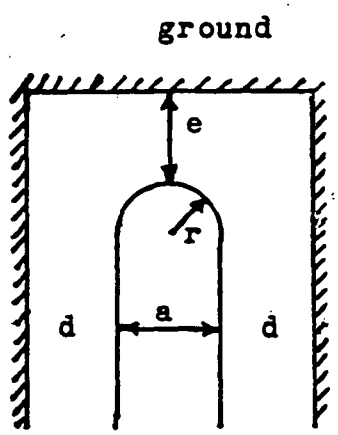

Dielectric Stress Concentration at Ends of Middle (Live) Strap

In Litz straps, ends are generally fully radiused, i.e. r = a/2. In that case, for the same dielectric stresses at the ends as in the main region, we must have:

$$\frac{V}{e}\left(1+0.25\,\frac{2e}{a}\right) = \frac{V}{d} \quad \text{or} \quad e = \frac{ad}{a-0.5d} \qquad (6.3)$$

For example, with a = 3 and d = 1 mm, e must be 1.2 mm, i.e. 20% more than d, the insulation thickness between the parallel straps. For smaller radius, say r = a/4, e = ad/(a-d)= 1.5, i.e. 50% more insulation at the ends. Recall that in Section 4.2, we proposed an indentation of the middle strap to reduce the fringing flux at the ends, which also serves the purpose of strengthening the end insulation as discussed in this section.

6.3 CORONA RESISTANCE

Among all the insulating materials, mica is the best known on earth for resisting high corona levels for a long time. Applying a mica tape next to the conductor strap was, therefore, considered at one time. However, this idea was dropped since the cable manufacturers considered it likely to cause difficulty in extruding a void-free insulation over the straps.

Further, a possibility of filling the inter-strand space was also considered to reduce corona and outgassing in vacuum. The filling can be achieved by pre-impregnating the straps with a suitable insulation. Such a filling, however, would hinder soldering operation on the straps at joints and terminations. Moreover, since the dielectric stresses within the straps are essentially zero, the inter-strand space does not need to be filled. The filling, therefore, was not recommended in the present design.

7.0 OTHER CONSIDERATIONS

7.1 ENVIRONMENTAL CONSIDERATIONS

The space environment is different than the earth environment in basically two ways, namely, vacuum and no gravity. The latter has no bearing in the present design considerations. Vacuum, on the other hand, influences the design in two major ways. First, the corona inception voltage of the cable, as determined by Paschen characteristic curve, will be much different. Second, the cooling must be done only by conduction and radiation as opposed to convection which is a primary cooling mode in electric power equipment on earth. These effects of vacuum on corona and cooling have been taken into account in the design.

7.2 MANUFACTURING AND FLEXIBILITY CONSIDERATIONS

As for manufacturing, the hollow coaxial cable appears to be the most difficult configuration. Manufacturing two concentric conductor tubes separated by an insulation tube is extremely difficult, as no clearance can be tolerated from the insulation point of view. Moreover, this configuration will be extremely rigid and almost impossible to handle during manufacturing and installation.

The hollow stranded configuration is somewhat less difficult to manufacture and less rigid. The strands can perhaps be spirally wound on the central supporting core. The core and the insulating tube, however, would make the cable rigid enough to cause handling difficulty.

The parallel Litz straps configuration appears to be easy to manufacture. The major insulation can be applied by established extrusion process. No special manufacturing equipment will be required, except a special set-up, as this configuration does not fall in the commercial catagory. The flexibility in handling and installation is a major attraction of this configuration.

As for the conductor material, aluminum offers significant weight advantage over copper. However, our discussion with Litz cable manufacturers indicated that aluminum, not being as ductile as copper, is extremely difficult to draw in thin strands and form Litz cables because of excessive breakage during the manufacturing process. None of the two leading Litz cable manufacturers make aluminum Litz cables, nor have shown interest in experimenting with it.

The above manufacturing considerations indicate that the parallel strap configuration is much easier to manufacture than the hollow configurations, and the copper strap is much easier to make than the aluminum strap with existing manufacturing technologies.

For applying the major insulation, two processes can be considered. First, the extrusion process in which the conductor passes through a reservoir of insulating material under heat and pressure. The insulating material melts and gets deposited on the conductor continuously. Another process is laminating in which the conductor straps, sandwiched between the insulation straps, pass through rollers under heat and pressure. Forming a good end insulation, however, appears to be difficult in this process. The extrusion process, therefore, was selected for manufacturing the present cable.

7.3 JOINTS AND TERMINATION CONSIDERATIONS

The hollow configuration would, in general, be difficult to join and terminate due to their concentric nature. The parallel Litz straps, on the other hand, are easy to join and terminate, as the two conductors can be sufficiently separated during splice and termination preparation, brought together again and insulated by applying insulation tape of required thickness (usually 50 to 100% more than the factory applied thickness).

For strand joints, aluminum cannot be soldered nor brazed. It can only be welded. Welding thin aluminum strands is

normally impractical, as they would quickly melt around the welding temperature. Copper strands, on the other hand, can be soldered or brazed, although brazing thin copper strands is also difficult. The solderability of copper strands is, therefore, a desirable attribute for joining strands during field installations and repairs.

The parallel straps can be easily terminated in conductor blades and bolted to other blades. Again, bolted joints on aluminum blades are known to loose pressure and cause arcing due to their higher mechanical creepage rate. Bolted joints on copper blades, on the other hand, have been successfully field proven in heavy power equipment over several decades.

For easy joint and terminations, it is desirable that the strand insulation be solderable without cleaning, or at least be chemically cleanable. Cleaning the strand insulation mechanically is impractical in this case with thousands of strands involved. As discussed earlier, Nylese (of Phelps Dodge) permits solder tinning.

Based on the above considerations, the copper conductor rates superior to aluminum and the parallel strap configuration rates superior to the hollow configurations from the joints and termination points of view.

8.0 ALL THE ALTERNATIVES COMPARED FOR FINAL SELECTION

Based on the configuration design studies, and the manufacturing, flexibility, joint and termination considerations presented in the previous sections, an overall comparison of various alternatives are summarized in Table 8.1. From Part A of the table, it is clear that the hollow parallel lines is the least desirable configuration. The hollow coaxial configurations have reasonably low loss, mass and reactance values. However, they occupy large volume, are difficult to manufacture, join and terminate and are extremely rigid in handling. Two parallel Litz straps, on the other hand, have all the desirable attributes, along with the excellent manufacturability, flexibility and ease of joints and terminations, while meeting the loss, mass and reactance goals. The 3-strap configuration offers less than half the inductance, while keeping all the desirable attributes of the 2-strap configuration, which make this configuration the most attractive.

Part B of the table indicates that aluminum strands excell over copper strands in loss and mass attributes, but suffer in manufacturability, joints and terminations. From the latter considerations, copper is the preferred conductor.

As for the major insulation, PVC has a high dielectric loss factor. Teflon has the lowest tangent δ, but was considered unextrudable over wide straps by the cable manufacturer. Polyethylene has low dielectric loss over a narrow temperature. Polypropylene has low loss over a wider temperature range, while being easily extrudable. The latter, therefore, has been selected in the final design.

As discussed later in Section 11.2, magnetic shielding is recommended, as it will be lightweight and less lossy than conductive shield.

Based on various considerations presented, the three Litz straps configuration with copper conductor and polypropylene as the major insulation was selected for the final design. The line parameters of the 600 V, 60 A, 3-strap design were given in Figure 4.5. The other design details now follow.

TABLE 8.1: OVERALL COMPARISON BETWEEN ALTERNATIVES

	Can Meet Loss, Mass and IX Goals	Total Volume	Manufac-turability	Flexi-bility	Joints & Terminations	Dielectric Loss Factor
A. CONFIGURATION						
Hollow solid coaxial	Good	Large	Poor	Extremely Poor	Difficult	---
Hollow stranded coaxial	Good	Large	Poor	Poor	Difficult	---
Hollow parallel lines	Poor	Very Large	Poor	Extremely Poor	Easy	---
Two Litz straps	Good	Small	Excellent	Excellent	Easy	---
Three Litz straps	Better	Small	Excellent	Excellent	Easy	---
B. CONDUCTOR						
Aluminum strands	Excellent	Large	Poor	Good	Poor	---
Copper strands	Good	Small	Excellent	Good	Excellent	---
C. MAJOR INSULATION						
PVC	---	---	Good	Good	---	High
Teflon	---	---	Poor on straps	Good	---	Lowest
Polyethylene	---	---	Good	Good	---	Low, unstable with temp.
Polypropylene	---	---	Good	Good	---	Low, more stable
D. SHIELD						
Conductive shield	Lossy, heavy	---	Good	Good	Good	---
Magnetic shield	Low loss, light	---	Good	Good	Good	---

9.0 THERMAL DESIGN

The cable may be cooled by radiation, conduction or both, and may be mounted in several alternative configurations. The temperature rises in three possible cooling configurations are calculated in this section for the 100 A, 1.5 inch wide cable with 20 mils major insulation and 10 mils outer jacket. The temperature rise with thicker insulation will be slightly higher.

9.1 RADIATION COOLING ALONE

The cable may be mounted in such a way that one face of it would radiate heat to the free space near absolute zero. In this configuration, the heat rejection would be primarily by radiation. To calculate the cable temperature rise under this condition, we assume 80°K reference temperature at the moment.

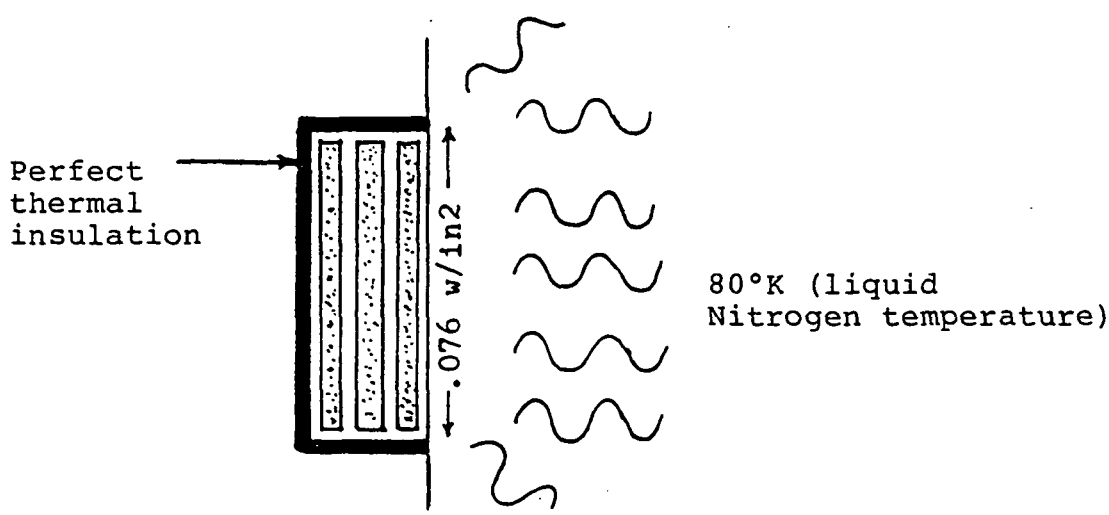

FIGURE 9.1: Radiation model under study with one face radiating to 80°K space and other three cable faces thermally insulated.

The heat radiated from a body at θ_1 temperature to the ambient at θ_0 is given by [12]:

$$q_r = \frac{3.66e}{1000} \left[\left(\frac{\theta_1}{100}\right)^4 - \left(\frac{\theta_0}{100}\right)^4 \right] \quad \text{watts/in}^2 \qquad (9.1)$$

where θ is in °K (°C + 273) and e is the emissivity of the radiating surface. Calculating the emissivity of a surface in free space, with simultaneous radiation and absorption of heat over a spectrum is involved. On earth, the emissivity of most industrial non-glossy gray-like paints ranges between 0.9 and 0.95. Jacob [11] shows that the emissivity of many electrical insulators exceeds 90%, and that almost all electrical non-conductors have the emissivity of at least 75%. For not knowing exactly the emissivity of the cable surface in free space, we calculate the cable temperature rise over a range of emissivity from 0.25 to 0.90.

The heat must be radiated from one side of the cable surface at the rate of 4.457 watts/meter or 4.457/(39.37 x 1.5) = .076 watts/in^2. Then, the calculations made with Equation (9.1) are summarized in Table 9.2 at the end of this section, which shows that the cable surface temperature is likely to be tens of degrees below zero degree centigrade. In this temperature, of course, the conduction temperature rise must be added to calculate the conductor temperature in the outer most strap. Since the insulation thickness and the heat flow (watts/in^2) are relatively small, the conduction temperature rise across the solid insulation is less than one degree, as calculated in the next section.

Thus, if the cable is radiating in free space, it will run quite cool.

With 0.75 emissivity, the cable surface temperature would be -40°C. At this temperature, the polypropylene and PVC insulation may develop cracks. This concern has to be addressed in the future if one face of the cable is exposed to free space in actual use.

9.2 CONDUCTION COOLING TO CONTINUOUS BASE PLATE

The cable may be mounted continuously on a base plate maintained at 60°C. In this configuration, the heat rejection would be by conduction alone.

The conduction cooling is governed by the basic equation $Q = -KA\Delta T/\Delta X$ where Q = heat flow rate (watts), K = thermal conductivity (w/m°C), A = area (m^2), ΔT = temperature difference (°C) across distance ΔX(m). This can be rearranged in the equivalent circuit form $\Delta T = Q.R$ where $R = \Delta X/KA$ is the thermal resistance (°C/W). The thermal conductivities of the cable materials are given in Table 9.1.

The loss in the cable is 4.457 w/m, 25% of which is in each of the two outer straps, uniformly distributed over the cable length. If the right hand surface of the cable in Figure 9.1 is in continuous contact with a 60°C base plate, then:

(a) The right hand outer PVC jacket conducts 100% of the heat through its thickness of 10 mils. The resulting temperature gradient across this thickness is therefore

$$4.457 = 0.15 \times 1 \times \frac{1.5}{39.37} \times \frac{\Delta T}{(.010/39.37)}$$

$$\therefore \Delta T = 0.20°C$$

(b) The right hand major insulation of 20 mils polypropylene conducts 75% of the heat, with the resulting gradient of 0.30°C, and

(c) The left hand major insulation of 20 mils thickness conducts only 25% of the heat, with the temperature gradient of 0.10°C.

The total temperature rise of the cable above the 60°C base plate is the sum of the above temperature gradients, i.e. 0.20 + 0.30 + 0.10 = 0.60°C. The operating cable temperature would then be less than 61°C.

TABLE 9.1

THERMAL PROPERTIES OF MATERIALS PROPOSED IN THE CABLE CONSTRUCTION

Material	Thermal Conductivity $wm^{-1}\ c^{-1}$	Steady-State Operating Limit (°C)
Copper	387	300°C
Strand Insulation	0.20	130°C
Polypropylene	0.15	120°C
Plasticized PVC	0.15	95°C

The low temperature rise in this mode is attributed to the low-loss design plus the wide face area available to dissipate the heat.

9.3 CONDUCTION COOLING BY INTERMITTENT MOUNTING SUPPORTS

The cable can also be mounted on regularly spaced supports conducting heat to a 60°C base plate. The objective of the following calculations is to specify the cooling contact area and their intervals that will keep the cable temperature below the thermal endurance limits of the materials proposed in the construction. The properties of these materials are summarized in Table 9.1.

The heat conduction paths are shown by arrows in Figure 9.2, where it is assumed that shaded areas C, distance ℓ apart, on both sides of the cable are in contact with the conduction coolers maintained at 60°C. The equivalent thermal circuit and the applicable symbols are shown in Figure 9.3.

As calculated earlier, the total losses in the cable are 4.457 w/m, one-fourth of which is in each of the outer straps. This gives q_1 = 1.11 watts/m. The copper length $\Delta X = \ell/2$ and the average cross sectional area of half the strap (assuming 40% fill-factor) is .0014 x .036 x .40 = 20.2E-6m^2. With K_C = 387 w/m°C (from Table), the copper thermal resistance is

$$R_C = \ell/2 \Big/ (387 \times 20.2E\text{-}6) = 64\ell\,°C/w.$$

The heat generation is uniformly distributed over the entire length, rather than lumped at one place. It can be analytically shown that in such situations, the temperature rise, ΔT, can be calculated by assuming that the total heat generated in length $\ell/2$ is conducted across the average distance $\ell/4$, the thermal resistance across which is $R_C/2$.

$$\therefore \Delta T = \left(q_1 \times \frac{\ell}{2}\right) \times \frac{R_C}{2} = \frac{q_1 \ell R_C}{4} \text{ along the strands.}$$

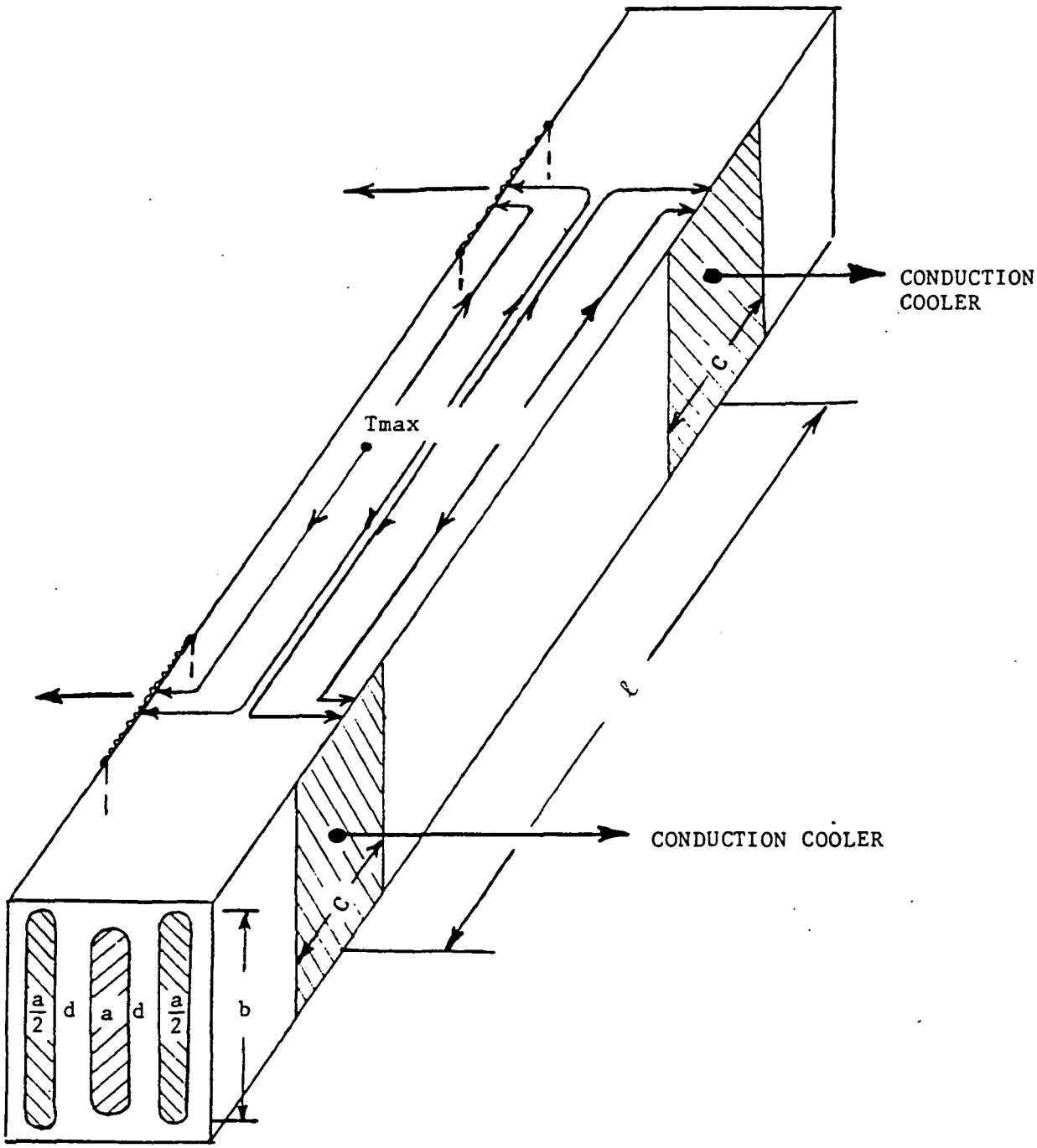

FIGURE 9.2: Conduction Cooling Configuration under Analysis. Shaded area represents cooling contacts C. Arrows indicate directions of heat flows.

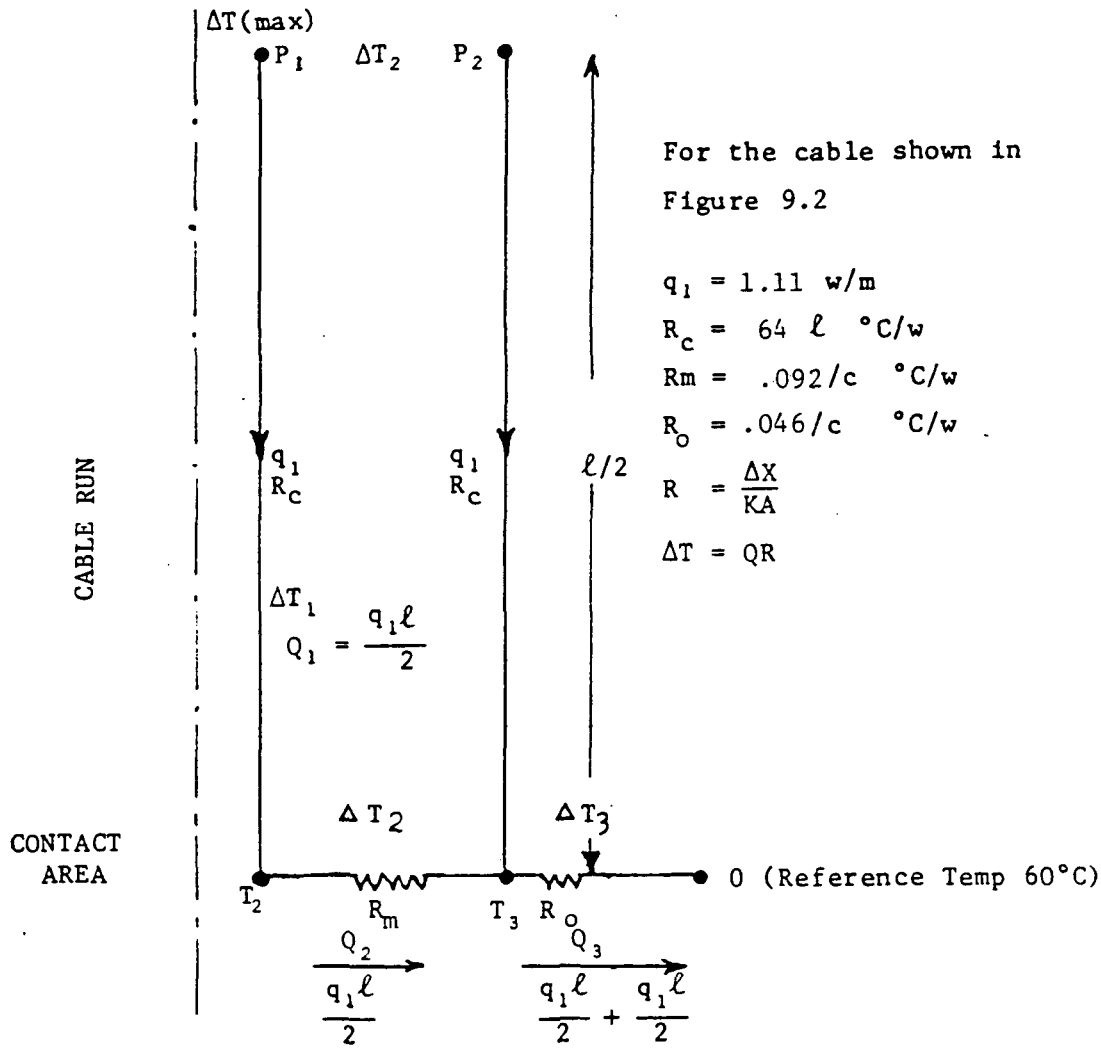

q_1 = Heat loss (watts) per meter length of outer strap

R_c = Th. Resistance of copper per meter length of outer strap

R_m = Thermal Resistance of major insulation) per one contact area bxc

R_o = Thermal Resistance of outer jacket)

ΔT = Temperature rise across the branch

→ = Heat flow (watts) through the branch

FIGURE 9.3: Equivalent Thermal Circuit used for Temperature Rise calculations with conduction alone. Due to symmetry, only half the cable thickness is considered in the model. The maximum temperature rise will be at point P_1

The thermal resistances of the major insulation of thickness d per side is:

$$R_m = \frac{d}{K_m x(bxc)} = \frac{.5}{0.15x36xc} = \frac{.092}{c} \quad °C/w$$

and for the outer jacket insulation:

$$R_o = \frac{.25}{0.15x36xc} = \frac{.046}{c} \quad °C/w.$$

The temperature rises shown in Figure 9.3 are:

$\Delta T_2 = Q_2 \ (R_m) = \frac{q_1 \ell}{2} \ (R_m)$ across the major insulation, and

$\Delta T_3 = Q_3 \ (R_o) = q_1 \ell \ (R_o)$ across the outer jacket.

The maximum temperature rise is then the sum of the above ΔTs, i.e.

$$\Delta T_{max} = \Delta T_1 + \Delta T_2 + \Delta T_3$$

$$= q_1 \ell \ (0.25R_c + 0.5R_m + R_o) \text{ after combining the terms.}$$

Substituting the values of R_c, R_m, R_p and q_1 calculated above, this equation becomes:

$$\Delta T_{max} = 1.11\ell \left(16\ell + \frac{.092}{c}\right) = 17.76\ell^2 + .102\frac{\ell}{c}$$

were ℓ and c in meters. The first term on the right represents the temperature rise along the copper strands at mid-span between the cooling contacts, while the second term is the rise across the insulation at the cooling contacts.

For the manufacture of the cable, we have chosen the operating temperature limit of 95°C for at least 10 years of life expectancy. Since the reference temperature of the conduction coolers is specified to be 60°C, we have the total allowable temperature rise, ΔT_{max}, of 35°C. As can be seen

from the above equations, the maximum permissible contact span is approximately $\sqrt{35/17.76} \simeq 1.4$ m when ℓ is large. Under this value, we have two degrees of freedom for limiting the temperature rise, that is by adjusting the contact area (c) or contact span (ℓ) or both. This choice can be exercised at any stage in the installation. However, the following relationship between c and ℓ must be met to limit ΔT_{max} to 35°C:

$$35 = 17.76\ell^2 + .102\frac{\ell}{c} \quad \text{where } \ell \text{ and c are in meters.}$$

A few possible combinations of ℓ and c which satisfy this cooling requirement are:

$\ell = 1.25$ m, c = 1.6 cm
$\ell = 1.00$ m, c = 0.6 cm
$\ell = 0.75$ m, c = 0.3 cm

Thus, for conduction cooling in this mode, we need at least 0.6 cm wide cooling contacts on both sides of the cable at one meter intervals.

9.4 SUMMARY OF THERMAL DESIGN CALCULATIONS

The calculated operating temperatures of the cable under the above three possible heat rejection modes are summarized in Table 9.2, which shows that the temperatures are well within the permissible limit except at the lower end. Both PVC and polypropylene at -40°C and below may pose a concern for embrittlement.

TABLE 9.2

OPERATING TEMPERATURES UNDER CONDUCTION ALONE AND RADIATION ALONE FOR 1000 V, 100 A, 1.5 INCH WIDE CABLE DESIGN

HEAT REJECTION MODE	COOLING CONDITION	OPERATING TEMPERATURE
Radiation to freespace (80°K)	80°K on one side of the cable with the cable surface emissivity as follows:	Cable surface temperature*
$q_r = \frac{3.67e}{1000}\left[\left(\frac{\theta_1}{100}\right)^4 - \left(\frac{\theta_0}{100}\right)^4\right]$ watts/in^2	e = 0.90 e = 0.75 e = 0.50 e = 0.25	-54°C -40°C -20°C +28°C
Conduction alone	60°C base plate continuous on one side of cable	61°C
Conduction to 60°C base plate from both sides of the cable	one cm wide contacts, one meter apart	Conductor temperature +95°C

* Due to the internal temperature rise due to conduction, the conductor temperature will be one degree higher than the cable surface temperature.

10.0 MECHANICAL FORCE CALCULATIONS

The mechanical force pattern in the three-strap configuration is such that the outer straps experience repulsion from the center strap and the center strap will experience the equal and opposite compression on itself. The repulsive force can be calculated by using 0.5 pu current in Figure 2.7, which holds for a wide range of the cable geometry. However, for the chosen geometry of extra-wide, closely-spaced straps, this force can be accurately calculated from the following analysis. The flux density Bx at the innerface of the outer strap is:

$$Bx = \mu_0 Hx = \mu_0 \times \frac{0.5 \times I\sqrt{2}}{b} \text{ Tesla (peak)}$$

where I is the cable current and b is the cable width (height). The flux density at the outer face of the outer strap is zero. The average flux density in the current carrying region of the outer strap is, therefore, Bx/2, i.e.

$$B_{avg} = \sqrt{2}\mu_0 I/4b \text{ Tesla.}$$

The force per meter length is then:

$$F_1 = B_{avg}\, I\sqrt{2} = 2\mu_0 I^2/4b = \mu_0 I^2/2b \text{ N/m (peak).}$$

If the straps were totally bonded face-to-face with the major insulation, the tensile stress in the bond and the insulation will be:

$$\sigma_b = \frac{F_1}{b} = \frac{\mu_0 I^2}{2b^2} \text{ N/m}^2 \text{ (peak).}$$

For the given cable, this turns out to be:

$$\sigma_b = \frac{4\pi E{-7} \times 60^2}{2 \times .037^2} = 1.6 \text{ N/m}^2 = 0.0003 \text{ psi (peak)}$$

which is quite small compared with the ultimate tensile

strength of about 2000 psi for the insulation. Since both polypropylene and PVC are anti-stick (peelable) materials, the strap would not be totally bonded face-to-face. In that case, this force is taken by the end insulation e (see sketch in Section 6.2), and the tensile stress in the insulation would be:

$$\sigma_e = \frac{F_1}{2e} = \frac{\mu_0 I^2}{4be} \text{ N/m}^2 \text{ (peak)}$$

With e = .0015 m, we have:

$$\sigma_e = \frac{4\pi E\text{-}7 \times 60^2}{4 \times .037 \times .0015} = 20 \text{ N/m}^2 = .003 \text{ psi}$$

which is very small to be of any concern.

The stresses are very small because the extra-wide straps chosen to keep the inductance low produces low flux density. The three-strap configuration is yet another reason for the low mechanical stresses.

11.0 ELECTROMAGNETIC INTERFERENCE

11.1 EMI FLUX DENSITY ESTIMATE

Electromagnetic interference radiating from the cable under development is a major concern. One of the applicable standards (MIL-STD-462, Section RE01) limits the radiation at 7 cm away from the worst radiating point to be less than 27 db above 1 picotesla. This flux density is difficult to calculate without a detailed finite-element electromagnetic study. However, it is shown below why it is expected to be low.

The "virtually concentric" 3-strap cable configuration selected for the final design can be viewed as two cable pairs, put side-by-side, carrying equal and opposite current of one-half the magnitude. One such pair, shown in the absence of the other in Figure 11.1, will radiate flux like a solenoid. The flux densities from the end (radiating point) of one such solenoid are calculated and tabulated under Figure 11.1 using the classical thin solenoid theory. It is seen that the flux density rapidly falls with the distance and becomes .042μT at 7 cm. If a one-turn search coil, one cable thickness (7.1 mm) wide and one meter long, is placed at this location, it will see the induced voltage of 26.7μV at 20 kHz (assuming uniform flux density within the search coil).

Now, if the other half of the cable is placed next to the first half considered above, it will produce about -26.7μV. The net resultant flux density will then be about zero, a subtraction of one "large" number from the other "large" number. The exact value of this subtraction could not be readily calculated by any closed form formula.

It should be pointed out that the above flux density estimates are without a shield around the cable. Any shield placed around the cable will reduce the above calculated flux densities.

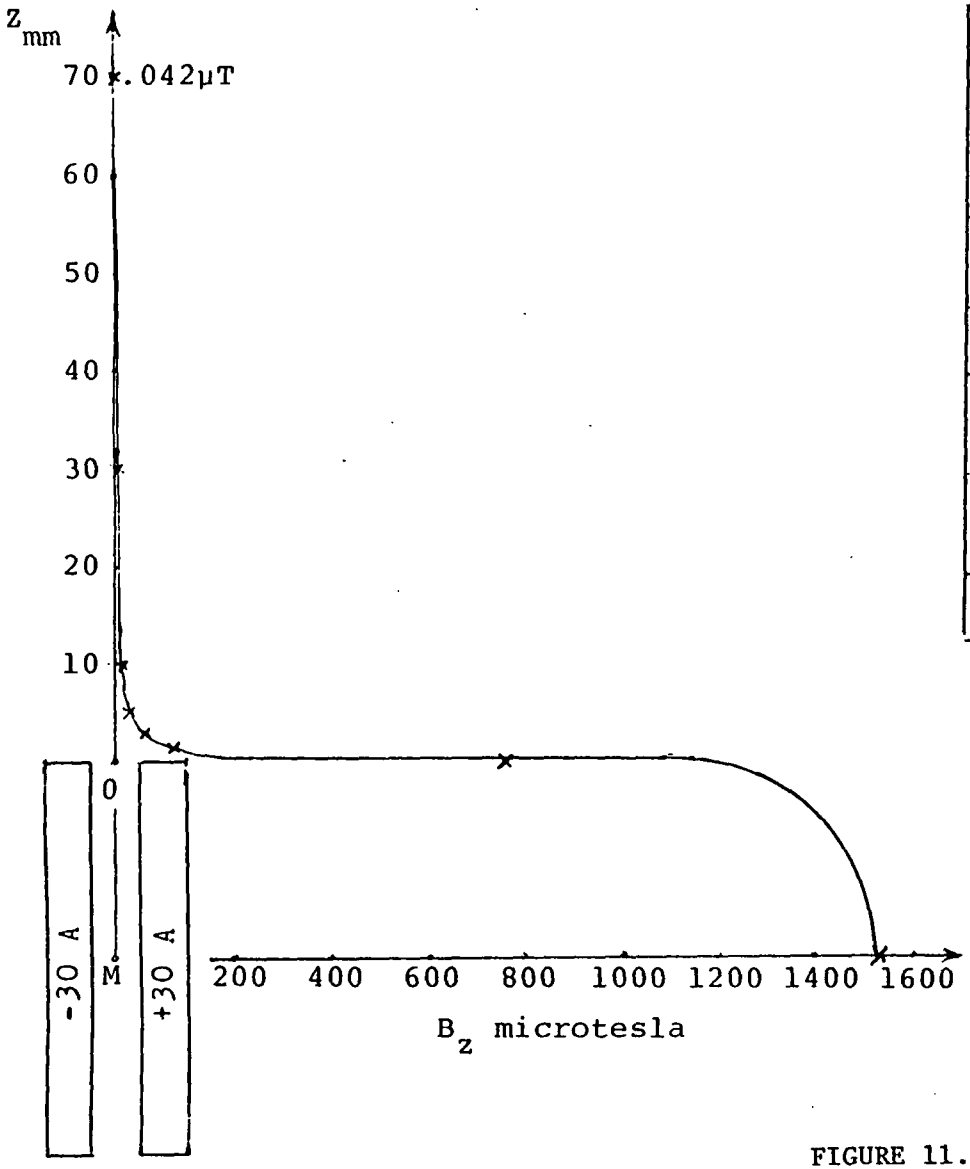

Z mm away from end	B (peak) without shield	
	per unit of B at Mid-Point M	Microtesla
-17.5 (Point M)	1.00	1523
0 (end point)	.50	762
1mm	.145	220
2mm	.053	81
3mm	.0256	39
5mm	.0097	14
7mm	.0050	7.6
10mm	.0025	3.8
70mm	28E-6	.042

FIGURE 11.1

Calculated flux density radiating from end of one-half cable without EMI shield. At 70 mm the other half cable will produce about equal and opposite flux density, thus cancelling each other.

11.2 EMI SHIELDING

One consequence of the three-strap configuration is that most of the magnetic flux is now internally contained, thus minimizing the electromagnetic shielding requirement. Furthermore, the indentation of the central high voltage strap with the grounded outer straps reduces also the electrostatic shielding requirement. Since the EMI field generated by the cable is mostly due to fringing, it is difficult to establish by analysis whether or not the shield is required. However, should the EMI tests indicate a shielding need, it can be applied later on.

There are two alternatives for the shielding material, the conducting material or the magnetic material. Experience in such situations indicate that the conducting shield would produce more losses with no extra benefits. The conductive shield keeps the flux away by the internally induced eddy currents, while the magnetic shield guides the flux along the designed paths. Therefore, if the shield is needed, the magnetic shielding material is expected to be better than the conductive shielding material.

12.0 FINAL DESIGN SUMMARIZED

12.1 DISCUSSION ON THE FINAL DESIGN

The final design, as developed in the previous sections, has been depicted in Figure 12.1. The loss, mass, inductance and capacitance per meter length of the cable with the revised ratings are summarized in Table 12.1, where the mechanical forces and temperature rises under conduction alone and radiation alone are also shown. In actual use, radiation will be the principle mode of heat rejection. The operating temperature of the cable, therefore, is expected to be tens of degrees below 0°C, depending on the exact emmissivity of the finally installed cable surface.

It is observed from the last column of Table 12.1 that the conductor loss in the revised 60 A cable is now 0.010% per meter versus 0.01% goal set for the original 100 A cable, and the mass 0.031 kg/kW/m versus 0.01 kg/kW/m goal for the 100 A cable. Since the cable current is now 0.6 times the original 100 A rating, the loss and mass both would now be reduced to 0.6 each, bringing the loss x mass product down to 0.6 x 0.6 = 0.36. Had we kept the same cable cross section, the loss would have been reduced to 0.36 (in proportion of I^2) and the mass remained the same (1.0), thus the mass x loss product again reducing to the same 0.36 ratio.

Had the original goals of .01% loss/m and .01 kg mass/kg/m were to be uniformly revised, they should now become 1/0.6 times the original values. The new goals should, therefore, be .017% loss/m and .017 kg mass/kW/m, respectively, with their product being 289 E-6. The last column of Table 12.1 indicates that these numbers for the revised 60 A cable, as designed, are .010% loss/m and .031 kg mass/kW/m, and their product 310 E-6. The last number, however, is calculated at 100°C. Since the operating temperature of the cable is expected to be much lower, the actual loss x mass product would be significantly lower than 310 E-6, thus meeting the goal. The loss is, however, lower and the mass higher than the uniformly revised goals. In other words, the design now gives the low-loss attribute a higher importance than the low-mass attribute.

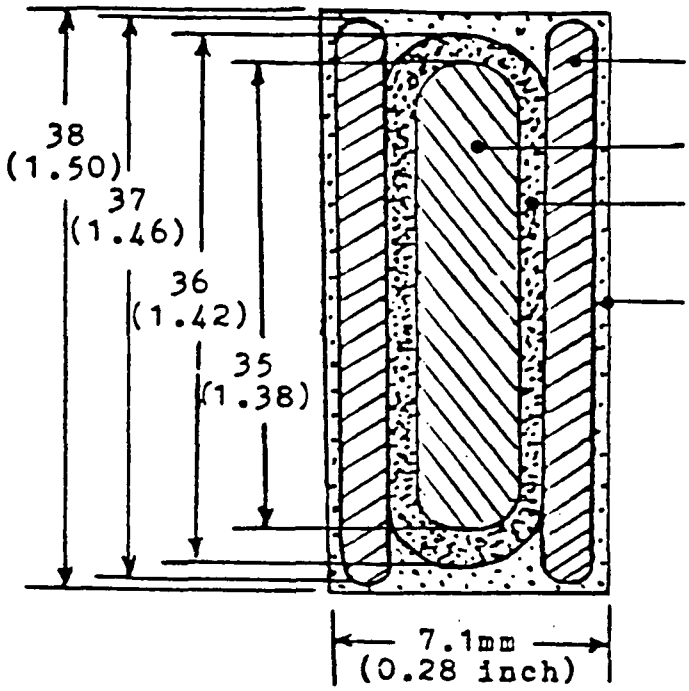

Outer straps 1.3 mm (.050 inch) thick
37 mm (1.46 inch) wide

Middle strap 3.0 mm (.120 inch) thick
35 mm (1.38 inch) wide

Middle insulation jacket, Polypropylene
0.5 mm (.020 inch) thick

Outer insulation jacket, PVC
0.25 mm (.020 inch) thick

No. of strands in the middle strap=1056 approximately (copper)

No. of strands in each outer strap=480 approximately (copper)

Strand Insulation: Solderable

Flexible (Aspect Ratio 5.4)

CALCULATED LINE PARAMETERS

Parameter	Unit	with major insulation 20 mils	30 mils
Resistance (100°C)	mΩ/m	1.043	1.043
Inductance	μH/m	.027	.032
Capacitance	μF/m	.003	.002
Mass	kg/m	1.102	1.103
Losses	Watts/m	3.755	3.755
IX drop	Volt/m	.203	.241
Charging current	Amp/m	.227	.151
Dielectric stresses	Volts/mil	30	20

FIGURE 12.1: Three-straps 1.5 inch wide design for 20 kHz, 600 V, 60 A cable. Aspect ratio 5.4.

TABLE 12.1: DESIGN SUMMARY OF 600 V, 60 A, 1.5 INCH WIDE CABLE, FINAL DESIGN WITH 20 MIL MAJOR INSULATION

DESIGN PARAMETER	PER METER LOOP	% OF RATING PER METER *
AC Resistance at 100°C, 20 kHz	1.043 mΩ/m	---
Conductor Loss (including 2.4% eddy loss)	3.755 watts/m	.010%
Inductance	0.027 μH/m	
IX voltage drop	0.203 v/m	.034%
Capacitance	0.003 μF/m	---
Charging current	0.227 A/m	.378%
Conductor Mass	1.102 kg/m	.031 kg/kW/m
Insulation Mass	0.057 kg/m	---
Force separating the straps	0.065 N/m	(.00036 Lbf/inch)
Tensile stress in end-insulation	20 N/m^2	(.003 psi)
Dielectric stresses in major insulation	1200 v/mm	(30 v/mil)
Dielectric Loss in Insulation	0.017 watts/m	---
Conduction cooling contacts required for 95°C operating temp.	1 cm wide, 1 m apart	
Operating temp. if one face radiating to freespace at 80°K	Tens of degrees below 0°C	
EMI shield requirement	Small	

* This column should be compared with the proportionately modified goals for the revised 60 A cable, as discussed in Section 12.1.

As seen in the above paragraph, the loss x mass product of the final design is as close as we can get, since the loss x mass product is invariant for a given current and a chosen conductor material. That is, the loss can be decreased by some percentage only by increasing the mass by about the same percentage. Within this fundamental engineering constraint, these two factors can be adjusted in any desired manner.

The major advantage of the 3-strap design is the significantly lower inductance and lower EMI than in the 2-strap configuration . Moreover, it offers the same flexibility in manufacturing, handling, joining and terminating.

12.2 SUMMARY OF BASIC FORMULAS FOR 3-STRAP DESIGN

The formulas for calculating the line parameters R,L,C and the mass for the parallel Litz straps configurations were developed during the contract period. These formulas for the 3-strap configuration are summarized in this section in SI units with the following symbols (see Figure 12.2):

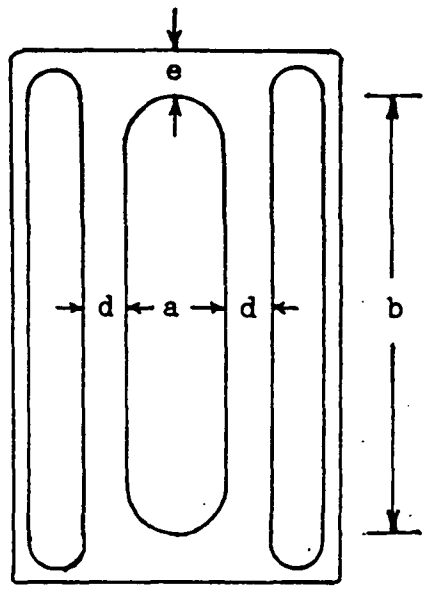

FIGURE 12.2: Dimension symbols of the 3-strap cable used in summarizing the design formulas

V, I = voltage and current ratings of the cable (rms).

a = thickness of the middle strap.

b = width (height) of the middle strap.

d = major insulating distance between straps.

e = end insulation over the middle strap.

K_c = cabling factor by which the spiraling strand length is greater than the straight cable length (≈ 1.15).

K_s = skin-effect eddy loss factor.

K_t = transverse flux eddy loss factor.

K_f = fill-factor of the straps (conductor cross-section area/ strap's gross cross-section area).

ρ, γ = resistivity and mass density of the conductor material.

μ_o, ε_o = permeability and permittivity of free space.

$\varepsilon, \varepsilon_\ell$ = absolute permittivity and loss factor of the major insulating material between straps.

E = dielectric stress in major insulation (rms).

f = frequency of operation.

d_o = conductor strand diameter.

N = number of strands in the middle strap.

For shielding and end-insulation considerations discussed earlier, the outer straps would be slightly wider than the middle strap width and thinner than one-half of the middle strap thickness. The dimensions are adjusted such that the middle strap cross-section equals that of the two outer straps combined.

Then, the line parameters per meter length of the cable are given by the following closed-form formulas:

Resistance	$R_{ac1} = K_s K_t K_c \dfrac{2\rho}{K_f ab}$	ohms/m loop	(12.1)
Inductance	$L_1 = \dfrac{\mu_o}{2b}\left(d + \dfrac{a}{3}\right)$	H/m loop	(12.2)
Reactive Drop	$IX_1 = 2\pi f L_1 I$	v/m loop	(12.3)
Capacitance	$C_1 = \dfrac{2\varepsilon b}{d}$	F/m loop	(12.4)

Charging Current	$I_1 = 2\pi f C_1 V$	A/m loop	(12.5)
Dielectric loss	$P_i = 2\pi f C_1 \tan\delta V^2$	watts/m loop	
	$= 2\pi f \varepsilon_o \varepsilon_\ell E^2$	watts/m^3 of insulation	(12.6)
Force	$F_1 = \frac{\mu_o I^2}{2b}$	peak N/m loop	(12.7)
Conductor Mass	$M_1 = 2K_c K_f ab\gamma$	kg/m loop	(12.8)

In the above formula for R_{ac1}, the skin-effect eddy loss factor K_s for 10 mil diameter copper strands at 20 kHz is very nearly unity. For practical Litz straps, the cabling (spiraling) factor K_c is about 1.15 and net copper fill-factor is about 0.4. The transverse flux eddy loss factor K_t for the 3-strap configuration is one-fourth of that derived in Appendix A of the First Quarterly Report since the flux density in the major insulating gap is now one-half of that in the two-straps configuration. The factor K_t is then:

$$K_t = 1 + \frac{0.2 f^2 N^2 d_o^{\,6}}{\rho^2 b^2 E l 2} \qquad (12.9)$$

For practical designs, this factor should generally fall between 1.0 and 1.05, i.e. the eddy losses generally kept below 5% of the DC I^2R losses

13.0 FAILURE MODES AND EFFECTS ANALYSIS

The reliability is as an important criteria in selecting the design configuration and the manufacturing process. A failure mode and effects analysis on the cable was made. Three possible causes of failures and their effects have been identified as follows:

13.1 EXPOSURE TO FREE-SPACE TEMPERATURE

As calculated in the thermal design, if one face of the cable is radiating to free space, the operating temperature at rated current (60 A) would be tens of degrees below 0°C. When the cable is under no-load, the cable temperature would be even lower, approaching the free-space temperature, which is assumed to be 80°K (-193°C) in the present study. At this temperature, most insulating materials become brittle and may crack. When resins are cooled down, they pass through a glass transition temperature, below which they become glassy (brittle). The selected insulations, the polypropylene and PVC, both have glass transition temperatures above 80°K. Both would, therefore, be brittle at 80°K. However, since the cable carries no mechanical load, other than its own mass, the chances of brittle cracks may be small.

Should a brittle crack develop across the thickness of the major insulation, it may lead to electrical failure over a period of time. A possible suggestion may be to use cryogenic insulations, such as Mylar and Kapton of E. I. DuPont, which have been successfully used in superconducting power equipment. These materials, however, have high dielectric losses, which are not of a concern in DC cryogenic applications, but are not practical for the present 20 kHz application.

13.2 EXPOSURE TO ULTRAVIOLET RADIATION

The cable side facing the free space would be exposed to ultraviolet radiation. Most polymer materials gradually

degrade under such exposures. Chemical additives are generally used to stabilize polymers against UV radiations. In the present application, it is likely that the outer PVC jacket insulation may not be directly exposed to the radiation. If a magnetic metal tape is wrapped around the cable for EMI shielding, the insulation would get adequate protection against such radiations. In case the EMI shield is not required and is not used, a Teflon tape may be wrapped around to protect the cable. Teflon is much more stable against UV rays.

13.3 VOIDS IN INSULATION

There are two kinds of voids that we should be concerned about. First, the void within the extruded insulation. The maximum permissible void size of this kind is calculated to be 5 mils in Section 6.0. The voids left in the extrusion process under heat and pressure are much less than half a mil. This failure mode is, therefore, not likely.

The second kind of void that may develop in the cable is under compressive force on the cable edges as shown in the Table 13.1 sketch. Under edgewise compression, the flat cable would tend to deform towards a spherical shape. If this deformation is under constant volume, no void formation is possible. The solid insulation would deform under essentially a constant volume, but the braided Litz straps may not, depending on how the strands get internally readjusted. Corona may start under such voids.

TABLE 13.1: FAILURE MODES AND EFFECTS ANALYSIS

CAUSE	EFFECT	FAILURE MODE	POSSIBLE REMEDY
Exposure to free space near absolute zero (especially at no-load)	Embrittlement of insulation, leading to possible cracks in major insulation	Electrical failure	Need suitable insulating material with low tan δ and cryogenic glass-transition temperature.
Exposure to free space UV radiation	Insulation instability against UV radiation	Gradual degradation of the insulating material	o Add additives in the insulation to stabilize against UV o Wrap metal (EMI shield) or Teflon tape over to protect insulation from UV exposure
Excessive compression between cable edges in installed condition	Buckling of major insulation, leading to gaps between conductor and insulation (which does not stick to the insulation, see Note and Figure)	Corona discharges, leading to electrical failure	o Make tests on manufactured cable and establish this possibility and/or its compression limit. Include this in Installation QC o Consider bleeding nitrogen along the cable insulation length o Consider adhesive bond between insulation and conductor straps

NOTE: Antistick insulation is desired for smooth extrusion process, good cable flexibility and easy jointing and terminations.

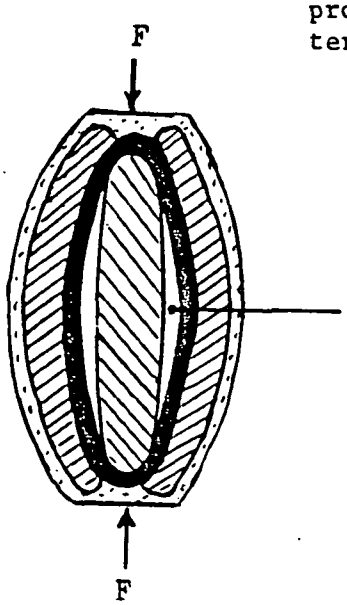

Possible delamination (void formation) under compressive force on cable edges

14.0 SAMPLE CONSTRUCTION AND TESTS

14.1 ONE METER LONG SAMPLE

After completing the final design and the subsequent Design Review at NASA LeRC, the construction of one-meter long sample was undertaken. The set-up for the sample construction is shown in Figure 14.1, which also includes major steps of the process. The actual process chosen for the 150-meter line is to extrude insulation over the Litz straps (with insulated strands). However, since Litz straps are not stock items and making one-meter Litz straps is not economical, the sample used readily and economically available bare copper straps. Such straps were vacuum-pressure impregnated with insulating varnish by the process shown in Figure 14.1. The straps were then tape-insulated by hand. Two passes of 5 mil, one-inch wide polypropylene tape were applied on the middle jacket in half-lap manner, thus building 20 mils jacket per side. The outer straps were then placed and the outer jacket applied again by hand-taping. Figure 14.2a, b and c show this cable.

Due to very low voltage required to test this sample, it was not possible to use the 100 kW, 1000 Vrms power supply which has been procured for testing the full cable. The sample was then tested with 1 kHz inductance-capacitance bridge and a DC milliohm meter. The measured inductance did not agree with the calculated value because the inductance of this short sample was much lower compared to both the lead inductance and the meter resolution.

Therefore, it was decided to make new samples with higher L so that it can be more reliably measured with the available bridge. These samples are described in the next section.

14.2 3.7 METER LONG SAMPLE

This sample was constructed with 3 parallel solid copper bars with dimensions shown in Figure 14.3. They were separated by 1/8 inch thick 0.75 inch diameter dimensionally stable

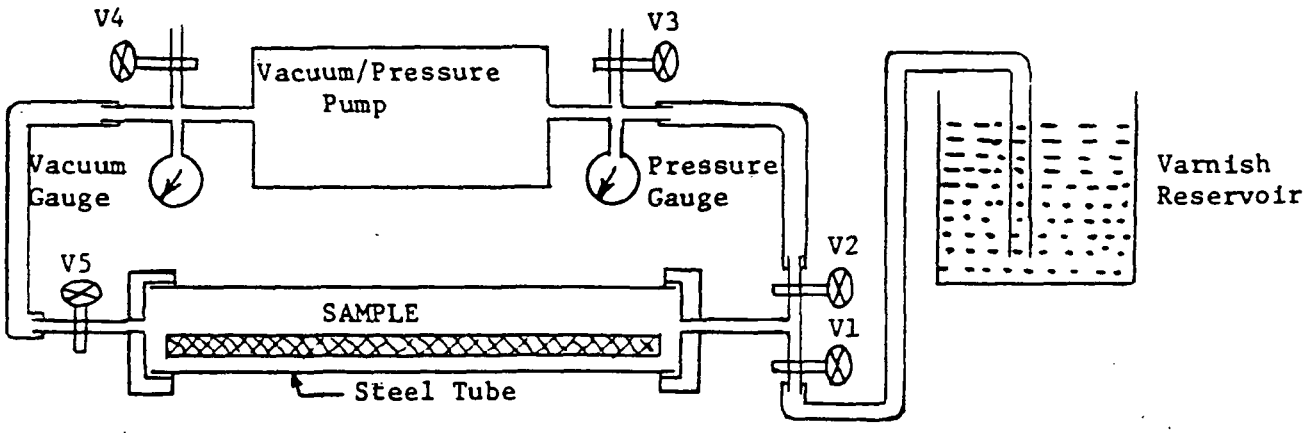

MAJOR PROCESS STEPS:

1) Close valves V1, V2, V4 and open V3, V5.
2) Start vacuum. Keep it on for an hour. Stop vacuum pump.
3) Close valves V3 and V5.
4) Open V1. Let varnish enter the sample by suction as much as it can.
5) Close V1. Open V4 and V2. Keep V3 closed.
6) Start compression. Keep it on for an hour. Stop compression pump.
7) Close V2 and open V3. Leave it this way overnight.
8) Open V1 slowly and drain the varnish completely.
9) Open left end of the sample tube and remove the sample.
10) Lay copper straps flat, sandwiched between polypropylene straps.
11) Let the assembly dry overnight under weight.
12) Wrap the assembly with adhesive backed insulating tape.

FIGURE 14.1: Equipment set-up and major process steps for constructing one meter-long sample. The varnish is vacuum-pressure impregnated on bare copper straps, which were then tape-insulated by hand.

ORIGINAL PAGE IS
OF POOR QUALITY

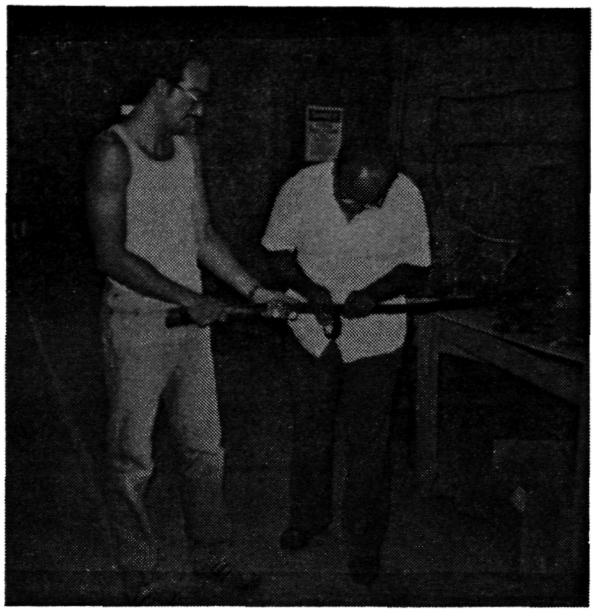

(a) Construction of one-meter cable sample. Outer jacket being taped.

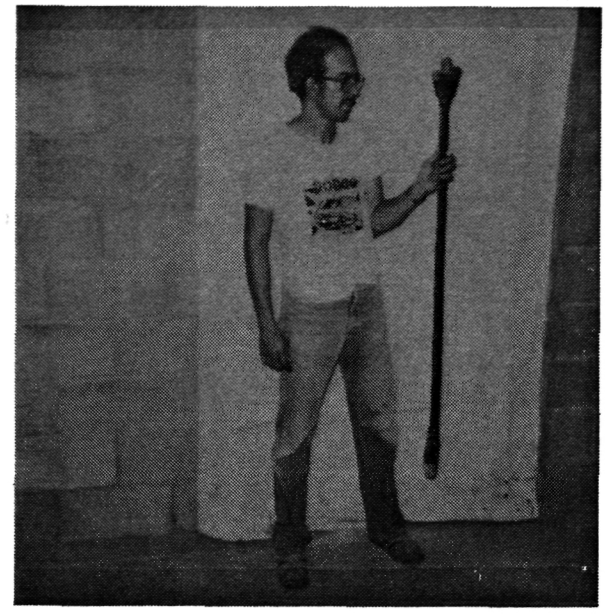

(b) Finished one-meter sample.

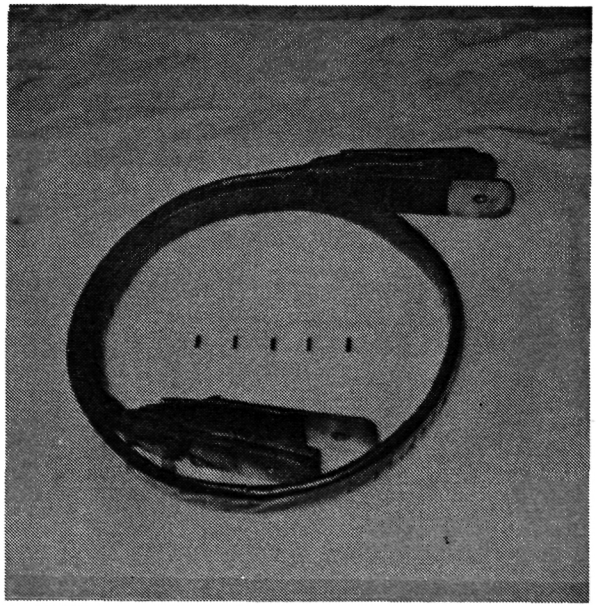

(c) The sample coiled on a 10 inch diameter circle, showing its flexibility (even with cured varnish on strands).

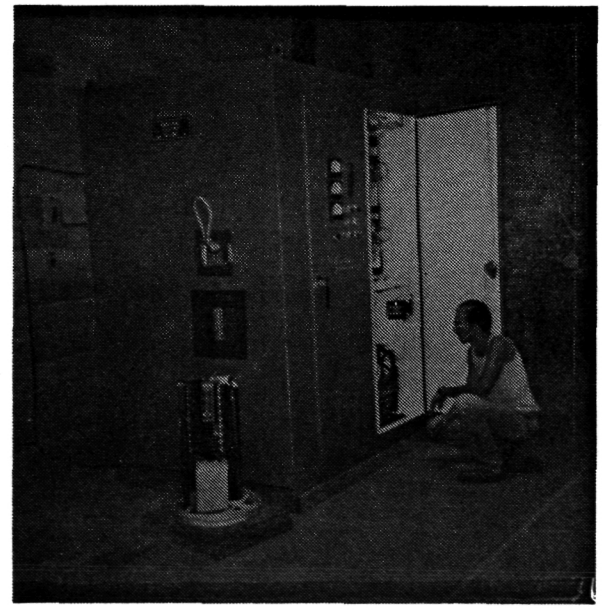

(d) 1000 V, 100 A, 20/10 kHz power supply received for testing full cable at full current.

FIGURE 14.2: ONE-METER SAMPLE CONSTRUCTION AND 100 KW POWER SUPPLY

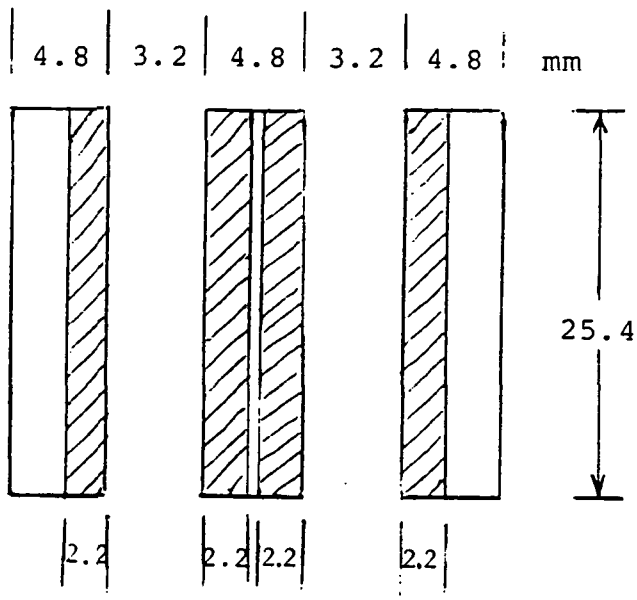

Solid Copper Bars

Length = 3.7m

δ_{skin} = 2.2mm
1 kHz

ε_{avg} = 1.75

Parameter	Calculated	Measured	Leads (deducted)
(A) 3-Bars (Concentric) Configuration:			
$L_{\mu H}$	.43	.4	.7
C_{PF}	910	1005	1
$R_{m\Omega}$ DC	.78	.8	0
(B) 2-Bars (Middle-Outer) Configuration:			
$L_{\mu H}$	.854	.8	.7
C_{PF}	455	509	1
$R_{m\Omega}$ DC	1.04	1.0	0

FIGURE 14.3: Geometrical Dimensions and Test Results of 3.7 m Sample

glass-fiber spacers ($\varepsilon = 6$) at 5 inch center-to-center spacing, and then banded together. The "continum average" dielectric constant of this arrangement was calculated to be 1.75. Since the inductance measurements were to be carried out at 1 kHz, the skin depth of 2.2 mm in the straps (shaded area in Figure 14.3) was used in calculating the inductance at this frequency. The DC resistance was calculated using the full strap area.

Two sets of measurements were taken, one in the 3-bar "virtually concentric" configuration and the other in the 2-bar configuration. The calculated values, along with the measured values of the R,L,C parameters for the above two alternative configurations, are reported under Figure 14.3. It is seen that the test results compare well with the calculated results. Notice that the inductance in the 2-bar configuration is almost twice that in the 3-bar configuration, as predicted.

14.3 FIVE METER LONG SAMPLE

One more sample, with 5-meter long straps of uninsulated strands and dimensions and separations closer to that adopted for the final design, was constructed as shown in Figure 14.4. The straps were separated by 70 mil thick solid (dimensionally stable) Quinergo Board 1200 (tradename of Quintex Corporation), which has the dielectric constant of about 7.5 in the raw (unheat-treated) form. This sample was tested four ways: (1) in a 3-strap configuration, (2) between middle-to-outer left strap, (3) between middle-to-outer right strap, and (4) between outer-to-outer straps. All these test results are summarized under Figure 14.4. They check reasonably well with the calculated values except for the inductance in the first configuration. The reason for this discrepancy could not be identified. However, it is suspected that large resolution and large lead inductance (although minimized by further twisting and shielding) compared to the quantity to be measured may be partly responsible for this discrepancy.

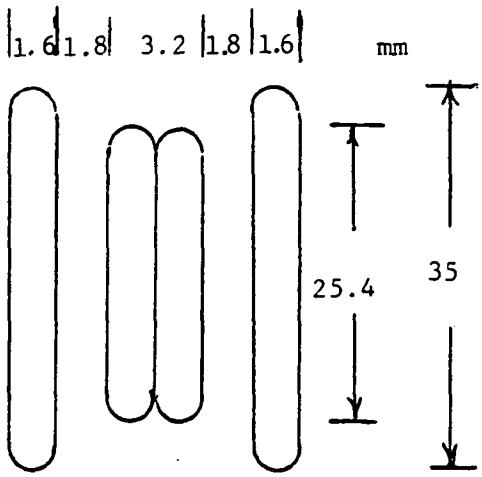

Stranded Straps With Solid Insulation Inbetween

Length = 5 meters

Straps same as in Sample No. 1, except separated by 70 mil thick solid insulation strips (instead of hand-taped).

$\varepsilon = 7.5$

Parameter	Calculated	Measured	Lead (deducted)
(A) 3-Straps (Concentric) Configuration:			
$L_{\mu H}$	.36	.6	.6
C_{PF}	11,060	10,130	1
$R_{m\Omega}$ DC	5.42	5.7	0
(B) 2-Straps (Middle-to-Outer Left) Configuration:			
$L_{\mu H}$	.84	.9	.6
C_{PF}	5530	4910	1
(C) 2-Straps (Middle-to-Outer Right) Configuration:			
$L_{\mu H}$	.84	.9	.6
C_{PF}	5530	5040	1
(D) 2-Straps (Outer-to-Outer) Configuration:			
$L_{\mu H}$	1.41	1.5	.6
C_{PF}	3230	2510	1

FIGURE 14.4: Geometrical Dimensions and Test Results of 5 m Sample

The general agreement between the calculated and measured values of the inductances and capacitances in the 3.7 and 5-meter long samples established the validity of the virtually concentric 3-strap cable concept and the analytical formulas developed for calculating its line parameters. At this stage, the 150-meter long full cable construction was released.

15.0 CONSTRUCTION OF FULL CABLE

The construction of 150-meter long, 600 V, 60 A cable followed the base line design depicted in Figure 12.1. There were a few manufacturing problems which needed to be resolved. These constructional difficulties are discussed here for future reference.

(1) Manufacturing the Litz braids to an accurately predictable dimension was difficult. For example, the finished unextruded strap measurements made by the writer at New England Electric Wire Corporation indicated the following sizes in inches:

	Middle Strap		Outer Strap	
	Actual	Planned	Actual	Planned
Thickness	.140	.120	.060	.050
Width	1.50	1.38	1.60	1.46

Thus, the strap sizes came somewhat larger than the planned. The increased thickness tends to increase the reactance, while the increased width tends to decrease the reactance. The thickness and width increasing together, therefore, partly compensate each other in determining the cable reactance.

To reduce the Litz straps to the planned sizes, the straps were run one more time through compactation rollers and the extrusion die was slightly opened-up to accomodate the increased width.

(2) The middle strap was then jacketed with polypropylene insulation by the extrusion process. Because of some concerns about tearing the insulation while extruding over a rough strap surface, a 30 mil thick jacket was applied instead of the 20 mils planned. The jacketed middle strap was tested for pinholes by a 4000 Vrms high-potential test on the cable. No pinholes were detected in this test.

The jacketed middle strap and the two outer straps then proceeded to the third step in manufacturing the finished cable, i.e. extruding the PVC jacket over the three-strap assembly. In its first attempt, the following problems were faced:

(a) The outer straps were wider than the middle strap before going in the extrusion die. However, in the finished cable on the other end of the die, the outer straps became somewhat narrower (by about 60 mils) than the middle strap, and also somewhat asymmetrically placed with respect to the middle strap (see Figure 15.1). It is suspected that the extrusion process built up pressure at four corners of a rectangular die, which in turn pushed the outer straps inward widthwise. This manufacturing phenomenon tended to increase the cable reactance.

(b) Due to the above pressure build-up, the PVC material penetrated the corners and also further down inbetween the middle and outer straps. This affects the cable design in three ways. It increases the reactance, increases the overbuild and decreases the flexibility.

(c) The first sample had a significant overbuild (almost 50%), mainly due to the PVC penetrating inbetween the straps.

As a result of these manufacturing problems, it was decided to eliminate the PVC penetration between the straps by wrapping a 1 mil Teflon tape, half-lapped, over the three-strap assembly before extruding the PVC jacket and by making appropriate changes in the die. After these measures were taken, the cable production was completed.

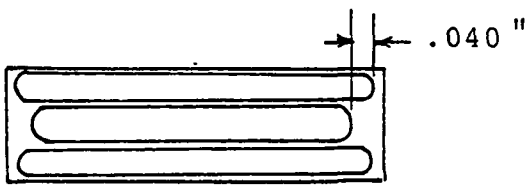

(a) This is how we planned

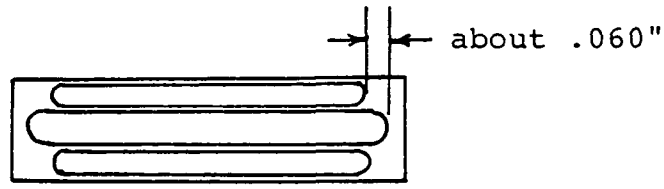

(b) This is how it came from extrusion die in the first attempt

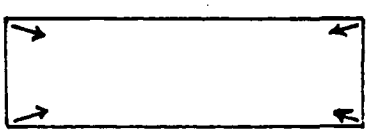

(c) It appears that the fluid pressure in the die built up at the corners. This pushes the outer straps widthwise, making them shorter than the middle strap.

FIGURE 15.1: Manufacturing Problems Encountered

16.0 TESTS ON FULL CABLE

A complete Test Plan was prepared and submitted to NASA for approval. It was accepted and followed for the tests reported in this section.

16.1 AC CORONA TESTS

AC corona tests were made on flat 5 mil thick samples of polypropylene, the insulating material selected for the major insulation between the straps. These tests were made at 60 Hz using ASTM standard brass disk electrodes as shown in Figure 16.1.

Two test series were conducted, one on a single layer of 5 mil thick sample and another on sets of 4 layers dielectrically piled in series (i.e. 20 mil total insulation thickness between the disk electrodes). The test results are summarized in Table 16.1. The corona inception voltage was recorded when the corona discharge exceeded 5 picocoulombs and the corona extinction voltage was recorded when the discharge fell below the 5 pc level.

The test results indicate that for 20 mil polypropylene insulation, the corona starts at 1550 volts (rms) and extincts at 1400 volts rms. This is comfortable for a cable with 440 V operating voltage (a safety factor of 3).

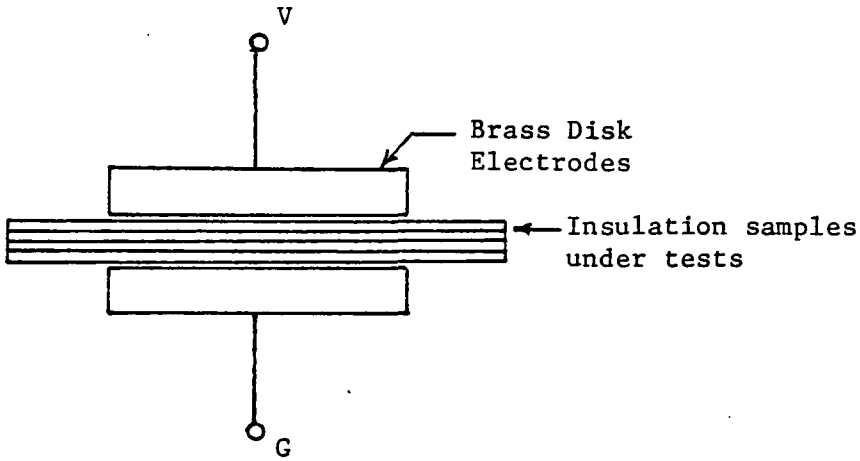

FIGURE 16.1: Corona Test Set-up

TABLE 16.1: CORONA TEST RESULTS ON FLAT INSULATION SAMPLES

Report No. 470057 Issued: 9/30/85

Equipment Used	Model	I.D. No.	Cal. Date
Corona Test Set	45	N065	6/86
Sensitive Research Electrostatic voltmeter	81247	V028	11/85

Test Method

The samples were placed into the Corona Test Set between two A.S.T.M. brass electrodes. Corona inception and extinction voltage was then measured on single samples and on sets of four piled dielectrically in series.

Test Results

Single Sample	Inception Voltage	Extinction Voltage
1	890	850
2	895	845
3	860	820
4	890	855
5	860	810

4 Layer Samples	Inception Voltage	Extinction Voltage
1	1550	1400
2	1600	1450
3	1550	1400
4	1550	1400
5	1600	1450

16.2 R,L,C TESTS

Two full cable lengths, 65 m and 123 m, were tested. Both the bridge measurements (Table 16.2) as well as the full current (short circuit) and full voltage (open circuit) tests under 20 kHz power excitation were made. The circuit diagram for the latter tests is shown in Figure 16.2. The results are tabulated for accuracy in Tables 16.3 to 16.6, and also plotted in Figures 16.3 to 16.5 to check the trends. Table 16.7 is a summary comparison of the calculated values with the test results. The inductance is higher and capacitance is lower than calculated due to the oversize that resulted in the final manufacture.

The capacitance is proportionately more lower, probably because the dielectric constant of the polypropylene is not precisely known at 20 kHz. The manufacturer's data gives $\varepsilon = 2.25$ only at two frequencies, 1 kHz and 1 MHz. We have assumed the same value at 20 kHz in the calculations, although it could be actually somewhat different.

The AC resistance values at 20 kHz are fairly close to the calculated values within the manufacturing tolerances.

The test results reported in this section on full cable once again prove the virtually concentric 3-straps cable concept and also verify the formulas developed for calculating the circuit parameters.

TABLE 16.2: BRIDGE MEASUREMENTS ON FULL CABLE LENGTHS

PARAMETER	ON 65 m CABLE				ON 123 m CABLE	
	Middle to Outer 1*	Middle to Outer 2	Middle to Both Outer	Per Meter	Middle to Both Outer	Per Meter
Resistance at DC (mΩ)	84.08	84.36	53.63	.825	102.2	.831
Inductance at 1000 Hz (μH)	5.5	5.2	2.5	.0385	4.3	.0350
Capacitance at 1000 Hz (μF)	.0362	.0423	.0751	.00116	.168	.00137

*This column gives the parameters between the middle to one of the outer straps. The next column are the parameters of the middle to the other outer strap and the next one is from the middle to both of the outer straps in parallel. Notice that the inductances and the capacitances of the two outer straps individually are not perfectly symmetrical with respect to the middle strap. This is attributed to the manufacturing variations. As discussed in Section 16.3, this asymmetry increases the EMI.

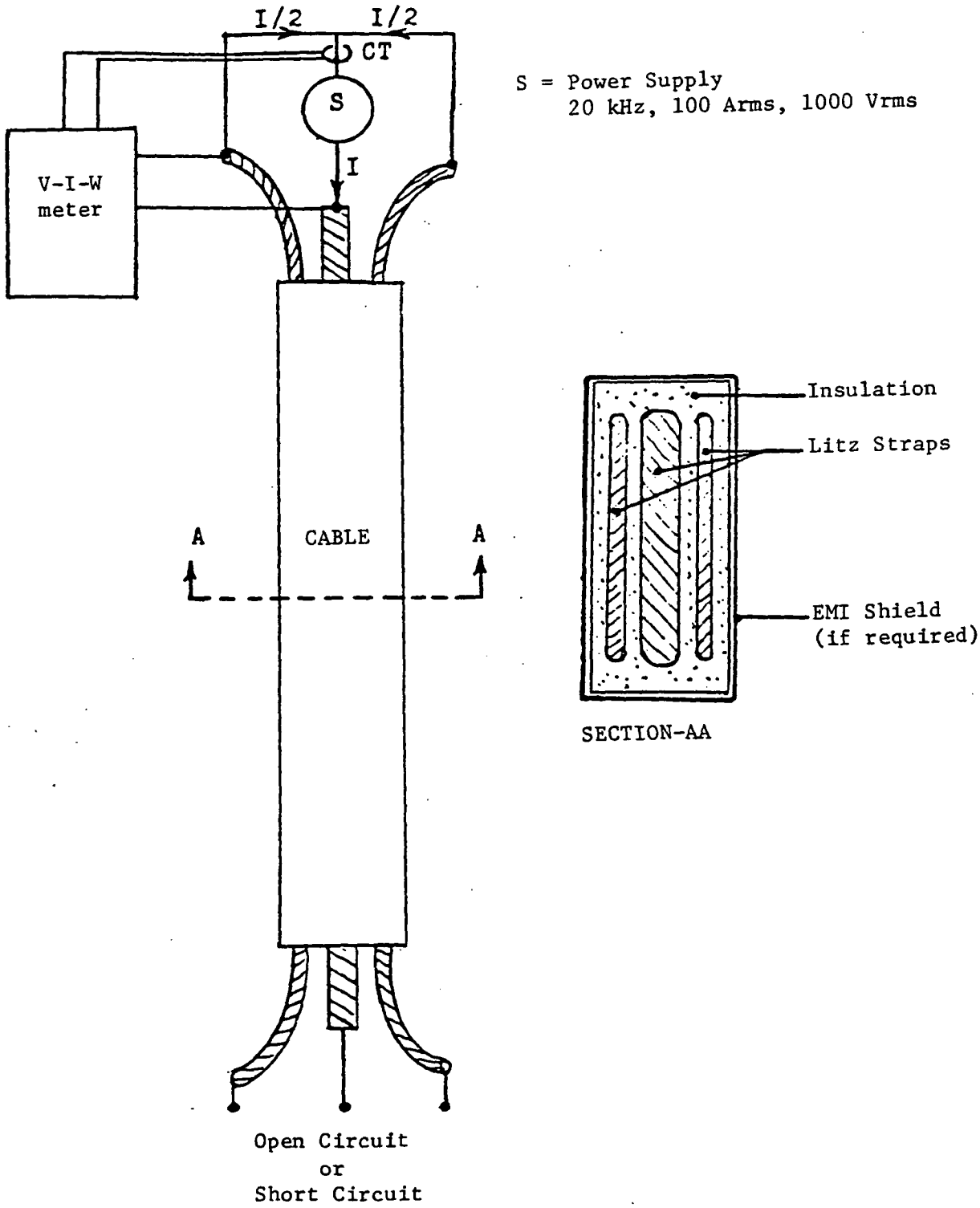

FIGURE 16.2: R,L,C Test set-up for 20 kHz
Open-Circuit and Short-Circuit Tests on Full Cable

TABLE 16.3: SHORT CIRCUIT TESTS ON 65 m CABLE

Current Amps	Voltage Volts	Power Watts	Power Factor	Frequency kHz
20	6.30	22	.184	20.07
30	9.31	48	.168	20.02
40	12.59	85	.163	20.02
60	18.79	191	.164	20.00
70	21.76	259	.165	20.00
80	24.76	334	.165	19.90

TABLE 16.4: OPEN CIRCUIT TESTS ON 65 m CABLE

Voltage Volts	Current Amps	Power* Watts	Power Factor*	Frequency kHz
200	1.784	4	.017	19.23
400	3.556	15	.011	19.23
600	5.317	31	.010	19.23
800	7.017	53	.010	19.09

*These readings, although reported, are to be disregarded. The nearly perfect capacitive nature of the cable under open circuit made these power and power factor measurements extremely inaccurate due to the instrument errors.

TABLE 16.5: SHORT CIRCUIT TESTS ON 123 m CABLE

Current Amps	Voltage Volts	Power Watts	Power Factor	Frequency kHz
20	10.80	43	.199	19.90
40	21.39	168	.191	19.76
60	32.20	390	.196	19.80
80	42.70	680	.199	19.70

TABLE 16.6: OPEN CIRCUIT TESTS ON 123 m CABLE

Voltage Volts	Current Amps	Power* Watts	Power Factor*	Frequency kHz
200	4.067	11	.013	18.95
403	7.998	40	.013	18.75
602	11.960	100	.013	18.81
801	15.830	190	.014	18.73

*These readings, although reported, are to be disregarded. The nearly perfect capacitive nature of the cable under open circuit made these power and power factor measurements extremely inaccurate due to the instrument error.

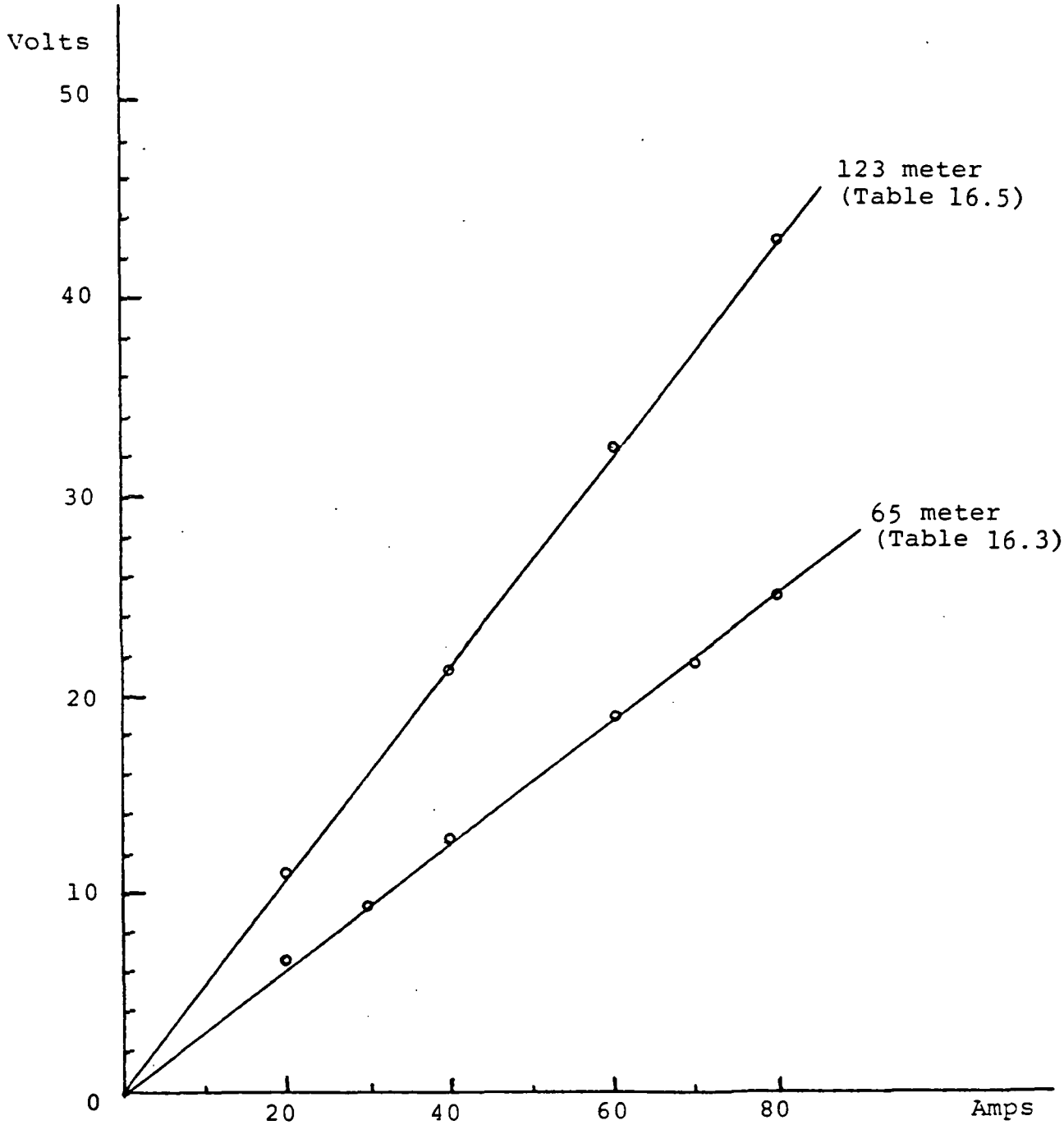

FIGURE 16.3: Reactive volts vs. Current during Short-Circuit Tests on full cable. The dots represent test data, which fall on linear scales, as expected.

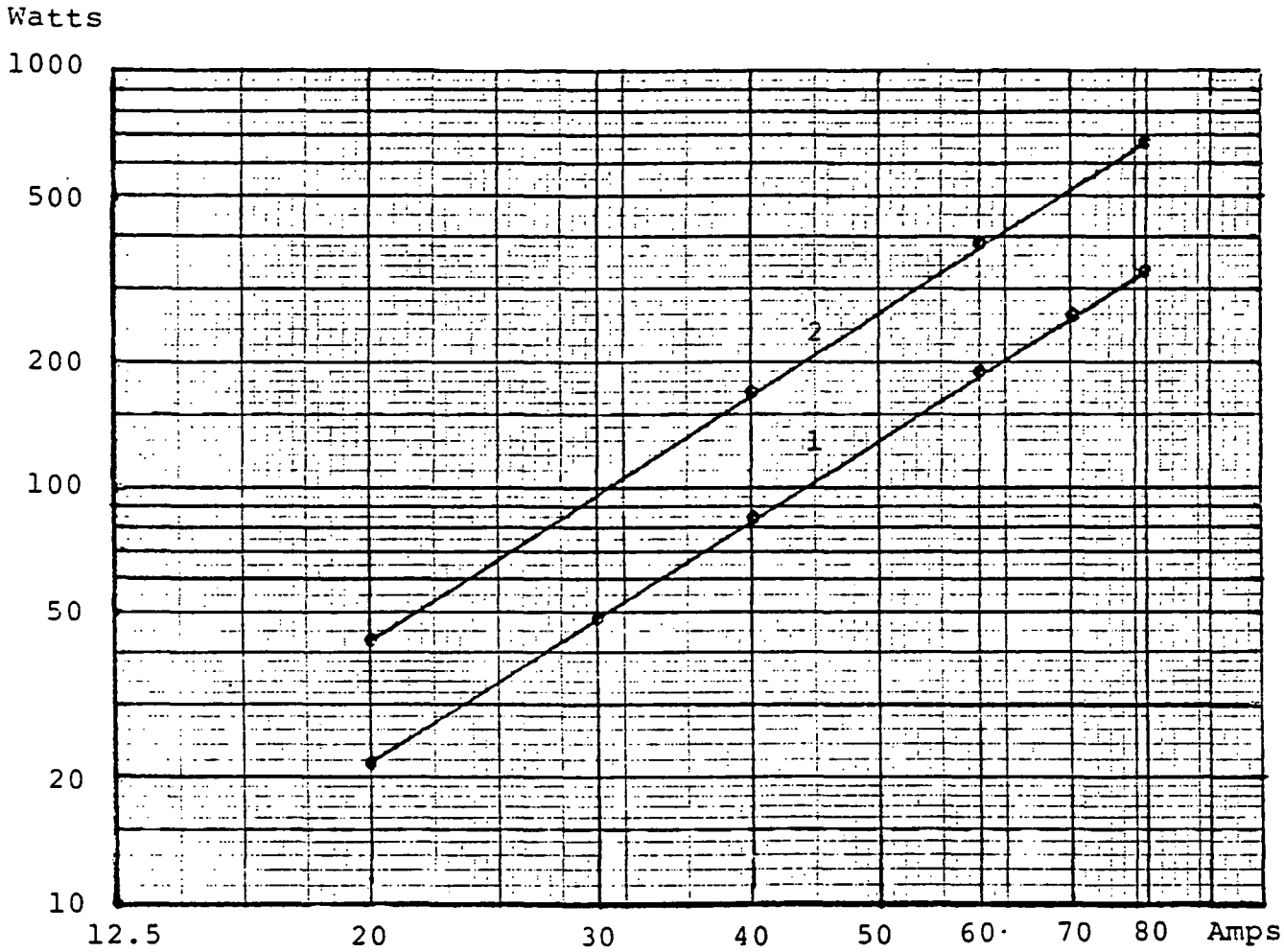

1. Lower curve represents 65 meter long cable (Table 16.3)
2. Upper curve represents 123 meter long cable (Table 16.5)

FIGURE 16.4: Loss vs. Current during Short-Circuit Test on full cable. The data (dots) fall on linear scale on log-log paper, as expected.

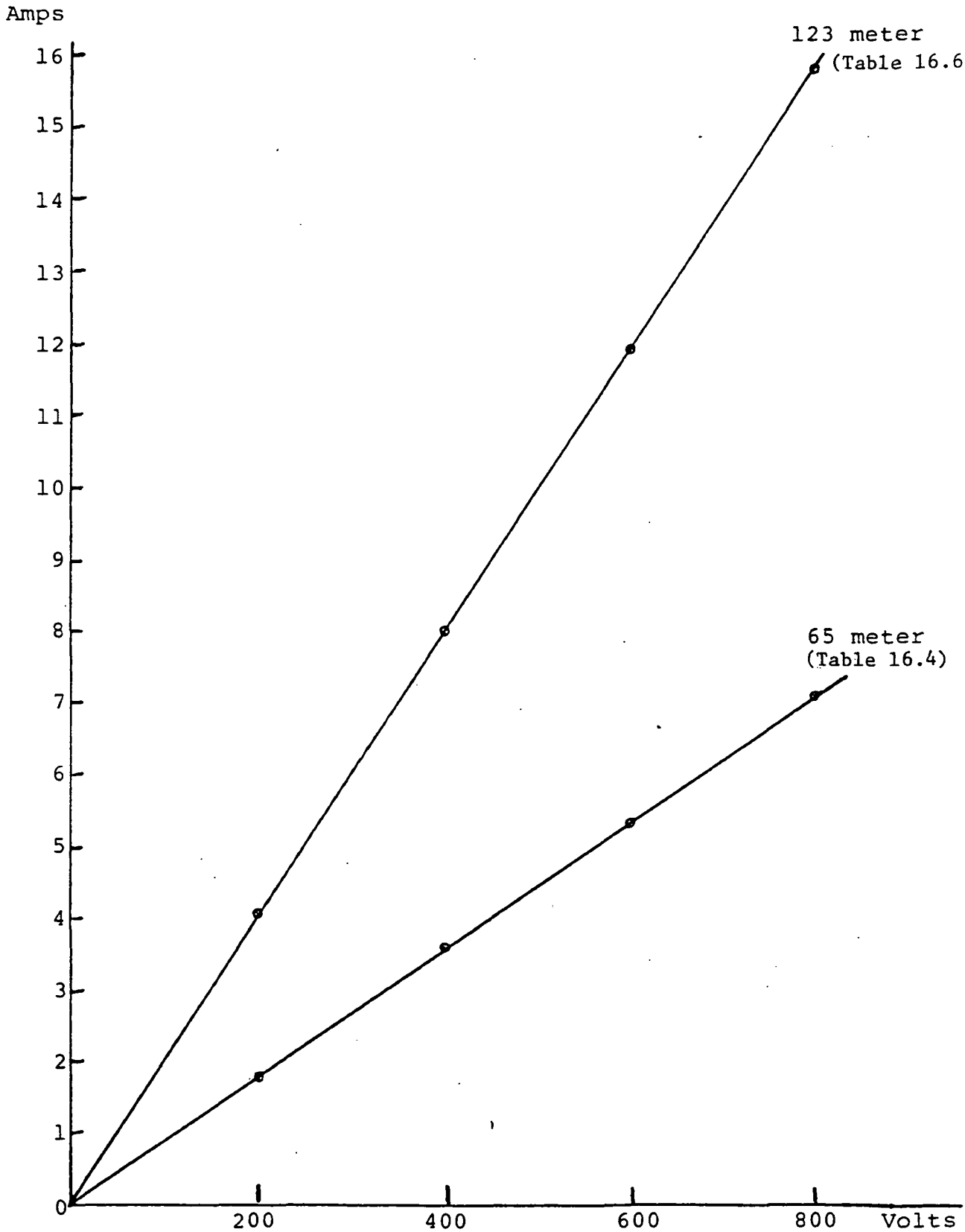

FIGURE 16.5: Charging current vs. Voltage during Open Circuit Tests on full cable. The data (dots) fall on linear scale, as expected.

TABLE 16.7: COMPARISON OF CALCULATED AND TESTED PARAMETERS

Quantity	Unit	Calculated With 30 Mil Insulation (1)	Tested on 65 m Cable		Tested on 123 m Cable	
			Bridge (3)	SC/OC (4)	Bridge	SC/OC
Resistance	mΩ/m	0.800 (2)	.825	.803	.831	.864
Inductance	μH/m	.032	.0385	.0385	.0350	.0345
Capacitance	μF/m	.00187	.00116	.00108	.00137	.00128

(1) Earlier tables reported calculated parameters with both 20 mil and 30 mil major insulation wall thickness on the middle strap. At the time of manufacturing, to avoid possible tearing of insulation during the extrusion process, the insulation thickness approaching 30 mil was adopted. Hence, this column contains calculated parameters with 30 mil insulation for comparison with test results.

(2) Corrected to room temperature (20°C) from previously reported value of 1.043 which was calculated at 100°C.

(3) These results come from Table 16.2.

(4) These results are average values derived from either short circuit or open circuit tests made under 20 kHz excitation as reported in Tables 16.3 to 16.6.

16.3 EMI TESTS WITH CABLE TERMINALS INSIDE THE CHAMBER

EMI tests in accordance with MIL-STD-462, Sections RE01, RE02 and RE04 were made at MET Electrical Testing Company in Baltimore, MD. The tests were made in a shielded chamber with the cable excited with 5 A, 20 kHz current and extrapolated to the cable rating of 60 A. The general set-up for these tests is shown in Figure 16.8. In the first test, the magnetic radiation at 7 cm away (RE01) was measured on a 5 m long cable with the cable terminals inside the chamber. The EMI in this setting significantly exceeded the MIL-STD-461B RE01 limit, which is 27 db above 1 picotesla at 7 cm from the cable. This was rather unexpected. Some of the possible reasons of not meeting the RE01 limit are identified as follows:

(1) The cable terminals were inside the shielded chamber. The cable-run is virtually concentric, thus minimizing the EMI to the maximum extent possible with the chosen configuration. The terminals at both ends of the cable, however, are not concentric. The terminations used in the EMI tests are shown in Figure 16.6, which make a small non-concentric loop at each end. These loops act as flux-generating solenoids, probably generating enough flux to exceed the RE01 limit. To eliminate this termination flux, another 10-meter long cable was tested with the cable ends outside the shielded chamber, and only the middle part of the cable running inside the chamber. The results of these tests are given in the next section.

(2) Another possible reason for exceeding the RE01 limit is the fact that the inductance of the middle strap with respect to the two outer straps is not perfectly symmetrical due to manufacturing variations. For example, the inductance measurements reported in Table 16.2 show that the inductance from middle to one of the outer straps was 5.5μH and from middle to the other outer strap was 5.2μH. Thus, the first value is about 6% higher than the other. The currents in the two outer straps are, there-

fore, not equally divided, and have an unbalance of about 6% of the outer strap current value, or 3% of the cable's rated current, with unbalance of 1.5% flowing in each of the two outer straps. This current unbalance was subsequently confirmed by actual current measurements in the two outer straps. This means that the cable, although designed to be virtually concentric, is only 98.5% concentric and 1.5% non-concentric due to the manufacturing inexactness that resulted in this first prototype construction. As shown in Figure 16.7, this 1.5% of the cable, then, acts as a simple solenoid, generating enough flux to exceed the stringent RE01 limit of 27 db above 1 picotesla.

16.4 EMI TESTS WITH CABLE TERMINALS OUTSIDE THE CHAMBER

Since paragraph (1) above indicated that the non-concentric cable terminals can create solenoidal flux, which does not represent the main part of the cable, it was decided to make further tests on a 10-meter long cable with the terminals placed outside the shielded chamber. The EMI was then measured under the following three different conditions:

(1) Unshielded cable
(2) Electro-magnetic shield around the cable (EMT)
(3) Conductive shield around the cable (copper tube)

The unshielded cable still exceeded the allowable limits. With end-terminals outside the chamber, this indicates that the magnetic flux radiated from the cable is mainly due to the non-concentric part of the cable as explained in para (2) of Section 16.3

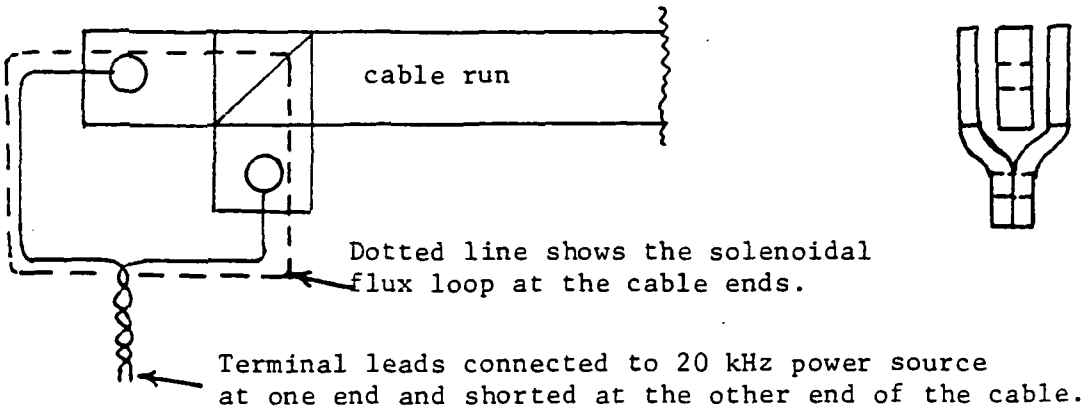

FIGURE 16.6: Non-concentric terminal-ends generate flux like a solenoid

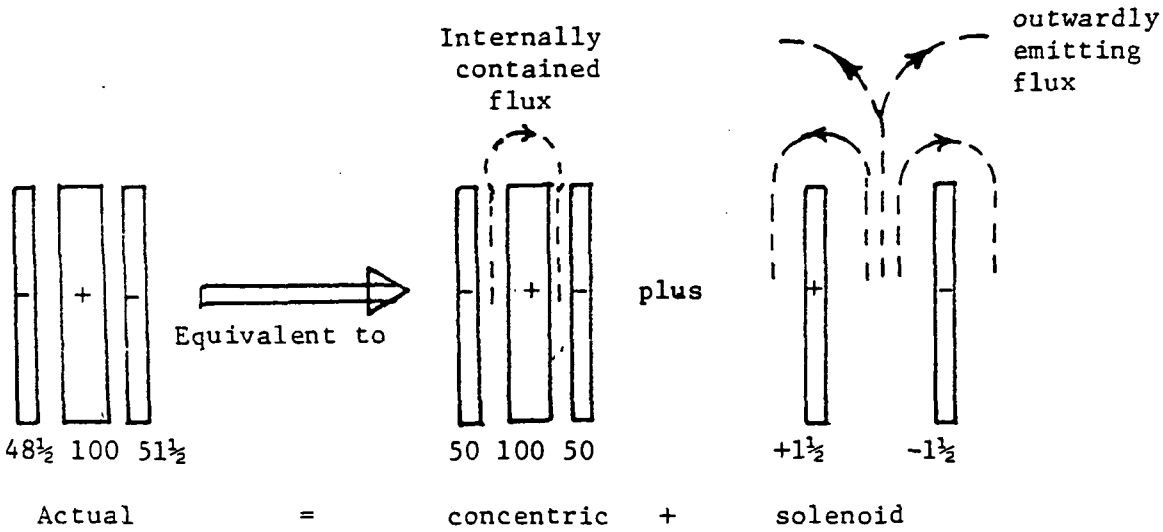

FIGURE 16.7: Difference in inductances of the middle to two outer straps makes the actual cable equivalent to a concentric cable plus a solenoid. The latter acts as a flux-emitter.

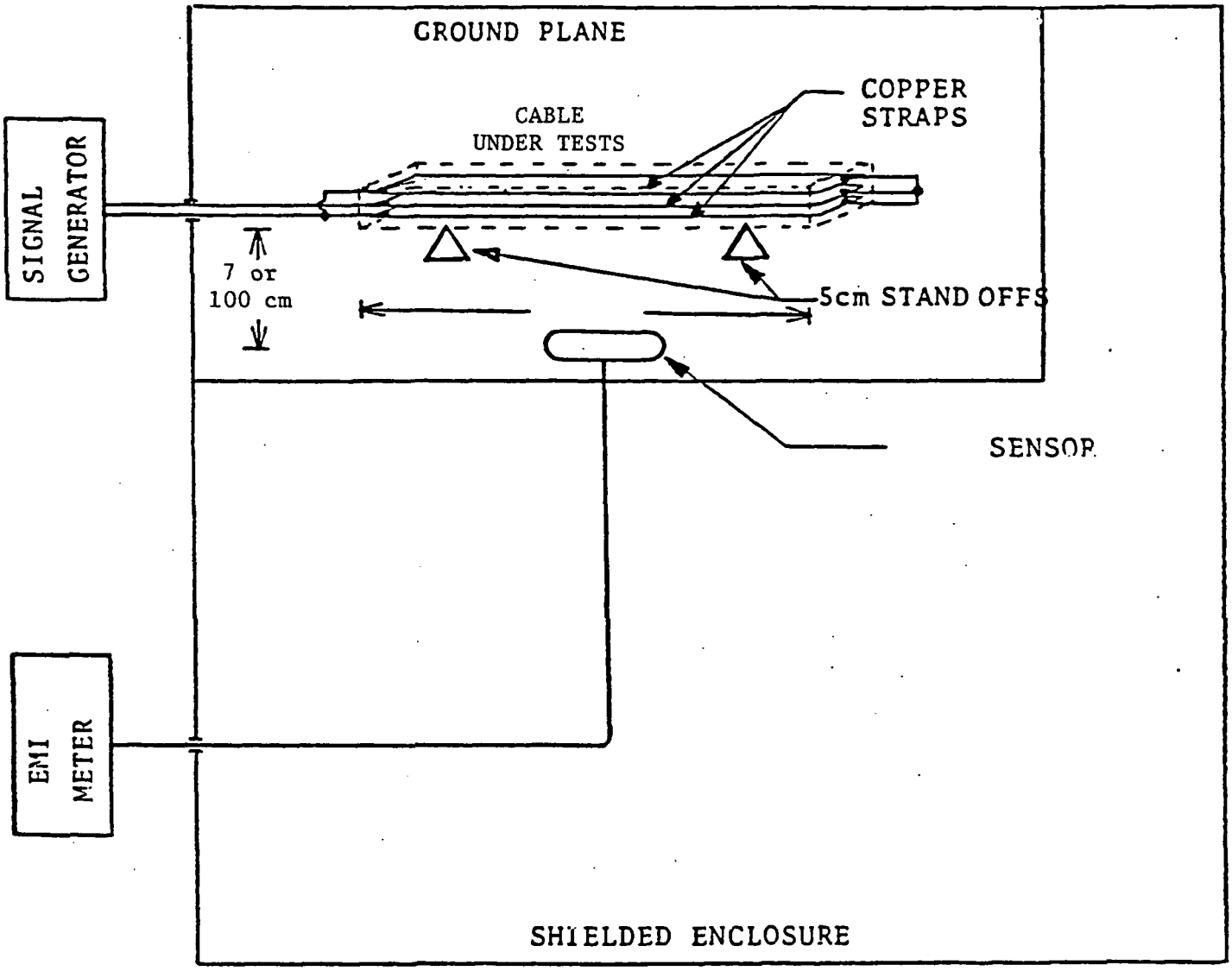

FIGURE 16.8: EMI Test Set-up for MIL-STD-462, Section RE01, RE02, RE04

Following is an estimate of the EMI due to the non-concentricity introduced by the cable manufacturing variations, which caused unequal inductances of the two outer straps with respect to the middle strap.

As shown in Figure 11.1, the magnetic flux at 70 mm away from half of the cable (equivalent to a 30 A solenoid) is .042 μT. A 60 A solenoid would then create .082 μT at 7 cm. The 1.5% solenoid, due to the above-mentioned unbalance current in the two outer straps, would create .015 x 82000 = 1230 picotesla. This converts to 20 log (1230/1) = 62 db above 1 pT, which clearly exceeds the RE01 limit of 27 db. The calculation shows that although the 1.5% non-concentric part of the cable sounds low, it creates sufficient solenoidal flux to exceed the specified EMI limit at 20 kHz. Unfortunately, such EMI calculations on a cable with symmetrical outer straps could not be made without an involved finite-element study. However, as mentioned in Section 11.1, the EMI flux produced at some distance away by the two halves of the cable would cancel each other, leaving virtually zero net flux. For this reason, the EMI from a cable manufactured with nearly perfect symmetry between the straps is expected to have significantly lower EMI. Finite-element electromagnetic flux plot study is required to investigate this in further details.

Since the unshielded cable did not meet the EMI limits (see Figure 16.9), the cable was shielded with 1/2-mil thick, one inch wide high permeability magnetic tape. This reduced the EMI only slightly, indicating that the amount of radiated flux probably saturated the thin tape. The cable was then shielded with a readily available 1/16-inch thick, 2-inch diameter mild steel conduit (EMT) and also with copper tubing of the same size. The reduction in EMI was more with copper tubing than with EMT. The EMT tube is partly magnetic and partly conductive, while copper is purely conductive. The conductive shield reduces the EMI by eddy currents induced in it which opposes the flux radiated by the cable. Theoretical

considerations indicate that a purely magnetic shield would generally perform better than EMT and copper shields at this frequency.

The full EMI test report has been separately submitted to NASA. However, the charts summarizing the results are depicted in Figures 16.9 to 16.19. The following notes apply to these curves:

1) The measurements were taken after scanning the EMI at different locations and in different antenna orientations. The reported EMI were at the point of maximum leakage, which was generally at the edges of the cable.

2) While measuring the EMI, the shielded chamber had sufficient ambient noise particularly at lower frequencies. For example, Figure 16.10 is ambient scan from 1 kHz to 50 kHz for the RE04 (and also RE01) setup. At 60 Hz, the ambient was 85 db, and at 400 Hz it was 40 db. Since we were primarily interested at 20 kHz and its higher harmonics, no significant efforts were made to locate the source of the low frequency ambient.

3) The second harmonic in the 20 kHz power source used for these tests introduced EMI at 40 kHz. For example, if there is 3% second harmonc present in the power source (a normal harmonic content in such equipment), it will introduce 40 kHz EMI which would be 20 log (1/.03) = 30.46 db lower than the fundamental 20 kHz EMI. This is about what we see in Figure 16.9.

4) The level of electric field radiation measured in the RE02 setup (Figures 16.14 to 16.16) was unexpected, nor can we explain at this time. However, significant ambient present in the shielded chamber makes this data doubtful.

EATON DATA ACQUISITION SYSTEM

E.U.T. : INDUCTION GENERAL/NASA CABLE DATE 07 F.
TEST PROCEDURE :RE01
COMMENTS :
TEST ENGINEER :B. SMITH

SCAN PARAMETERS						TEST TITLE :RE01 NASA CABLE
Rvr	Start Freq	Stop Freq	Bandwidth	Atten	Detector	Transduc
7	10 kHz	50 kHz	1 kHz	0 dB	PEAK	ALP-10

GLOBAL PARAMETERS

BROAD BAND CORRECTION: NO | SWEEP RATE: MAX

LIMIT LINE : RE01

SCANS PER SEGMENT : 1

SEG 1 START TIME: 13:19:21 STOP TIME: 13:19:49

Maximum Scan Data : RE01 NASA CABLE

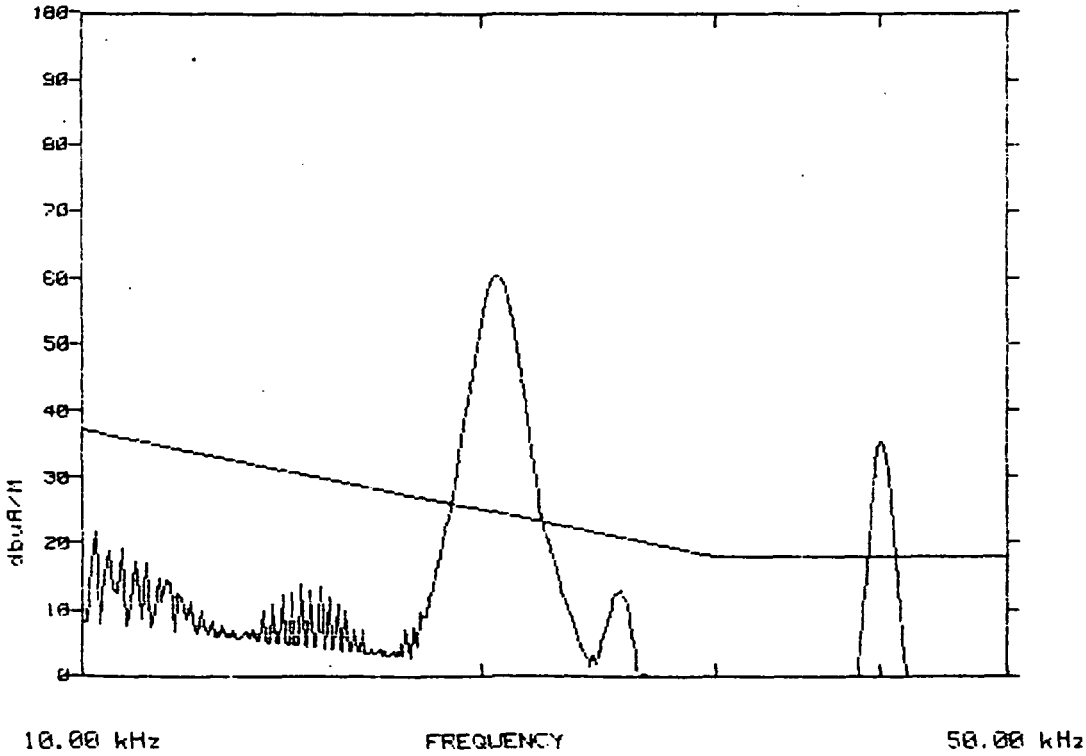

FIGURE 16.9: EMI RE01 Pre-Scan on Unshielded Cable, showing significant radiation at fundamental (20 kHz) and its 2nd harmonic. The hash at lower frequency is ambient noise.

EATON DATA ACQUISITION SYSTEM

E.U.T. : INDUCTION GENERAL/NASA CABLE DATE 08 FE
TEST PROCEDURE :RE04 PRESCAN
COMMENTS :AMBIENT
TEST ENGINEER :B. SMITH

SCAN PARAMETERS						TEST TITLE :RE04 PRESCAN
Rvr	Start Freq	Stop Freq	Bandwidth	Atten	Detector	Transduc
7	1 kHz	50 kHz	100 Hz	0 dB	PEAK	ALP-10

GLOBAL PARAMETERS

BROAD BAND CORRECTION: NO | SWEEP RATE: 1000 Samples/Sec

LIMIT LINE : RE04

SCANS PER SEGMENT : 1

SEG 1 START TIME: 08:46:55 STOP TIME: 08:47:46

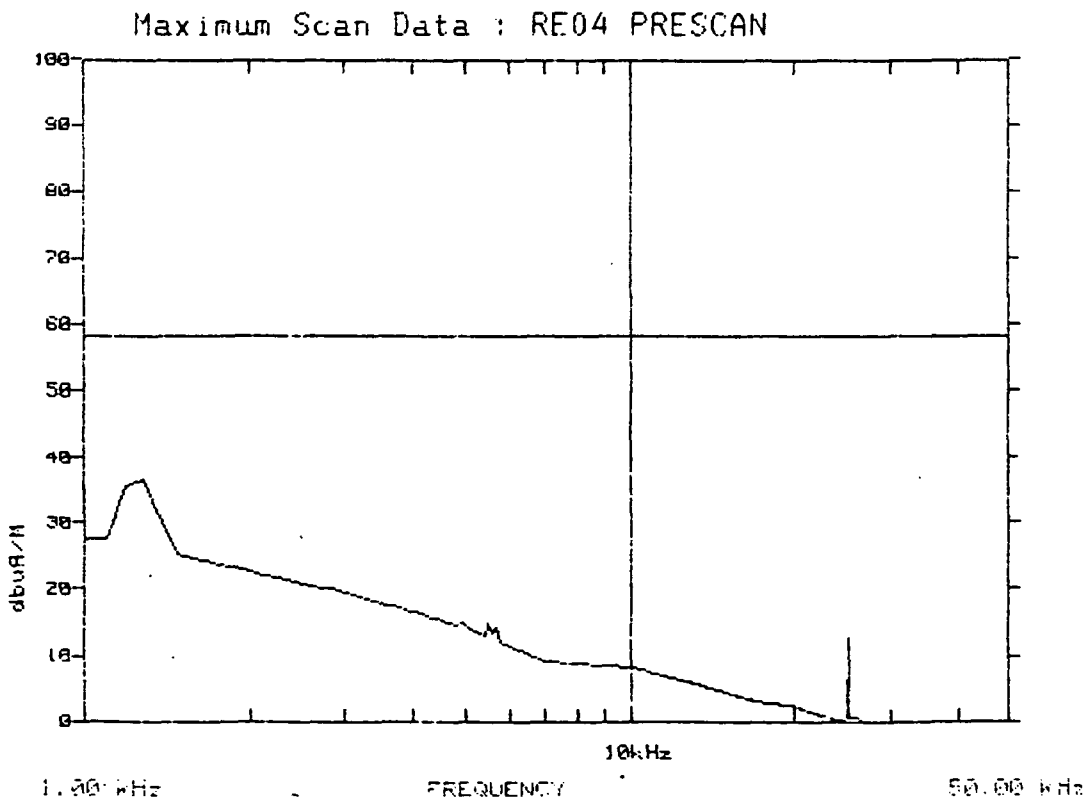

FIGURE 16.10: EMI RE04 (and RE01) Ambient Scan, showing higher ambient at lower frequencies.

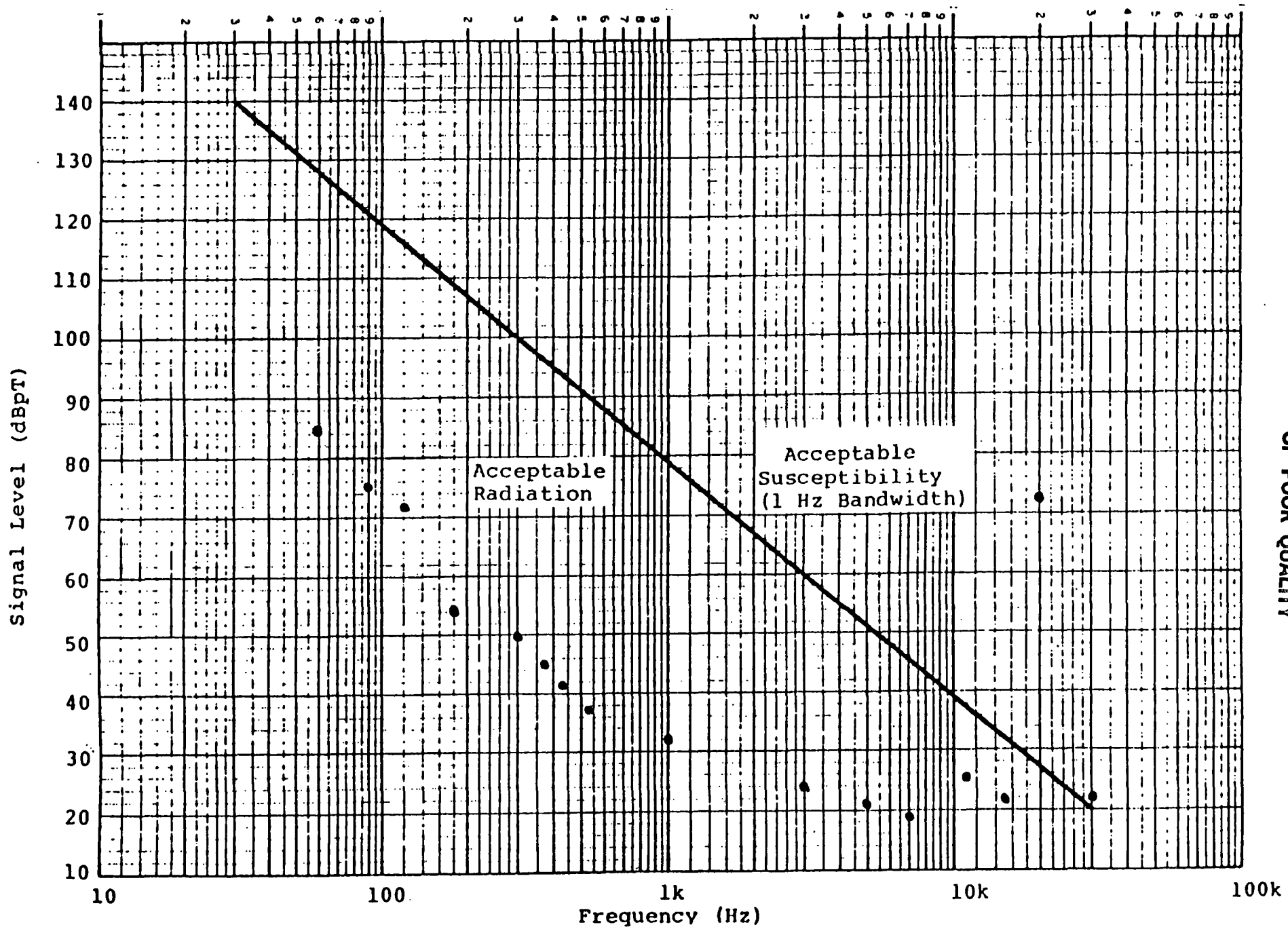

FIGURE 16.11: EMI RE01 Test Results on Unshielded Cable

ORIGINAL PAGE IS
OF POOR QUALITY

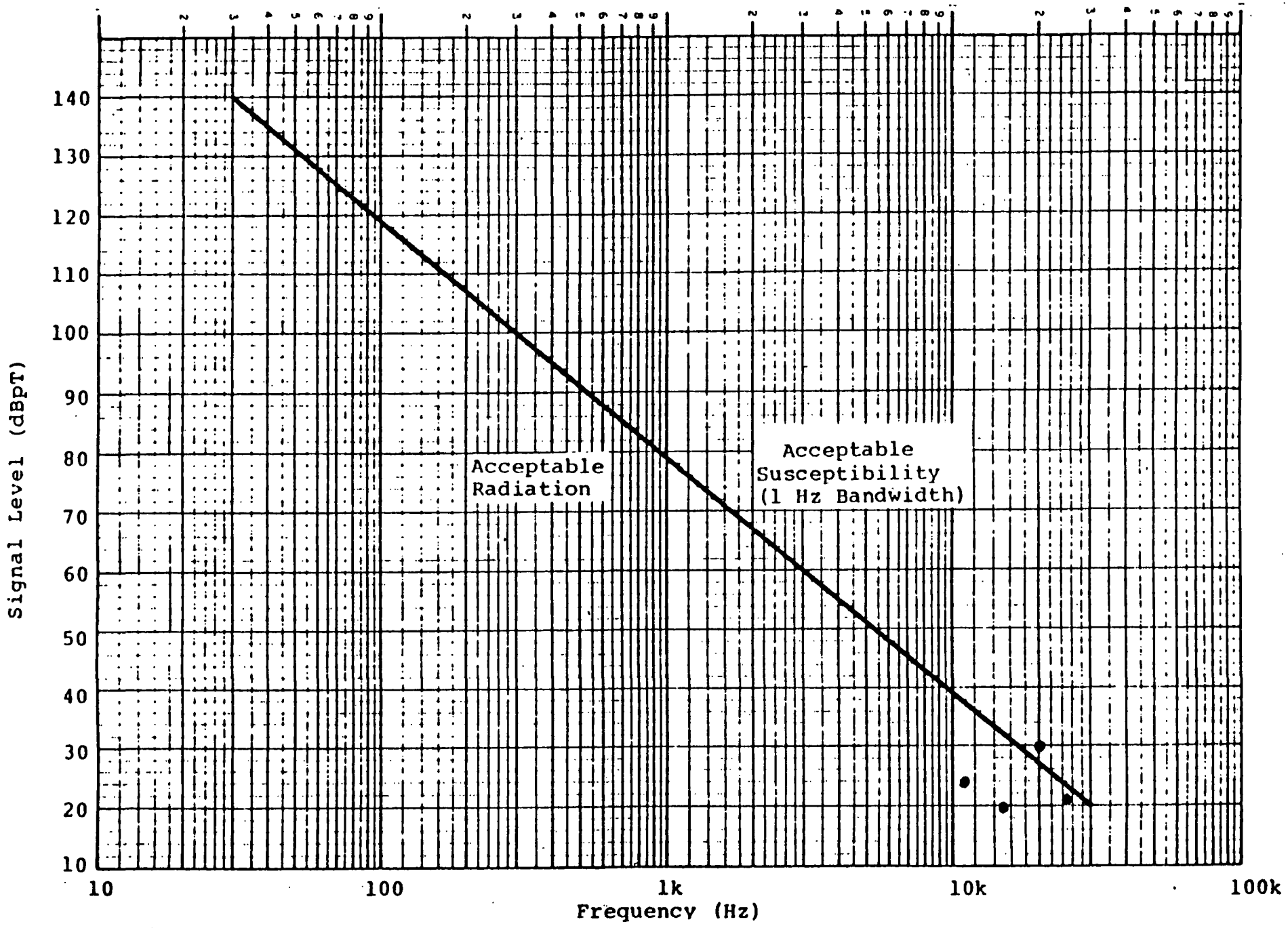

FIGURE 16.12: EMI RE01 Test Results on Cable Shielded with 2-inch EMT

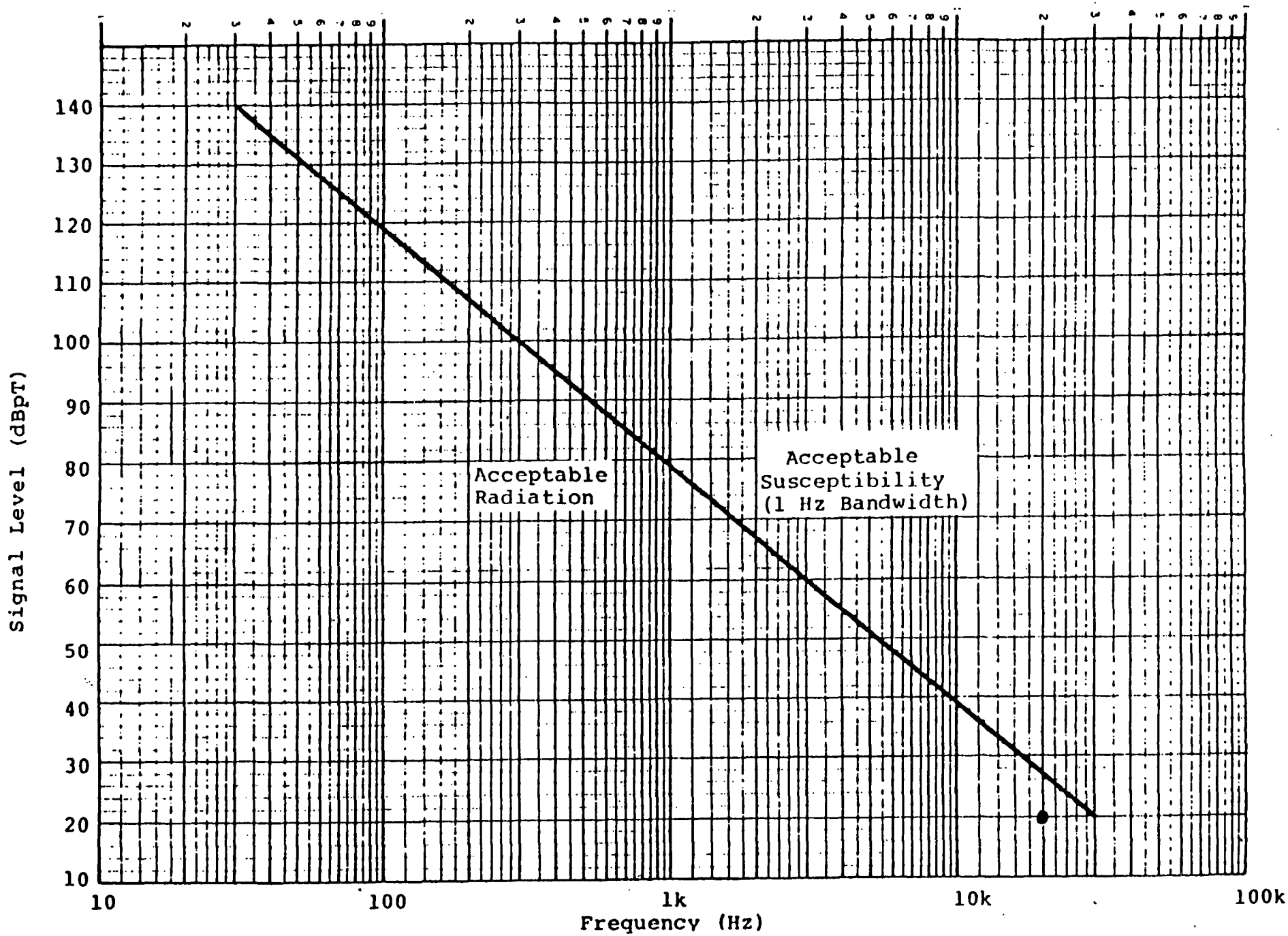

FIGURE 16.13: EMI RE01 Test Results on Cable Shielded with 2-inch Copper Tube

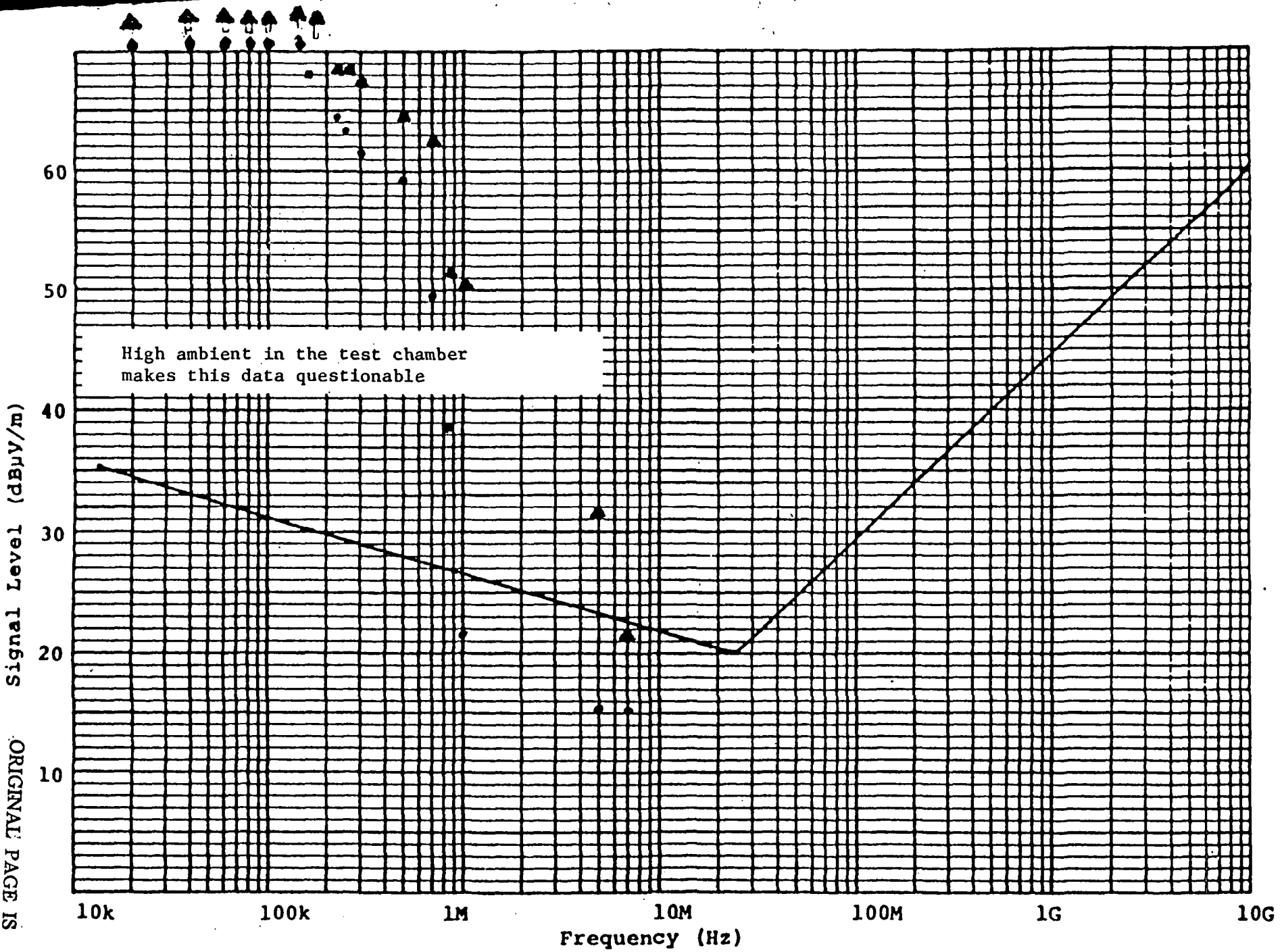

FIGURE 16.14: EMI RE02 Narrow Band Test Results on Unshielded Cable

ORIGINAL PAGE IS
OF POOR QUALITY

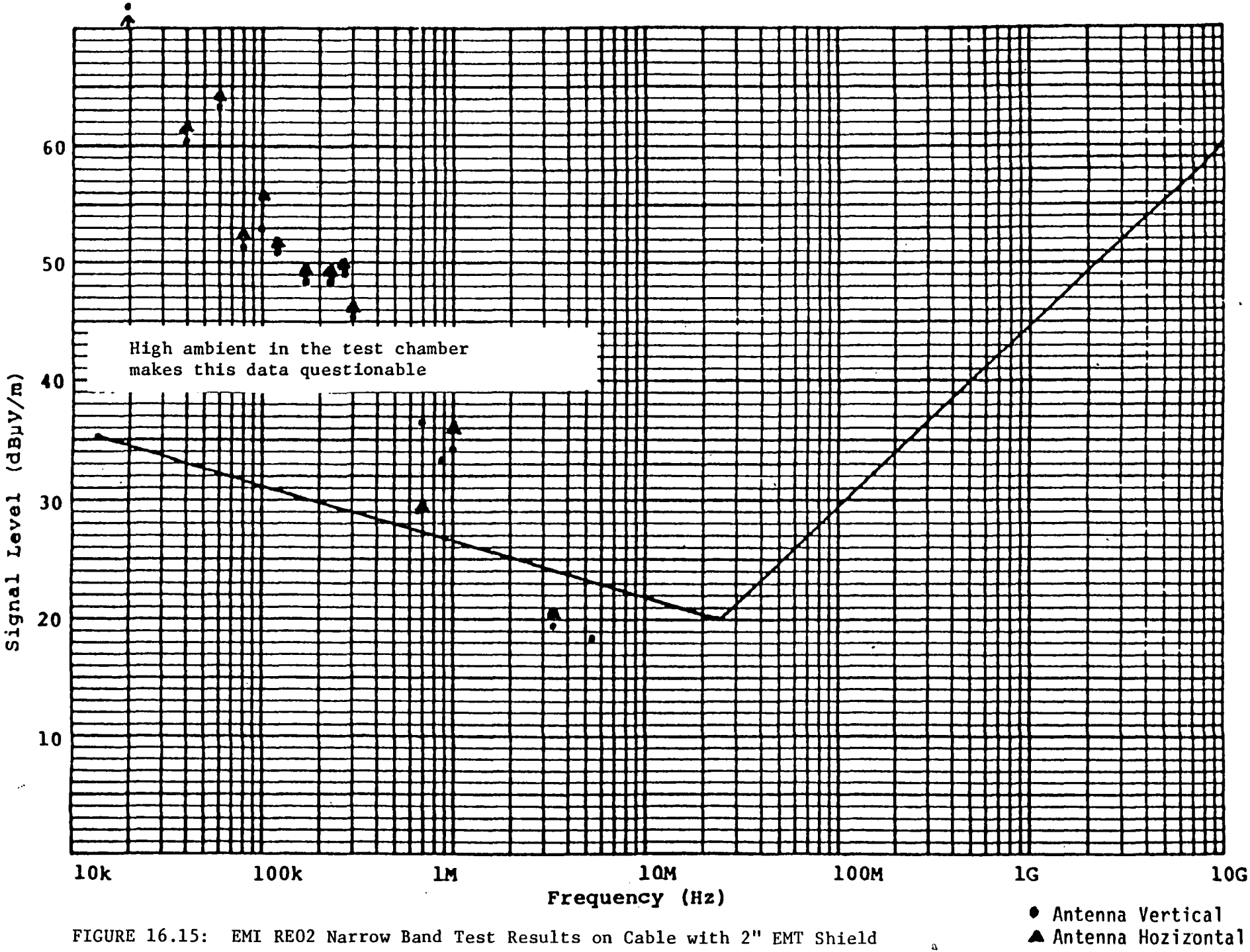

FIGURE 16.15: EMI RE02 Narrow Band Test Results on Cable with 2" EMT Shield

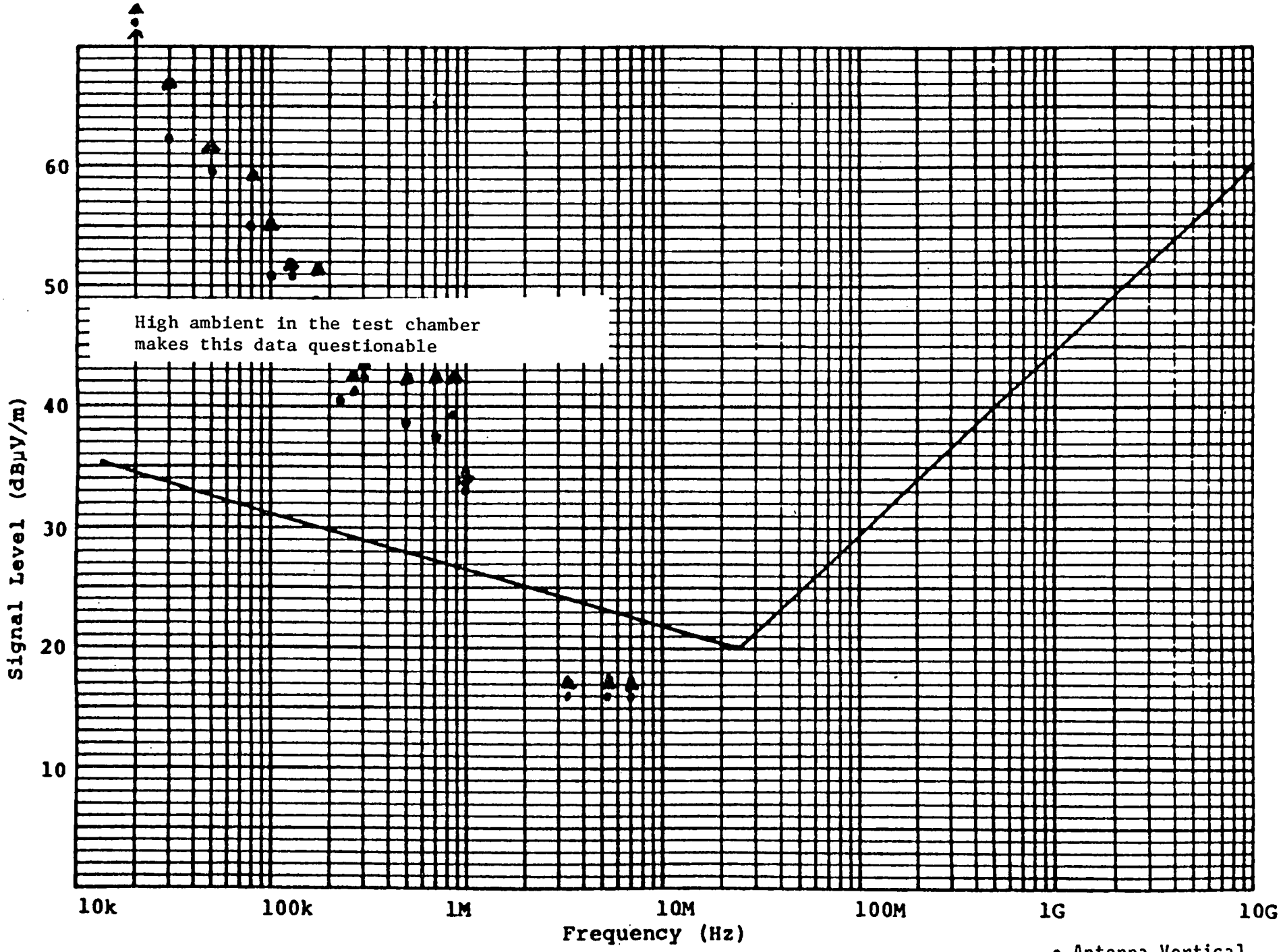

FIGURE 16.16: EMI RE02 Narrow Band Test Results on Cable with Copper Shield

• Antenna Vertical
▲ Antenna Horizontal

ORIGINAL PAGE IS
OF POOR QUALITY

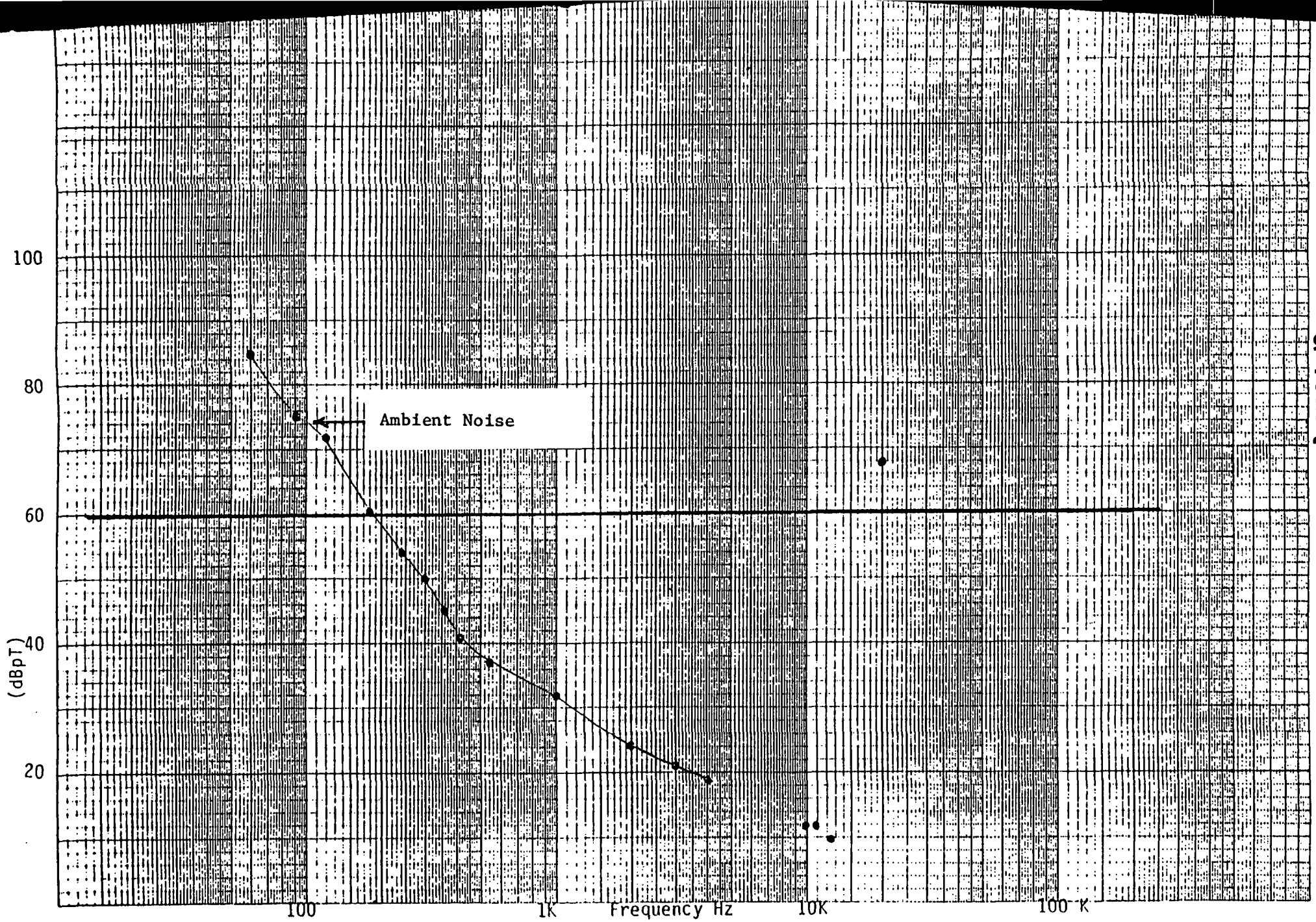

FIGURE 16.17: EMI RE04 Test Results on Unshielded Cable (Antenna Vertical)

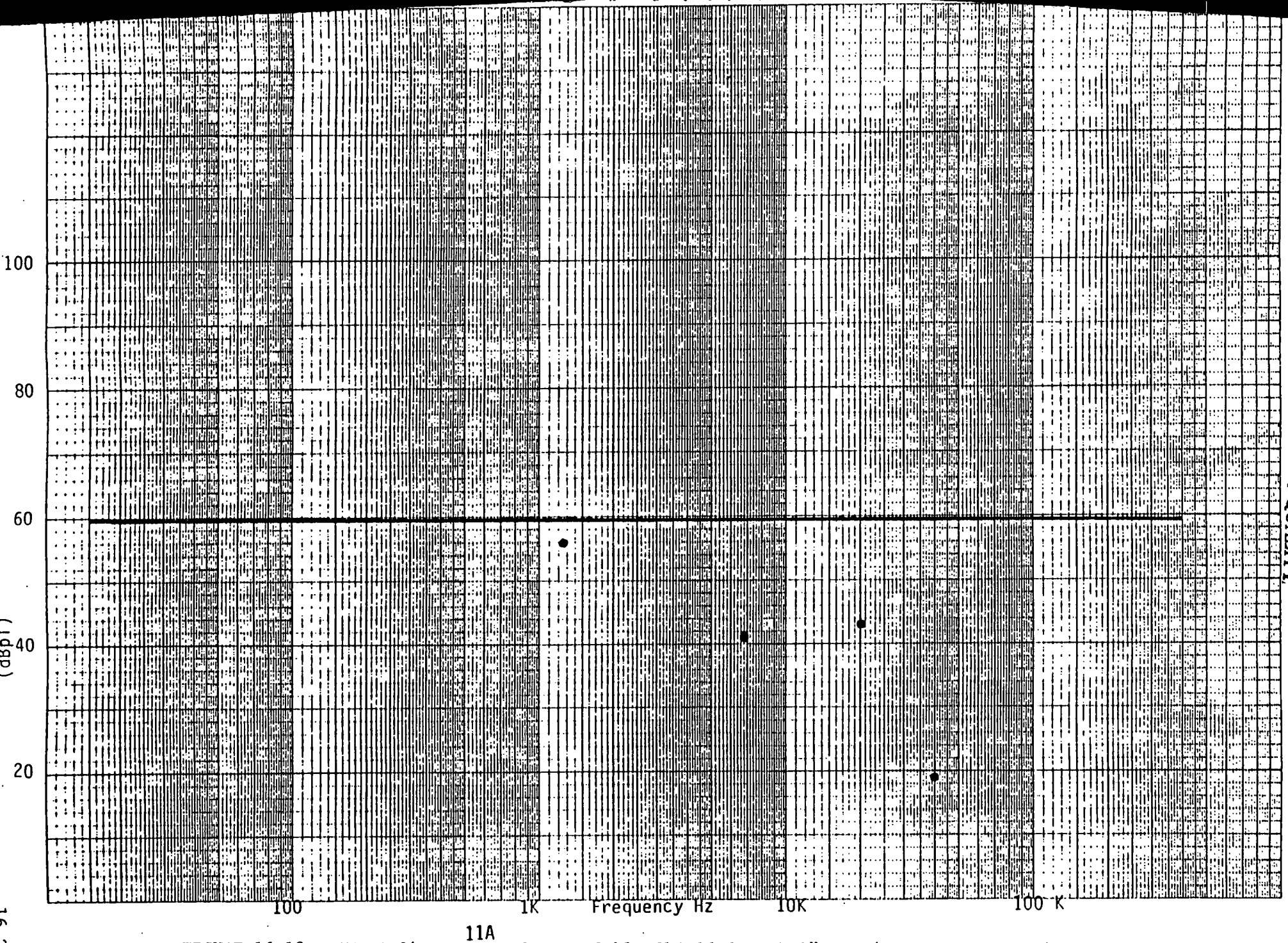

FIGURE 16.18: EMI RE04 Test Results on Cable Shielded with 2" EMT (Antenna Vertical)

ORIGINAL PAGE IS
OF POOR QUALITY

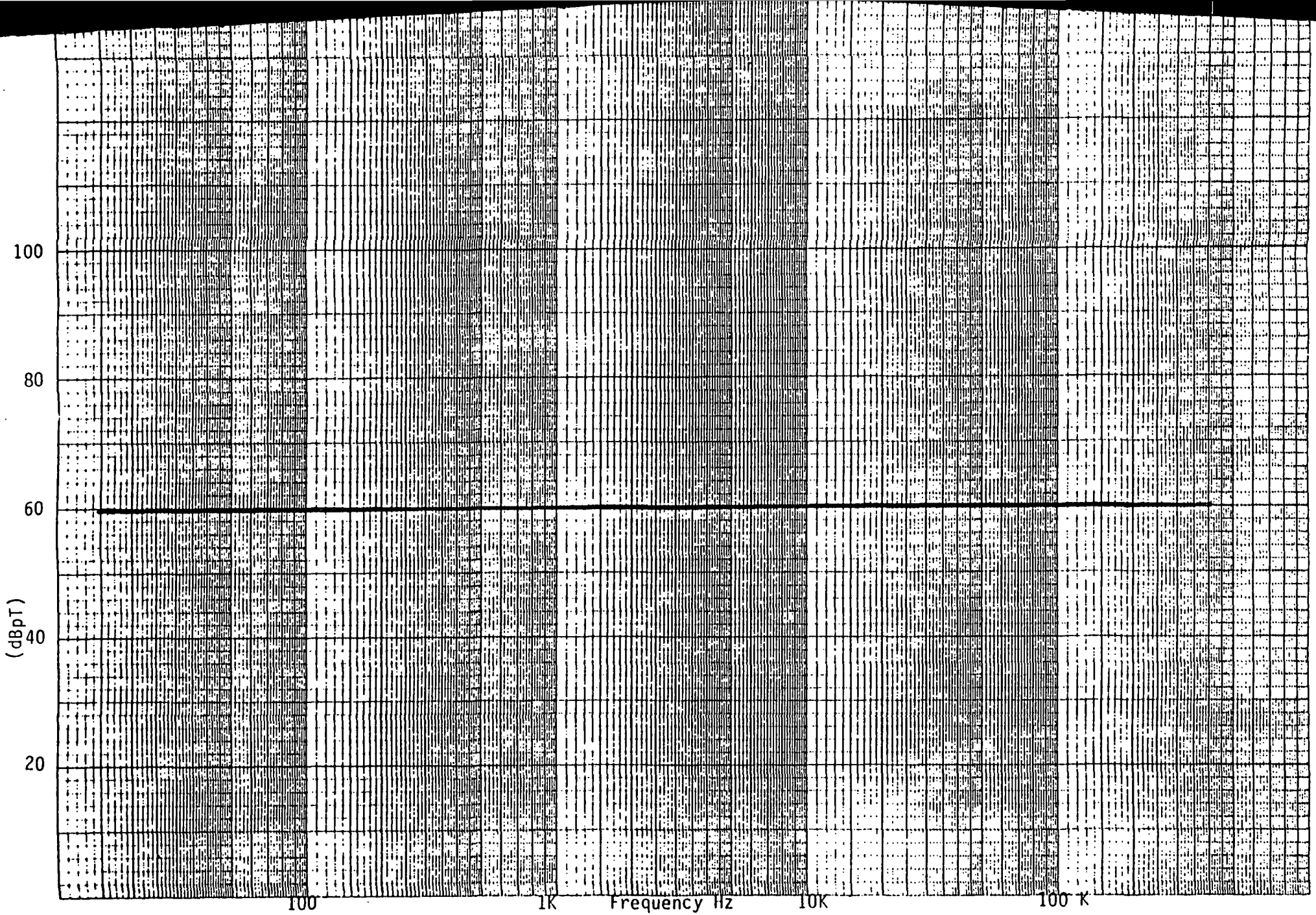

FIGURE 16.19: EMI RE04 Test Results on Cable Shielded with 2" Copper Tubing. All readings were below the detection system sensitivity (zero db).

ORIGINAL PAGE IS OF POOR QUALITY

Since the magnetic radiations, RE01 at 7 cm and RE04 at 1 meter, at 20 kHz are of our primary interest at present, they are summarized in Table 16.8. The RE04 data in that table is questionable, as the EMI of EMT shielded cable at 1 meter (RE04) shows higher db than that at 7 cm (RE01) distance. This conflicts with the engineering judgment. At any rate, the table indicates that the unshielded cable does not meet the magnetic radiation limits of MIL-STD-462, Section RE01. The reasons for this, as identified earlier, are as follows:

1) The pressure buildup in the extrusion die discussed in Section 15.0 made the middle strap wider than the outer straps. This caused the end-fringing flux to extend farther from the cable. If the middle strap was shorter than the outer straps (as was designed), the end flux would have been contained close to the cable, as explained in Section 4.2.

2) The manufacturing variations caused inductances of the two outer straps, with respect to the middle strap, to be unequal. The resulting unequal currents in the outer straps caused a small part of the cable to act as a flux-emitting solenoid, as explained in para (2) of Section 16.3.

Both of the above sources of the EMI are related with the manufacturing difficulties experienced in the first prototype construction. Future manufacturing improvements, based on the experience gained, can eliminate both of the above EMI sources. For example, Figure 16.20 shows how the end-fringing flux can be minimized by rolling the outer straps over the middle strap. The cable, thus made with symmetrical outer straps, is expected to meet the EMI limits, possibly without a shield or with a shield of thin, high permeability magnetic tape (one mil thick of negligible weight) wrapped around it.

TABLE 16.8
SUMMARY OF EMI MEASUREMENTS ON THE CABLE
PER MIL-STD-462 AND 461B

TEST CONDITION	EMI db at 20 kHz over 1 picotesla[1]	
	RE01 at 7 cm (limit 27 db)	RE04 at 1 m (limit 58 db)
Unshielded Cable	73 db	68
Cable shielded with EMT, electromagnetic (mild steel) tubing	30	43[2]
Cable shield with conductive (copper) tubing	20	Less than meter sensitivity

(1) These tests were made at 5 A cable current. To extrapolate them to the rated current of 60 A, add 20 log (60/5) = 22 db in these readings.

(2) This, being at a 1-meter distance, does not make sense, as it is higher than 30 db measured at 7 cm.

(3) See Figure 16.20 for recommended manufacturing improvements to reduce EMI to the specified limits.

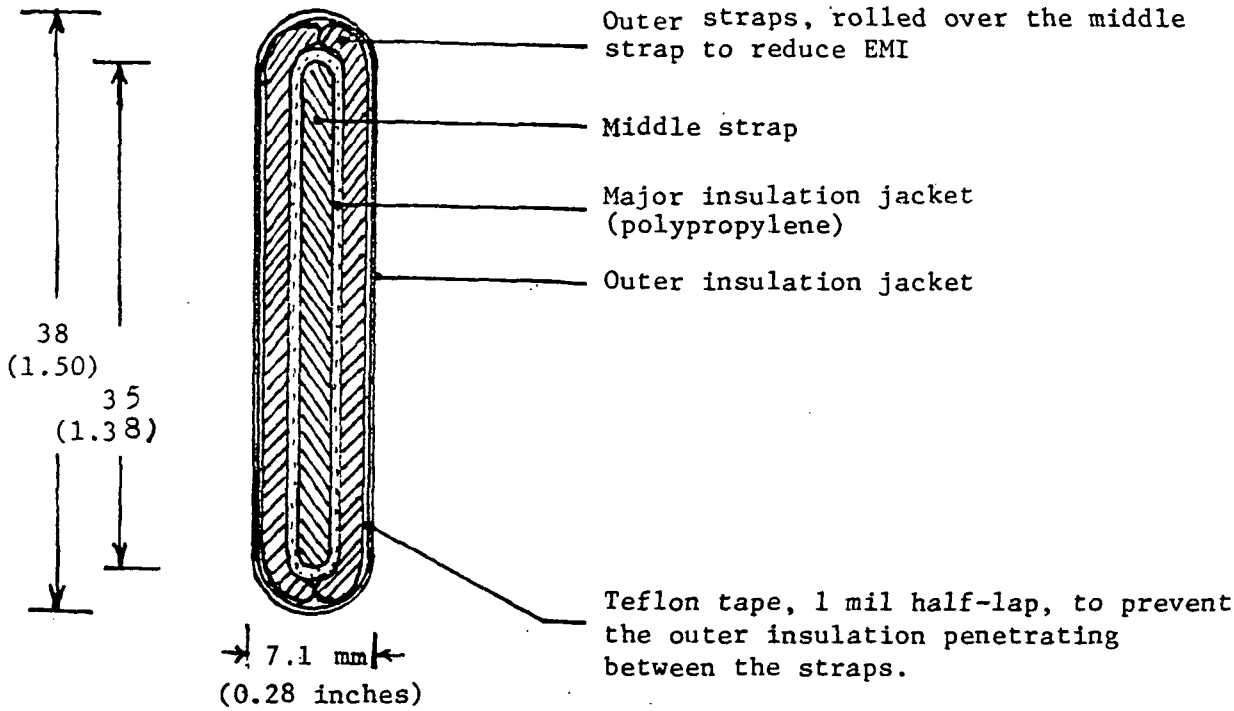

FIGURE 16.20: RECOMMENDED MANUFACTURING IMPROVEMENTS.

Outer straps rolled over the middle strap will close the main leakage point at the cable edges, thus further minimizing the EMI. Such a cable made with improved symmetry in the outer straps is expected to meet the specified EMI limit.

APPENDIX A

EDDY LOSSES IN LITZ STRAPS LINES DUE TO TRANSVERSE FLUX

Let us consider a round wire situated in an alternating magnetic flux, the flux density being distributed linearly as shown in Figure A.1. We shall neglect the demagnetizing effect of the eddy currents on the magnetizing flux. This is possible when the wire diameter is much smaller than the skin depth, as is true in the present case.

Consider a longitudinal cross section of the wire as shown in Part (C) of Figure A.1. An alternating e.m.f. will be induced in the conductor and short circuited eddy currents will flow as shown. To quantify the phenomenon, let us consider an elemental width dx at distance x from the wire axis.

Let J_x = current density at distance x

B_x = flux density at distance x

$\emptyset_x$ = flux linking with the loop at x

l = length of the current path (loop)

t = time

d_o = wire diameter or dimension perpendicular to the flux in rectangular conductor

ρ = resistivity of the conductor material

As eddy current path is short circuited, the difference in e.m.f.s is equal to the difference in voltage drops in the short-circuited paths at x and at x+dx, i.e.

$$\frac{\partial B_x}{\partial t}\, l dx = \left(J_x + \frac{\partial J_x}{\partial x}\, dx\right) d\cdot dx \;\; \frac{\rho l}{d\cdot dx} \;\; - J_x d\cdot dx \; \frac{\rho l}{d\cdot dx}$$

or $$\frac{\partial B_x}{\partial t}\, dx = \rho \, \frac{\partial J_x}{\partial x}\, dx$$

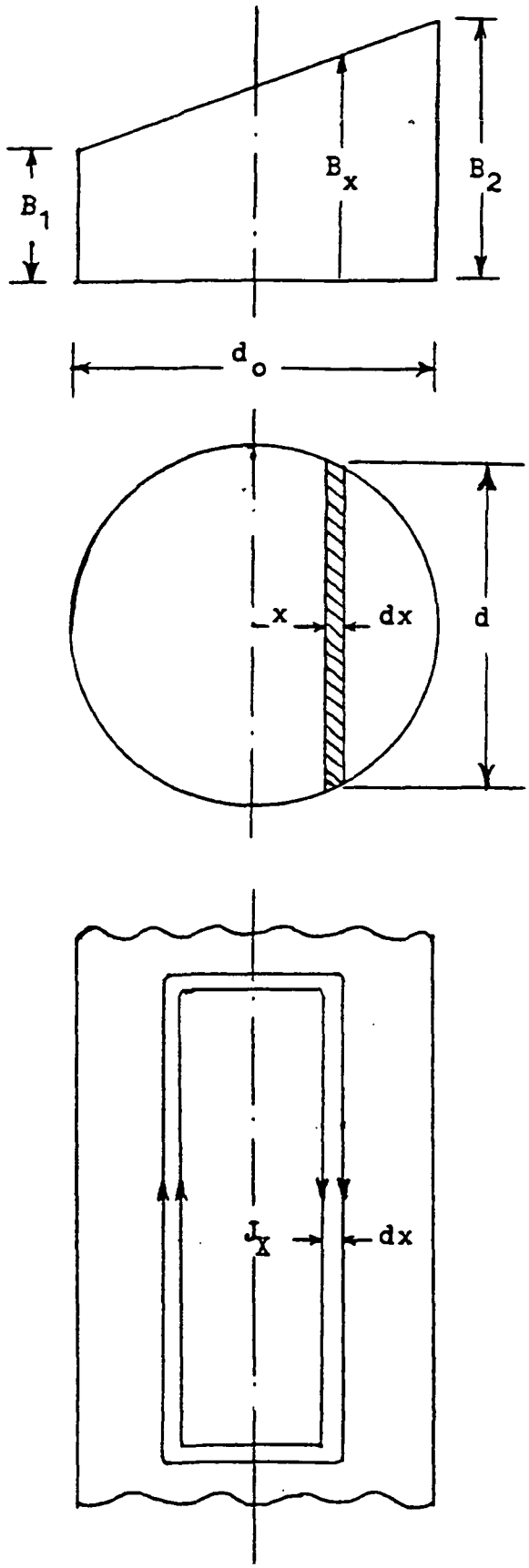

(a) Space varying magnetic field

(b) Elementary volume under analysis

(c) Eddy current loop

FIGURE A.1: Eddy Currents in Round Conductor placed in transverse magnetic field

We neglected the leakage reactance drop because it is small in comparison with the resistance drop. For sinusoidal time variations, substituting $\partial/\partial t = \omega$, the above equation becomes:

$$\rho \frac{\partial J_x}{\partial x} = B_x \omega$$

From Figure A.1 (a),

$$B_x = \frac{B_2+B_1}{2} + \frac{B_2-B_1}{d_o} x = A + Bx, \text{ say}$$

$$\text{where} \quad A = \frac{B_2+B_1}{2} \quad \text{and} \quad B = \frac{B_2-B_1}{d_o} .$$

$$\text{Thus,} \quad \frac{\partial J_x}{\partial x} = A \frac{\omega}{\rho} + Bx, \text{ whose solution is:}$$

$$J_x = \frac{\omega}{\rho} \left(AX + B \frac{x^2}{2} \right) + C$$

The integration constant C can be found from the condition that the sum of all eddy currents in the conductor cross section is equal to zero, because the eddy currents are short circuited ones. Another way of looking at this is that the eddy currents at +x and -x are equal and opposite. Therefore,

$$\int_{-do/2}^{+do/2} J_x dx = 0, \text{ from which we get}$$

$$C = -\frac{\omega B do^2}{24\rho}$$

$$\therefore J_x = \frac{\omega}{\rho} \left[AX + \frac{Bx^2}{2} - \frac{Bd_o^2}{24} \right]$$

If we use rms values of the flux densities A and B, then J_x will be rms. The eddy current losses per unit volume at x is $J_x^2\rho$, and per elementary volume of one meter length, width dx and height d is $J_x^2\rho d \cdot dx$. The total eddy losses per meter length are then given by integrating this, i.e.

$$P\ eddy = \int_{-\frac{do}{2}}^{+do/2} d \cdot \rho\ J_x^2 \cdot dx \qquad (A.1)$$

We now define the transverse eddy loss factor

$$K_t = \frac{\text{DC Losses + Eddy Losses}}{\text{DC Losses}} \quad \text{, so that}$$

$$R_{ac} = K_t R_{dc} \ .$$

The dimension d in round wire varies with x. The eddy losses in the entire round wire is then found by double integration of the above equation. If there are N strands arranged as shown in Figure A.2, and the flux density varies from B_o at the inner edge to zero at the outer edge of the strap, then the total eddy losses can be found by the third integration over all the strands. At the end of these three integrating processes, we found the factor K_t

$$K_t = 1 + \frac{0.8 f^2 N^2 d_o^{\ 6}}{\rho^2 b^2 E12} \text{ for round wires,} \qquad (A.2)$$

where d_o is the dimension perpendicular to the flux direction.

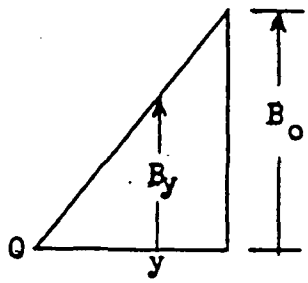

(a) Magnetic field linearly varying from zero to maximum across the strap thickness dimension

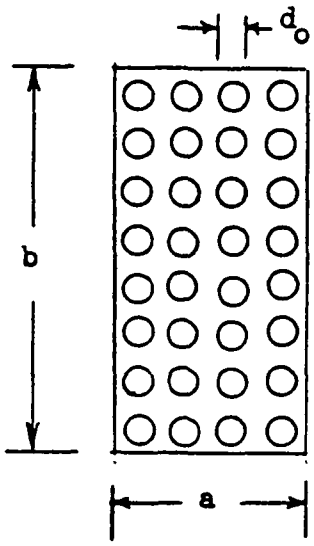

(b) Strap made of numerous fully transposed conductor strands of diameter d_o

FIGURE A.2: Rectangular Strap of Round Strands placed in transverse magnetic field varying from B_o at one edge and zero at the other edge

APPENDIX B

PARAMETRIC STUDY ON 2-STRAP CABLE CONFIGURATION

This Appendix contains the following:

(1) Computer Program Listing (BASIC)

(2) List of Computer Symbols (SI Units)

(3) Computer Output Sample (Copper and PVC)

(4) Figures B.1 to B.5, depicting Resistance, Inductance, Capacitance and Mass of 2-strap cable with copper and aluminum conductors. Computations were made for major insulation thickness d ranging from 1 to 3 mm, strap thickness a from 1 to 4 mm, and strap width from 50 to 100 mm.

LIST OF COMPUTER SYMBOLS IN SI UNITS

D1=MASS DENSITY OF CONDUCTOR
D2=MASS DENSITY OF INSULATION
KF=FILL(SPACE) FACTOR OF STRAP
D0=STRAND DIAMETER
R0=RESISTIVITY OF CONDUCTOR
F=FREQUENCY
E=RELATIVE PERMITIVITY OF INSULATION
E0=ABSOLUTE PERMITIVITY OF FREE SPACE
M0=ABSOLUTE PERMEABILITY OF FREE SPACE
J=CASE(RUN) NUMBER COUNTER
PI=3.1416
D=INSULATION THICKNESS BETWEEN STRAPS
A=CONDUCTOR STRAP THICKNESS
B=CONDUCTOR STRAP WIDTH(HEIGHT)
N=NUMBER OF STRANDS IN ONE STRAP
KS=SKIN EFFECT EDDY LOSS FACTOR
KC=CABLING(STRAPING) LENGTH FACTOR
KT=TRANSVERSE FLUX EDDY LOSS FACTOR

RA=AC RESISTANCE, MILLIOHMS
L=INDUCTANCE, MILLIHENRIES
C=CAPACITANCE, MICROFARADS
WC=WEIGHT OF CONDUCTOR
WI=WEIGHT OF INSULATION
WT=TOTAL WEIGHT WITHOUT SHIELD
V/MM=DIELECTRIC STRESS, VOLTS/MM
V/MIL=DIELECTRIC STRESS, VOLTS/MIL
L = EXPONENT

COMPUTER PROGRAM LISTING (BASIC)

```
5 LPRINT CHR$(30) "HI-FREQ TR. LINE DESIGN"
6 LPRINT "  "
10 READ D1,D2,KF
20 DATA 8640,1340,0.40
30 READ D0,R0,F
40 DATA 0.25E-3,2.2E-8,20E3
50 READ E,E0,M0,PI
60 DATA 2.7,8.85E-12,12.5664E-7,3.1416
70 LPRINT CHR$(30) "INPUT DATA"
80 LPRINT "  "
90 LPRINT CHR$(30) "D1,D2,KF=";D1;D2;KF
100 LPRINT
110 LPRINT CHR$(30) "D0,R0,F=";D0;R0;F
120 LPRINT
130 LPRINT "E,E0=";E;E0
135 LPRINT "P1,M0=";PI;M0
140 LPRINT "  "
150 REM MAIN COMPUTATIONS
155 LPRINT
156 J=1
160 FOR D=.001 TO .003 STEP .0005
170 FOR A=.001 TO .003 STEP .0005
180 FOR B=.050 TO .100 STEP .010
190 N=4*KF*A*B/(PI*D0[2)
210 KS=1.00
220 KC=1.15
230 KT=D0[6/(R0[2*B[2*1E12)
240 KT=1+0.8*F[2*N[2*KT
250 RA=100*KS*KC*KT*R0*1E3/(KF*A*B)
260 L=50*M0*(D+0.667*A)*1E6/B
270 C=50*B*E*E0*1E6/D
280 WC=100*KF*A*B*D1*KC
290 WI=50*3*D*B*D2
300 WT=WC+WI
304 LPRINT"  "
305 LPRINT "CASE NO. ";J
306 LPRINT "  "
310 LPRINT "B,A,D=";B;A;D
320 LPRINT
330 LPRINT "N,KT=";N;KT
335 LPRINT "  "
338 LPRINT "V/MM,V/MIL=";1/D;.025/D
340 LPRINT "  "
344 LPRINT "MAIN LINE PARAMETERS"
346 LPRINT "  "
350 LPRINT "RA,L,C=";RA;L;C
360 LPRINT
370 LPRINT "WC,WI,WT=";WC;WI;WT
380 LPRINT "  "
385 J=J+1
390 NEXT B
395 LPRINT
400 NEXT A
405 LPRINT
410 NEXT D
415 LPRINT "  "
450 END
```

ORIGINAL PAGE IS
OF POOR QUALITY

COMPUTER OUTPUT SAMPLE (COPPER AND PVC)

HI-FREQ TR. LINE DESIGN

INPUT DATA

```
D1, D2, KF= 8640   1340   .4
D0, R0, F= 2.5E-04   2.2E-08   20000
E, E0= 2.7   8.85E-12
PI, M0= 3.1416   1.25664E-06
```

CASE NO. 1

```
B, A, D= .05   1E-03   1E-03
N, KT= 407.435   1.01072

V/MM, V/MIL= 1000   25

MAIN LINE PARAMETERS

RA, L, C= 127.856   2.09482   .0597375
WC, WI, WT= 19.87   10.05   29.92
```

CASE NO. 2

```
B, A, D= .06   1E-03   1E-03
N, KT= 488.922   1.01072

V/MM, V/MIL= 1000   25

MAIN LINE PARAMETERS

RA, L, C= 106.547   1.74568   .071685
WC, WI, WT= 23.85   12.06   35.91
```

•
•
•

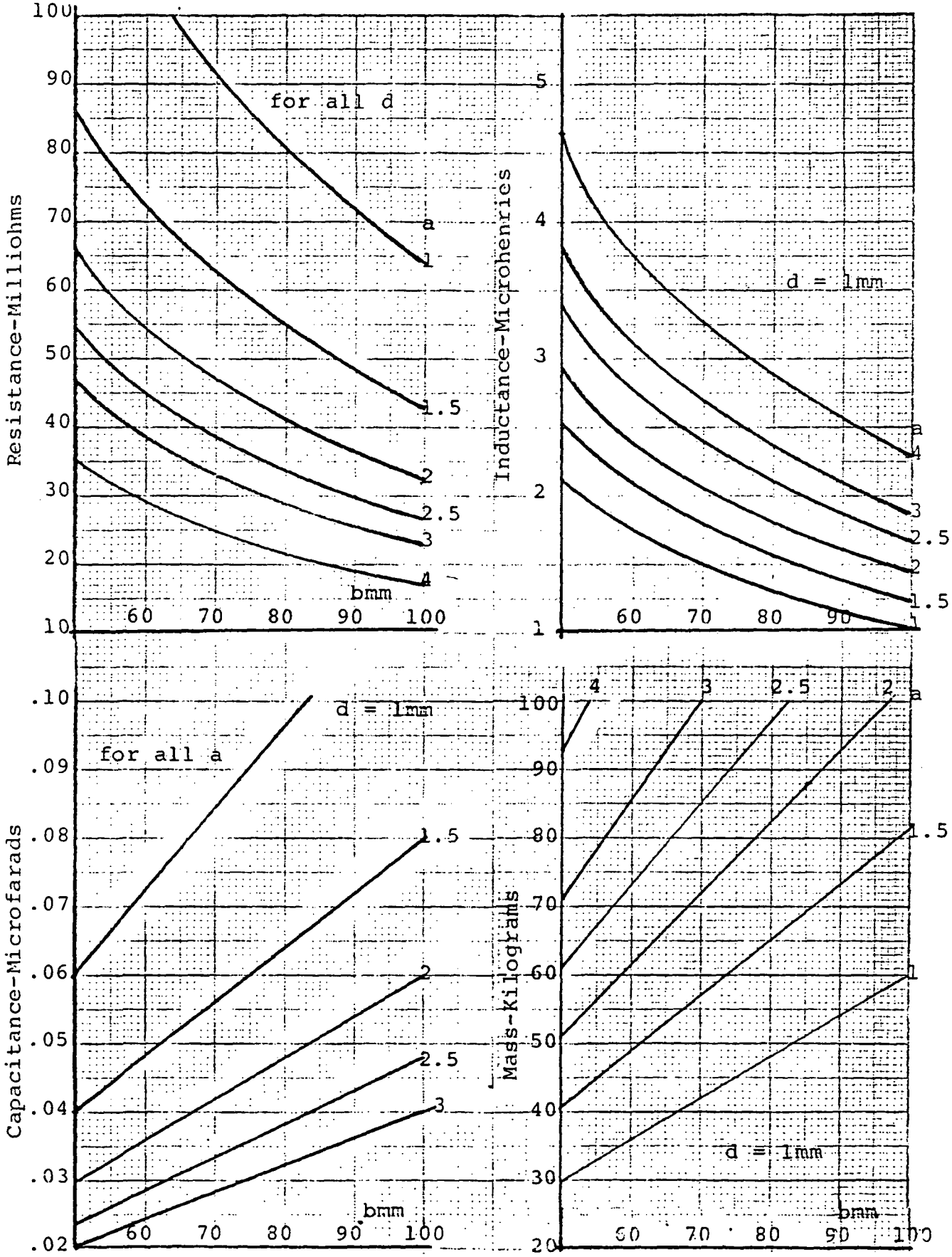

FIGURE B.1: Resistance, Inductance, Capacitance and Mass of two Parallel Straps with Copper Conductor and 1 mm insulation thickness

ORIGINAL PAGE IS
OF POOR QUALITY

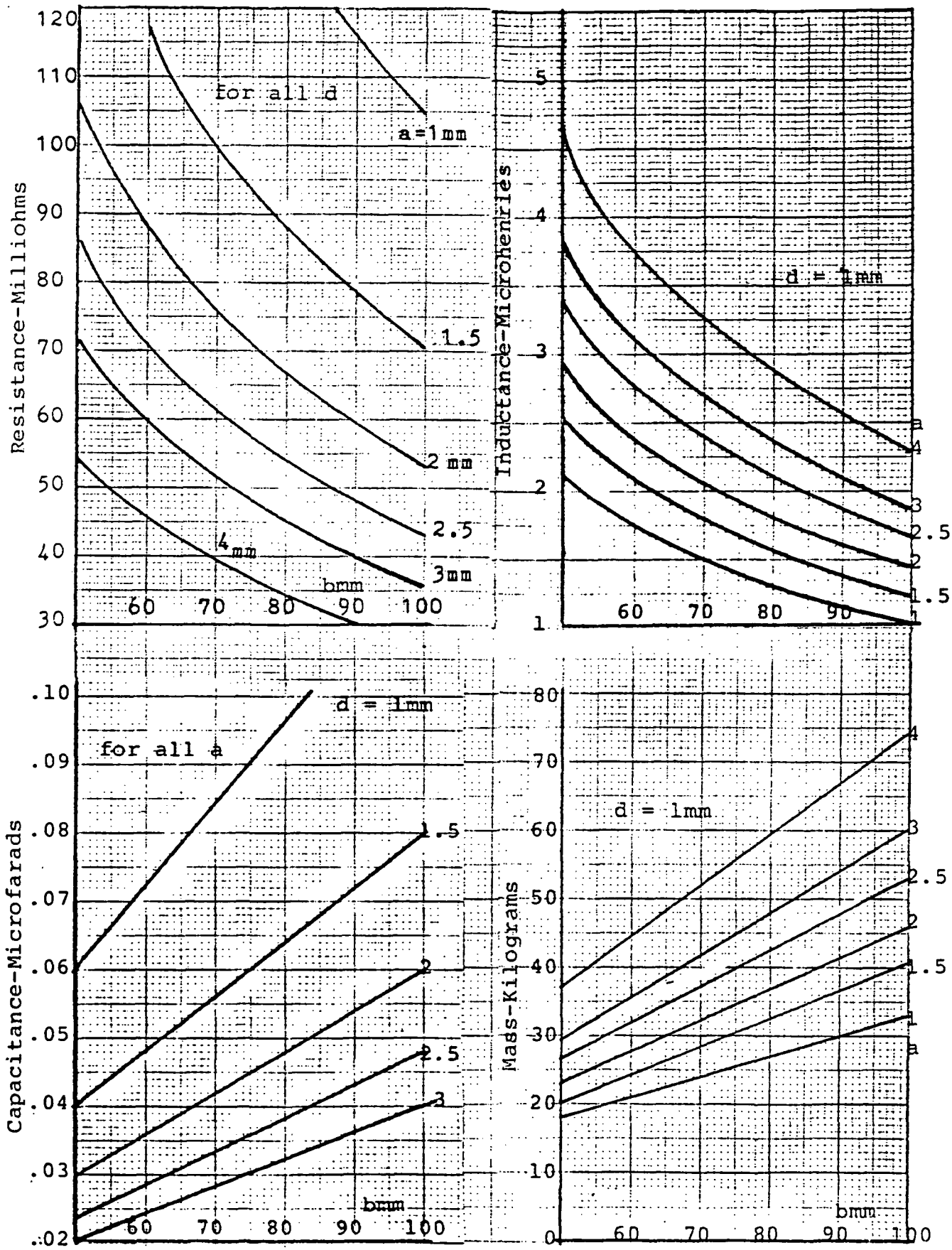

FIGURE B.2: Resistance, Inductance, Capacitance and Mass of two Parallel Straps with Aluminum Conductor and 1 mm insulation thickness

ORIGINAL PAGE IS
OF POOR QUALITY

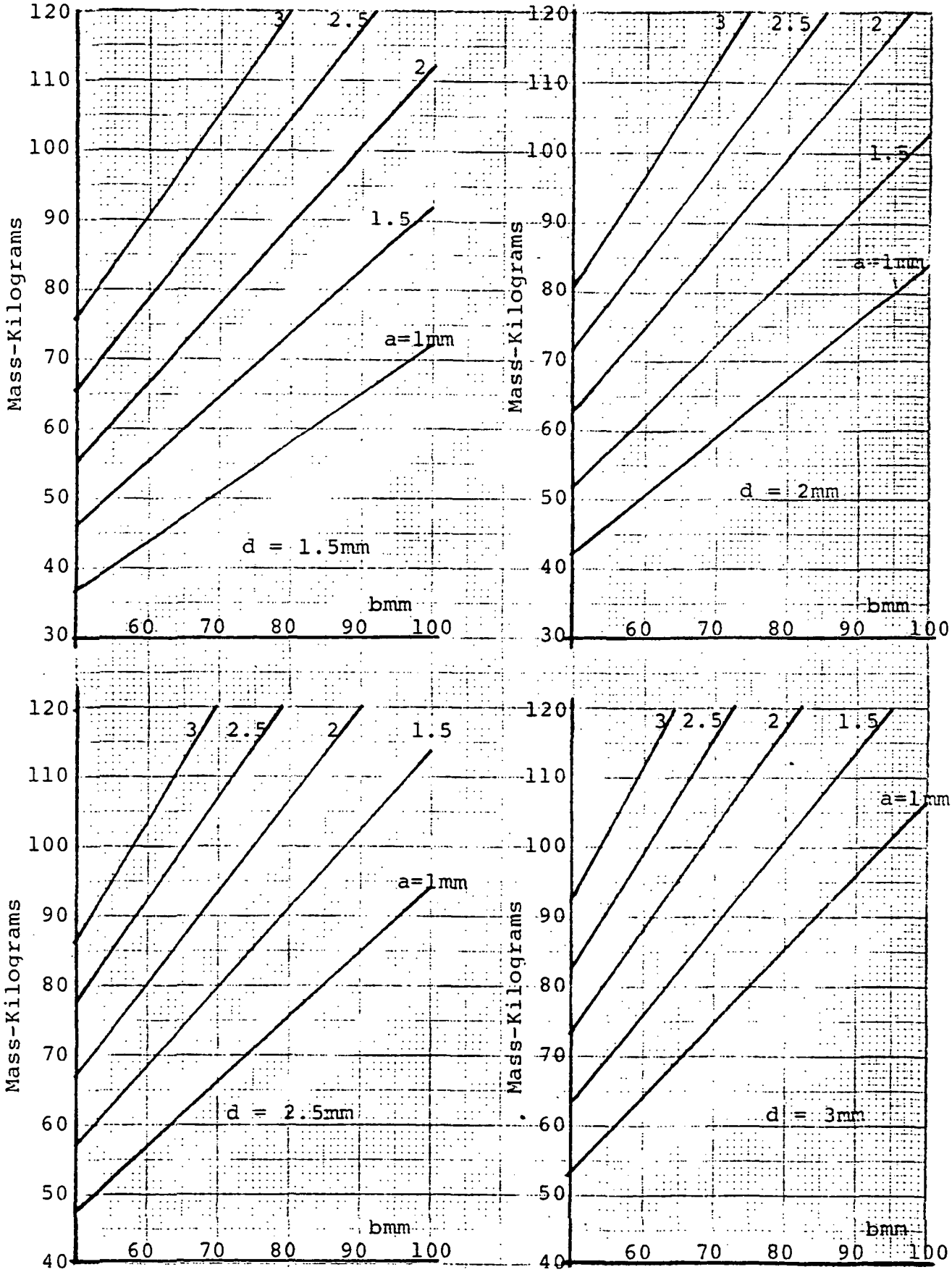

FIGURE B.3: Mass of Parallel Straps with Copper Conductor and different insulation thicknesses

ORIGINAL PAGE IS OF POOR QUALITY

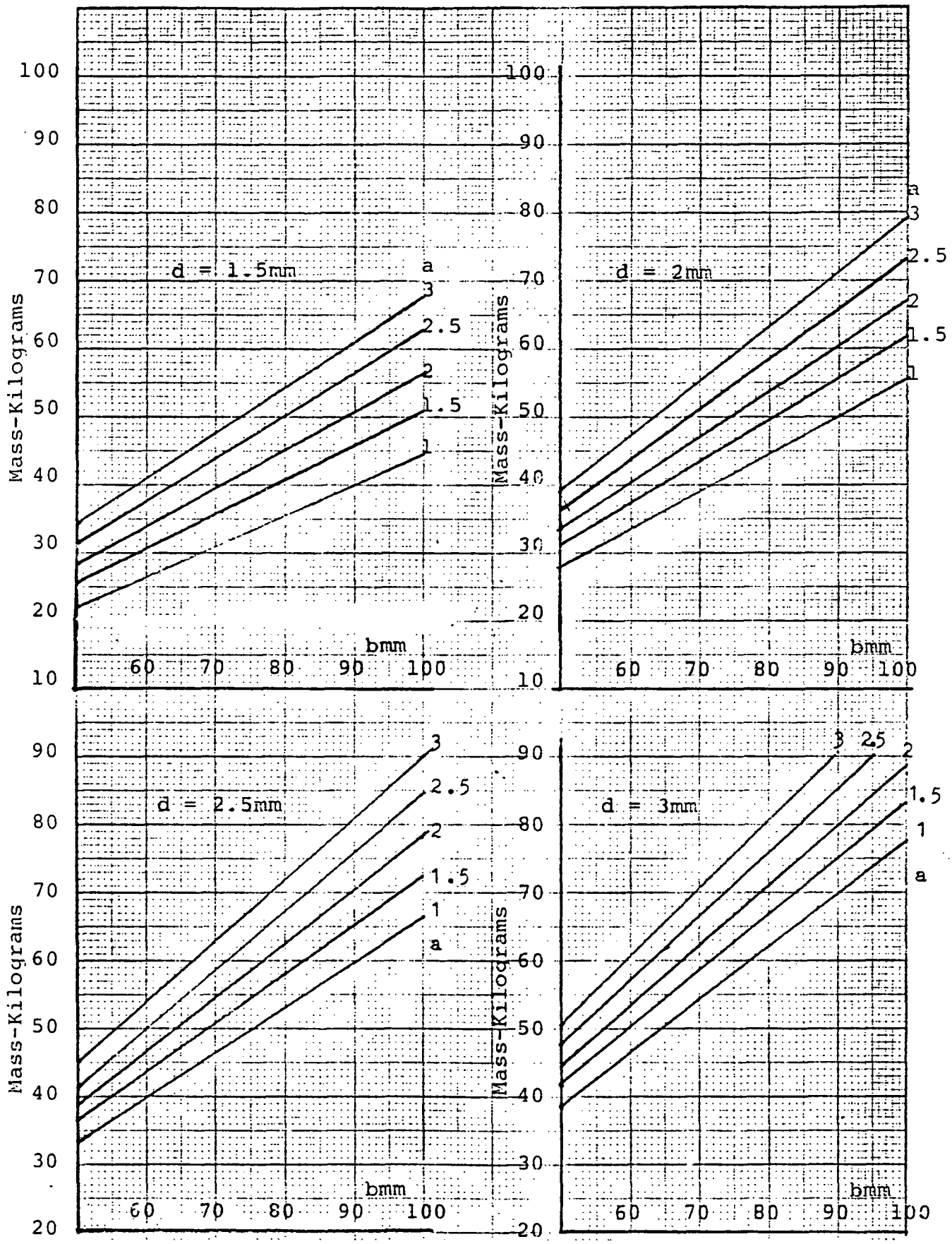

FIGURE B.4: Mass of Parallel Straps with Aluminum Conductor and different insulation thicknesses

ORIGINAL PAGE IS
OF POOR QUALITY

ORIGINAL PAGE IS
OF POOR QUALITY

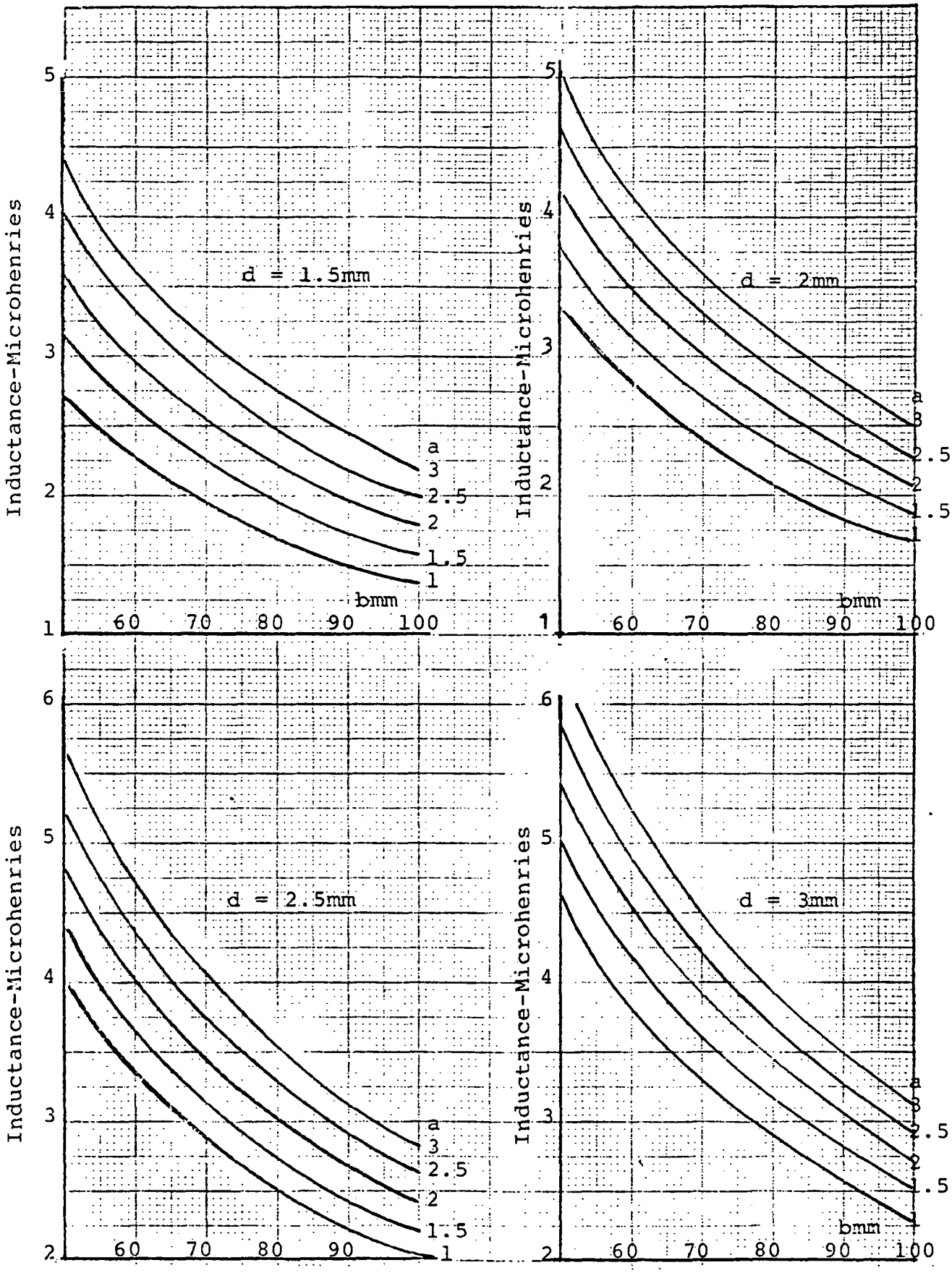

FIGURE B.5: Inductance of Parallel Straps with Copper and Aluminum Conductors with different insulation thicknesses

LIST OF FIGURES

			PAGE
Figure	2.1:	Hollow configurations investigated by previous workers	2.02
Figure	2.2:	Two parallel Litz strap lines	2.04
Figure	2.3:	Ratio of AC to DC resistance for a round wire in self magnetic field	2.08
Figure	2.4:	Characteristic of proximity effect on the peripheral distribution of current density	2.09
Figure	2.5:	Reactance of rectangular flat conductors at 60 Hz	2.13
Figure	2.6:	The strap lines as a capacitor	2.14
Figure	2.7:	Force between rectangular flat conductors for different geometrical spacings	2.16
Figure	4.1:	Three parallel straps (virtually concentric) configuration, evolution	4.02
Figure	4.2:	Finite-element flux plot of 3-phase bus bars with central bus carrying peak current	4.04
Figure	4.3:	Indentation of the middle strap improves EMI and end-insulation design	4.05
Figure	4.4:	Three-straps 2.0 inch wide design for 1000 V, 100 A cable with aspect ratio of 5.1	4.08
Figure	4.5:	Three-straps 1.5 inch wide design for 600 V, 60 A cable with aspect ratio of 5.4	4.10
Figure	5.1:	Dielectric loss tangent vs. frequency at room temp. for some low-loss insulating materials	5.09
Figure	5.2:	Dielectric loss tangent vs. temperature for some insulating materials	5.10

LIST OF FIGURES

		PAGE
Figure 6.1:	Paschen curve, electrical breakdown stress versus pd for air	6.02
Figure 6.2:	Corona inception voltage vs. laminar void size	6.04
Figure 9.1:	Radiation model under study with one face radiating to free space	9.01
Figure 9.2:	Conduction cooling configuration under analysis	9.06
Figure 9.3:	Equivalent thermal circuit used for temperature rise calculations with conduction alone	9.07
Figure 11.1:	EMI flux density estimate of one-half of the cable, with the other half cancelling	11.02
Figure 12.1:	Three-strap 1.5 inch wide design for 600 V, 60 A cable	12.02
Figure 12.2:	Dimension symbols of the 3-straps cable as used in summarizing the design formulas	12.04
Figure 14.1:	Equipment set-up and major process steps for constructing one-meter long sample	14.02
Figure 14.2:	One-meter sample and the 100 kW power supply	14.03
Figure 14.3:	Geometrical dimensions and test results of 3.7 m sample	14.04
Figure 14.4:	Geometrical dimensions and test results of 5 m sample	14.06
Figure 15.1:	Manufacturing problems encountered	15.03
Figure 16.1:	Corona test set-up	16.02
Figure 16.2:	R,L,C test set-up for 20 kHz open-circuit and short-circuit tests on full cable	16.06
Figure 16.3:	Reactive voltage vs. current during short-circuit tests on full cable	16.09

LIST OF FIGURES

		PAGE
Figure 16.4:	Loss vs. current during short-circuit tests on full cable	16.10
Figure 16.5:	Charging current vs. voltage during open-circuit tests on full cable	16.11
Figure 16.6:	Non-concentric terminal-ends generate flux like a solenoid	16.15
Figure 16.7:	Difference in inductances of the middle to two outer straps makes the cable act as a flux-emitter	16.15
Figure 16.8:	EMI test set-up for MIL-STD 462, Sections RE01, RE02 and RE04	16.16
Figure 16.9:	EMI RE01 pre-scan on unshielded cable	16.19
Figure 16.10:	EMI RE04 (and RE01) ambient scan	16.20
Figure 16.11:	EMI RE01 test results on unshielded cable	16.21
Figure 16.12:	EMI RE01 test results on cable shielded with 2-inch EMT	16.22
Figure 16.13:	EMI RE01 test results on cable shielded with 2-inch copper tube	16.23
Figure 16.14:	EMI RE02 narrow band test results on unshielded cable	16.24
Figure 16.15:	EMI RE02 narrow band test results on cable shielded with 2-inch EMT	16.25
Figure 16.16:	EMI RE02 narrow band test results on cable shielded with 2-inch copper tube	16.26
Figure 16.17:	EMI RE04 test results on unshielded cable	16.27
Figure 16.18:	EMI RE04 test results on cable shielded with 2-inch EMT	16.28
Figure 16.19:	EMI RE04 test results on cable shielded with 2-inch copper tube	16.29
Figure 16.20:	Recommended manufacturing improvements	16.32

LIST OF FIGURES

		PAGE
Figure A.1:	Eddy currents in round conductor placed in transverse magnetic field	A.02
Figure A.2:	Rectangular strap of round strands placed in space varying transverse magnetic field	A.05
Figure B.1:	Resistance, inductance, capacitance and mass of parallel straps with copper conductor and 1 mm insulation thickness	B.05
Figure B.2:	Resistance, inductance, capacitance and mass of parallel straps with aluminum conductor and 1 mm insulation thickness	B.06
Figure B.3:	Mass of parallel straps with copper conductor and different insulation thicknesses	B.07
Figure B.4:	Mass of parallel straps with aluminum conductor and different insulation thicknesses	B.08
Figure B.5:	Inductance of parallel straps with copper and aluminum conductors with different insulation thicknesses	B.09

LIST OF TABLES

		PAGE
Table 1.1:	Initial specifications and goals as set by NASA	1.02
Table 3.1:	Comparison of various configurations for 100 kW, 1000 V, 100 A, 50 m long transmission line	3.02
Table 4.1:	Comparison between 2-strap and 3-strap 1000 V, 100 A designs	4.06
Table 5.1:	Alternative conductor materials	5.02
Table 5.2:	Electrical and mechanical properties of common conductors	5.03
Table 5.3:	Properties of major electrical insulating materials	5.07
Table 5.4:	Candidate insulating materials compared from manufacturing viewpoints	5.08
Table 5.5:	Properties of the selected major insulating material, Pro-Fax SE-191 propylene copolymer of Hercules, Inc.	5.12
Table 8.1:	Overall comparison between alternatives	8.02
Table 9.1:	Thermal properties of materials proposed in the cable construction	9.04
Table 9.2:	Operating temperatures under conduction and radiation for 600 V, 60 A, 1.5 inch wide cable design	9.10
Table 12.1:	Design summary of 600 V, 60 A, 1.5 inch wide cable selected as the final design	12.03
Table 13.1:	Failure modes and effects analysis on the cable	13.01
Table 16.1:	Corona test results on flat insulation samples	16.03
Table 16.2:	Bridge measurements on full cable lengths	16.05
Table 16.3:	Short-circuit tests on 65 m cable	16.07

LIST OF TABLES

		PAGE
Table 16.4:	Open-circuit tests on 65 m cable	16.07
Table 16.5:	Short-circuit tests on 123 m cable	16.08
Table 16.6:	Open-circuit tests on 123 m cable	16.08
Table 16.7:	Comparison of calculated and tested parameters	16.12
Table 16.8:	Summary of EMI Measurements on the cable per MIL-STD-462 and 461B	16.31

LIST OF REFERENCES

[1] Jefferies, K. S. and Renz, D. D., Parametric Analysis of Hollow Conductor Parallel and Coaxial Transmission Lines for High Frequency Space Power Distribution, NASA Technical Memorandum 83601, Lewis Research Center, Cleveland, Ohio, March, 1984.

[2] Renz, D. D., et. al., Design Considerations for Large Space Electric Power Systems, NASA Technical Memorandum 83064, Lewis Research Center, Cleveland, Ohio, April, 1983.

[3] Grover, F. W., Calculations of Mutual and Self-Inductances, Dover Publication, New York, 1955.

[4] Grivet, P., Physics of Transmission Lines at High and Very High Frequencies, Vol. I, Academic Press, New York, 1970.

[5] Dwight, H. B., Electrical Coils and Conductors, McGraw-Hill Book Co., New York, 1945.

[6] McNutt, W. J. and Patel, M. R., The Combined Effects of Thermal Aging and Short Circuit Stresses on Transformer Life, IEEE Transactions, Vol. PAS-95, pp. 1275-1286, 1976.

[7] Hansen, I., Description of a 2.3 kW Power Transformer for Space Application, NASA Technical Memorandum 79138, Lewis Research Center, Cleveland, Ohio, February, 1979.

[8] Dunbar, W. G., High Voltage Design Guide for Spacecrafts, Air Force Wright Aeronautical Laboratory/Boeing Aerospace Company Report No. AFWAL-TR-82-2057, Vol. V, January, 1983.

[9] Machine Design, Penton/IPC Publication, Cleveland, OH, April 1985 issue.

[10] Bradwell A., Electrical Insulation, Peter Peregrinus Ltd. and IEE London (Publishers), 1983.

LIST OF REFERENCES

[11] Meek and Craggs, Electrical Breakdown of Gases, John Wiley & Sons, New York, 1978, p. 689.

[12] Jacob M., Heat Transfer, Vol. I and II, John Wiley & Sons (Publishers), NY, 1949.

REPORT DISTRIBUTION LIST

CONTRACT NAS3-23894

NASA CR-175071

One copy per name unless indicated in ()

NASA Lewis Research Center
21000 Brookpark Road
Cleveland, OH 44135

ATTN:	M.A. Beheim	M.S. 3-7
	M.E. Goldstein	M.S. 5-9
	R.W. Graham	M.S. 5-9
	D. Soltas	M.S. 7-3
	Librarian	M.S. 60-3 (2)
	Report Control	M.S. 5-5
	R&QA Office	M.S. 500-211
	H.W. Brandhorst	M.S. 301-3
	I.T. Myers	M.S. 301-2
	G.R. Sundberg	M.S. 301-2 (20)
	G.E. Schwartz	M.S. 301-2 (3)
	I.G. Hansen	M.S. 501-14
	F.F. Terdan	M.S. 501-14
	D.D. Renz	M.S. 501-14 (30)
	A.F. Forestieri	M.S. 501-15
	D. Bentz	M.S. 301-5
	Jack Heller	M.S. 301-5

NASA Scientific & Technical Information Facility
P.O. Box 8757
Baltimore/Washington International Airport, MD 21240
Attn: Accessing Department (25)

NASA George C. Marshall Space Flight Center
Marshall Space Flight Center, AL 35812
Attn: R.E. Kapustka
R. Bechtel

NASA Lyndon B. Johnson Space Center
Houston, TX 77058
Attn: Robert Robinson
Irene Hackler
Robert Hendrix

NASA Goddard Space Flight Center
Greenbelt, MD 20771
Attn: R. Biehman
F. Ford

Wright Patterson Air Force Base
Wright Patterson, OH 45433
Attn: W. Berger, AFWAL/PDCA
J. Weimer, AFWAL/PDCA
E. Lake, AFWAL/PDCA

University of Toledo
Department of Electrical Engieering
2801 W. Bancraft St.
Toledo, OH 43606
Attn: Dr. T.A. Stuart

Department of Energy
1000 Independence Avenue
Washington, DC 20585
Attn: Dr. R. Eaton, CE 32

SDI Office
1717 H. Street N.W.
Washington, DC 20301
Attn: Dr. JH. Hammond, SDE/KE
R. Wiley, SDI/SLKI

Jet Propulsion Laboratory
California Institute of Technology
4800 Oak Grove Drive
Pasadena, CA 91109
Attn: J.A. Stallkamp
Dr. G. Wester M.S. 198-220

Power Conditioning Laboratory
University of Texas
P.O. Box 19016
Arlington, TX 76019
Attn: W.C. Nunnally

General Dynamics
Space Systems Division
P.O. Box 85990
San Diego, CA 92138
Attn: Jim Mildice, C1-7103

University of Oklahoma
202 West Boyd, CEC Room 448B
Norman OK 73019
Attn: Dr. L.W. Zelby

Boeing Commercial Airplane Co.
P.O. Box 3707
Seattle, WA 98124
Attn: C.W. Clay
S. Silverman

New England Electric Wire Corp.
Lisbon, NH 03585
Attn: R.F. Meserve

University of Wisconsin - Madison
Dept. of Electrical & Computer
Engineering
1415 Johnson Drive
Madison, WI 53706
Attn: Dr. T. Lipo

McDonnell Douglas Aircraft Company
3855 Lakewood Blvd.
Long Beach, CA 90846
Attn: D.H. Blyther, 36-43

U.S. Army Electronics Technology
& Devices Laboratory
Fort Monmouth, NJ 07703
Attn: Dr. M. Weiner, SLCET/ML
S.Levy, SLCET/ML

The Pentagon
Washington, DC 20301-7100
Attn: R. Verga, OSD/SDIO - SLKT

T.R. Burkes, Inc.
P.O. Box 16577
Lubbock TX 79490
Attn: T.T. Burkes

Laser laboratory
university of Rochester
250 E. River Road
Rochester, NY 14623
Attn: W.R. Donaldson

HQ DNA
5801 Telegraph Road
Alexandria, VA 22811
Attn: J. Farber, RAEV

State University of New York
4232 Ridge Lea Road
Amherst, NY 14226
Attn: Dr. W.J. Sarjeant

W.J. Schafer Assoc,, Inc.
1901 North Fort Meyer Dr. - Suite
No. 800
Arlington, VA 22209
Attn: P.N. Mace

Electric Power Research Institute
3412 Hillview Avenue
P.O. Box 10412
Palo Alto, CA 94303
Attn: N.G. Hingorani

General Dynamics
P.O. Box 748
Forth Worth, TX 76101
Attn: J.R. McKenzie, Jr.

Texas Technical University
Electrical Engineering Dept.
Lubbock, TX 79409
Attn: Dr. W. Portnoy

Sandia National Laboratory
P.O. Box 5800
Albuquerque, NM 87115
Attn: W. McCollough

Westinghouse Electirc Corp.
P.O. Box 989
Lima, OH 45802
Attn: D. Baker

RCA/Aerospace and Defense
Astro-Electronics Division
P.O. Box 800
Princeton, NJ 08540
Attn: J.A. D'Arcy

Goodyear Aerospace Corp.
1210 Massillon Road
Akron, OH 44315
Attn: C.K. Lavan, Jr.

Boeing Aerospace Co.
P.O. Box 3999
Seattle, WA 98124
Attn: I.S. Mehdi, M.S. 47-03
A.L. Angell

Rockwell International
P.O. Box 4192
3370 Miraloma Ave.
Anaheim, CA 92803
Attn: P.E. McCollum

Plessey Dynamics Corp.
1414 Chestnut Avenue
Hillside, NJ 07205
Attn: G. Bochnak